

Nanomechanics of Biomaterials using Atomic Force Microscope

A thesis

Submitted in partial fulfilment of the requirements

Of the degree of

Doctor of Philosophy

By

JYOTI YADAV

20153408



Indian Institute of Science Education and Research, Pune-411008

2021

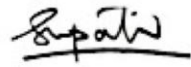
To

Father, Mother, Son &

Husband

Certificate

Certified that the work incorporated in this thesis entitled 'Nanomechanics of Biomaterials using Atomic Force Microscope' submitted by Jyoti Yadav, was carried out by the candidate, under my supervision. The work presented here or any part of it has not been included in any other thesis submitted previously for the award of any degree or diploma from any other University or institution.



Dr. Shivprasad Patil

Thesis Supervisor

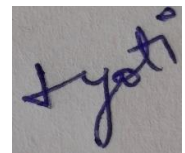
Indian Institute of Science Education and Research

Pune, Maharashtra

Date: November 2021

Declaration

I declare that this thesis is a presentation of my original research work. Wherever contributions of others are involved, every effort is made to indicate this clearly, with due reference to the literature, and acknowledgment of collaborative research and discussions. I also declare that I have adhered to all principles of academic honesty and integrity and have not misrepresented or fabricated or falsified any idea/data/fact/source in my submission. I understand that violation of the above will be cause for disciplinary action by the institute and can also evoke penal action from the sources which have thus not been properly cited or from whom proper permission has not been taken when needed.

A small, square image showing a handwritten signature in blue ink that reads "Jyoti".

Jyoti Yadav

Enrolment no. – 20153408

Date: November 2021

Acknowledgements

I would like to acknowledge my supervisor Dr. Shivprasad Patil for his support and kind behavior. I especially thank him for his freedom to learn different things from other labs also. He was always available for the discussions.

I would like to acknowledge my research committee members Dr. Amrita B. Hazra (IISER Pune) and Dr. Deepa Subramanyam (NCCS Pune) for evaluating my work improving the quality of my research and their collaborations.

I would like to thank Dr. A.S.R. Koti (TIFR Mumbai) for providing plasmid for titin I27 octamer, Dr. Sabyasachi Rakshit (IISER Mohali) for providing I27 monomer plasmid and Dr. Sudhakaran Prabakaran for providing plasmid for PTEN protein.

I would like to specially thank to Dr. Amrita B. Hazra (IISER Pune) and Dr. Santosh Kumar Jha (NCL Pune) for providing protein extraction and purification facility. Special thanks to Yashwant Kumar (IISER Pune) and Nirbhik Acharya (NCL Pune) for teaching protein extraction and purification. I also thank to Gayathri S. Singaraju, Ridim D Mote, Surya Bansi Singh, Mahak Tiwari, Shinde Laxmikant V (NCCS Pune) for experiments and discussions.

I acknowledge my current and past lab members Shatruhan, Ajith, Surya, Viplove, Vikhyaat, Aadarsh, Umashankar, Saurabh, Mayank, Dr. Amandeep Sekhon, Dr. Arpita and Dr. Monika for keeping the lab joyful. Special thanks to Shatruhan, he has helped me in learning the AFM instrument. Special thanks to Dr. Amrita B. Hazra's group, they were always available for the discussion.

I acknowledge all the staffs: technical, academic, teaching, non-teaching, hostel, housekeeping for helping me out, directly or indirectly, to make my academic and non-academic life better.

This journey would not have been possible without my family and friends. I can never forget the time spent with Yashwant, Manu, Satish, Divya, Yamini, Rupali and Nishant. Special thanks goes to my father, husband and mother in law who supported me at every step. Without their support, this journey would not have been possible. Writing thesis with my son was a lovely journey. I do not have words to explain that.

I also thank University Grant Commission for providing funding so that I finish my research work and Perkin Elmer (IISER Pune) facility for fluorescence measurements.

-Jyoti

November 2021

Table of contents

List of figures	xii
List of tables	xvii
Abstract	xviii
Abbreviations used	xix
1 Introduction	1
1.1 Mechanics of Biomaterials	1
1.1.1 Mechanical properties of proteins	2
1.1.2 Mechanical properties of cells	4
1.1.3 Techniques used.....	6
1.1.3.1 Nanoindentation.....	6
1.1.3.2 Traction Force Microscopy.....	7
1.1.3.3 Biomembrane Force Probe.....	8
1.1.3.4 Optical Tweezer.....	8
1.1.3.5 Hybrid nanomechanical investigation technique.....	9
1.2 Protein-drug interaction	10
1.2.1 Proteins	10
1.2.2 Drug	11
1.2.3 Methods to study protein-drug interaction	11
1.2.4 Atomic Force Microscope (AFM)	15
1.3 Stem Cells	16
1.4 Organization of thesis	16
2 Methods	19

2.1	Introduction	19
2.2	Experimental methods	19
2.2.1	Atomic Force Microscope (AFM)	19
2.2.1.1	Principle of Operation.....	20
2.2.1.2	Sample preparation.....	23
2.2.1.3	Cantilevers.....	24
2.2.1.4	Applications.....	24
2.2.2	Fluorescence Spectroscopy	29
2.2.2.1	Intrinsic Fluorescence in Proteins.....	30
2.2.2.2	Mechanism of fluorescence quenching.....	31
2.2.2.3	Equilibrium denaturation method.....	32
2.3	Theoretical methods	33
2.3.1	Worm-Like Chain (WLC) model	33
2.3.2	Hertz model	35
2.3.3	Molecular modelling	38
3	Interaction of Chloramphenicol with titin I27 using single-molecule force spectroscopy	40
3.1	Introduction	40
3.2	Methods.....	42
3.2.1	Protein	42
3.2.2	Protein expression and purification of I27 monomer (I27) ₁ and I27 octamer (I27) ₈	43
3.3	Fluorescence spectroscopy	45
3.3.1	Sample preparation	45
3.4	Docking studies	46
3.5	Atomic force spectroscopy	46
3.5.1	Calibration of the cantilever	48
3.5.2	Sample preparation	49
3.5.3	Analysis	49
3.6	Equilibrium denaturation of (I27) ₁	50

3.6.1	Sample preparation	50
3.7	Results	50
3.7.1	Fluorescence	50
3.7.2	Atomic force spectroscopy	54
3.7.3	Equilibrium denaturation experiment	58
3.8	Discussion	60
3.9	Conclusion	62
4	Assessment of the mechanical properties of mouse embryonic stem cells lacking clathrin heavy chain using AFM	63
4.1	Introduction	63
4.2	Materials and methods	64
4.2.1	Bead attachment on cantilever	64
4.2.2	Cell mechanics using AFM	65
4.2.3	AFM analysis	65
4.3	Results	73
4.3.1	<i>Cltc</i> knockdown results in increase in cell stiffness	73
4.3.2	F-actin depolymerizing agents reduce the stiffness of <i>Cltc</i> deficient mESC.....	78
4.4	Conclusion	83
5	Expression and purification of PTEN and T4 Lysozyme mutant protein	84
5.1	Introduction	84
5.1.1	PTEN protein	84
5.1.2	T4 Lysozyme	86
5.2	Materials and Methods	87
5.2.1	Materials	87
5.2.2	Optimization for purification of WT-PTEN protein	87
5.2.3	Large scale purification of WT – PTEN	88

5.2.4	Purification of mutant (Mu) – PTEN	89
5.2.5	Optimization for purification of T4 Lysozyme mutant protein	89
5.2.6	Large scale purification of T4 Lysozyme	90
5.2.7	Matrix-assisted laser desorption/ionization (MALDI)	91
5.2.8	Formation of polymers from monomer of T4 Lysozyme	91
5.3	Results	92
5.3.1	Agarose gel of PTEN and T4 Lysozyme protein.....	92
5.3.2	Optimization of overexpression of PTEN protein	92
5.3.3	Large scale purification of WT- PTEN	95
5.3.4	Purification of Mu-PTEN	95
5.3.5	Optimization of overexpression of T4 Lysozyme	96
5.3.6	Large scale purification of T4 Lysozyme.....	97
5.3.7	MALDI of T4 Lysozyme protein	98
5.3.8	SDS-PAGE of the polymeric T4 Lysozyme protein	101
5.4	Conclusion	101
6	Conclusion and future possibilities	103
6.1	Conclusion	103
6.1.1	Interaction of Chloramphenicol with titin I27	104
6.1.2	Mechanical properties of mouse Embryonic Stem Cells (mESCs)	105
6.2	Future possibilities	105
6.2.1	Effect of temperature and chemical denaturants on protein-drug complex.....	105
6.2.2	Interaction of various antibiotics and muscle relaxants on titin I27 protein	106
6.2.3	Mechanics of PTEN and T4 Lysozyme.....	106
	References	108

List of figures

2.1 Schematic of AFM where a laser beam is allowed to fall on the back of the cantilever. Laser beam reflects from the cantilever surface and falls on the photodetector. The photodetector gives the signal which is proportional to bending of the cantilever. A polypeptide is tethered between the sample surface and the cantilever tip.....	21
2.2 Jablonski diagram showing the fluorescence emission spectrum.....	30
2.3 Schematic showing static and dynamic quenching.....	31
2.4 Worm-like chain model is used to describe the entropic elasticity of polymer which basically describes the relationship between force (F) and extension (x) of protein using contour length (L_c) and persistence length (P), respectively.....	35
2.5 AFM schematic showing the interaction of glass bead with the cell where d_0 and z_0 shows the initial cantilever deflection and the movement, and d_1 and z_1 shows the final cantilever deflection and the movement.....	37
3.1 Crystal structure of titin I27 (PDB - 1TIT).....	43
3.2 15% SDS-PAGE gel image of titin I27 monomer. Lane 1 shows marker and Lane 2 shows monomer of I27.....	44
3.3 SDS-PAGE gel for titin I27 octamer. Lane 1 shows the marker and Lane 2 shows the octamer of I27.....	45
3.4 a) Schematic of I27 octamer tethered between AFM cantilever and gold coated coverslip, b) One of the domains gets unfolded when the applied force reaches a critical value resulting in relaxation of cantilever to its equilibrium position, c) Unfolding of last domain. Further pulling will result in the stretch of the unfolded domain followed by the tip-molecule detachment.....	47
3.5 Force extension curve of $(I27)_8$ at room temperature at 1500 nm/sec. The characteristic sawtooth pattern showing 7 unfolding events.....	48

3.6 The Trp fluorescence emission spectra of I27 excited with 295 nm wavelength after the addition of CLM to the solution. The arrow indicates increasing concentrations of CLM (0, 10, 20, 30, 40, 50, 75 and $100 \times 10^{-6} \text{ molL}^{-1}$). We observed that the fluorescence is quenched with the addition of CLM to the solution. 10 mM PBS (pH 7.4) buffer is used for the protein as well as for CLM solution.....	52
3.7 Docking studies to check the proximity of CLM to Trp34 of titin I27 protein. a) I27 (PDB ID: 1TIT) docked with CLM using PatchDock, b) Interaction of CLM with Trp34 within 5 Å. It suggests that the fluorescence quenching is due to attachment of CLM to the protein in vicinity of Trp.....	53
3.8 Stern-Volmer plot for quenching of I27 at different drug concentrations (pH is 7.4, the excitation wavelength, $\lambda_{\text{ex}} = 295 \text{ nm}$). The concentration of I27, $[\text{I27}] = 40 \times 10^{-6} \text{ M}$, the drug concentration is varied, $[\text{Q}] = 20, 30, 40, 50, \text{ and } 75 \times 10^{-6} \text{ M}$	54
3.9 Representative measurements for the unfolding of polyprotein without and with the drug a) I27-WT, and b) I27 with 40 μM CLM . The force required to unfold the domain is more for I27 with 40 μM CLM compared to I27-WT. Solid red line represent the WLC model fitted to the force versus extension curve.....	55
3.10 Unfolding force frequency histograms followed by Gaussian fit for I27 only and I27 with different drug concentrations.....	56
3.11 The graph shows the domain-wise unfolding force after the addition of the drug at various concentrations. The peak number suggests the number of unfolded domains. The sample size is 160 and 98 for the I27-WT and I27 with 40 μM CLM respectively. The unfolding force is higher for 40 μM CLM concentration. The difference is of $\sim 25 \text{ pN}$ for each domain, the error bars are standard errors which is standard deviation divided by square root number of measurements.....	57
3.12 The domain-wise persistence length of I27-WT and I27 with 40 μM CLM. The error bars are standard errors.....	58

3.13 Equilibrium denaturation experiments on monomers of I27-WT and I27 with different drug concentrations followed by Trp emission fluorescence spectroscopy. The denaturation data is plotted in terms of denatured fraction. a) The data in black filled squares are I27-WT, yellow filled circles are I27 with 30 μ M CLM concentration and filled blue triangles are of I27 with 50 μ M CLM concentration, b) The data in black filled squares are I27-WT, red filled stars are I27 with 40 μ M CLM concentration. Solid lines are fit to a two-state model.....	59
3.14 Plot of ΔG_D versus GdmCl molarity for calculation of ΔG_D (H_2O). a) The data in black filled squares are I27-WT, yellow filled circles are I27 with 30 μ M CLM concentration and filled blue triangles are of I27 with 50 μ M CLM concentration, b) The data in black filled squares are I27-WT and red filled stars are I27 with 40 μ M CLM concentration.....	60
4.1 Schematic of AFM where a spherical glass bead of diameter 5 μ m is attached on the tipless cantilever. The inset shows the SEM image of the glass bead attached on the cantilever.....	65
4.2 Force vs indentation curves fitted with Hertz model for a) shScrambled, b) shCltc1, c) shCltc3, d) retinoic acid respectively. The grey area shows the region over which the hertz model is fitted, that area describes the region where the cell is elastically deformed. The E value describes the stiffness of the cell 269 Pa, 627.5 Pa, 405.7 Pa, 745 Pa, respectively.....	67
4.3 Force vs indentation curves fitted with Hertz model for a) shScrambled, b) shCltc1, c) shCltc3 cells treated with LatA, respectively. The grey area shows the region over which the hertz model is fitted, that area describes the region where the cell is elastically deformed. The E value describes the stiffness of the cell 240 Pa, 298.9 Pa and 277.3 Pa, respectively.....	69
4.4 Force vs indentation curves fitted with Hertz model for a) shScrambled, b) shCltc1, c) shCltc3 treated with CytoD, respectively. The grey area shows the region over which the hertz model is fitted, that area describes the region where the cell is elastically deformed. The E value describes the stiffness of the cell 280.8 Pa, 228.5 Pa and 276.8 Pa, respectively.....	71
4.5 Representative force curves on samples: Representative force curves on all samples plotted together. This data is used to estimate the Young's modulus reported in Fig. 1 and Fig. 2. Raw data clearly reveals variation in stiffness in mESCs after various treatments and KDs. Glass cover-slip is a reference and the tip-glass contact is assumed to be non-deforming.....	74

4.6 Young's modulus (E) of shScrambled, shCltc1, shCltc3 and RA treated mESCs. ***p<0.0001 by Student's T-test. The error bars denote standard error over 22-25 cells with 100 measurements on each cell with 3 μm x 3 μm grid. ~ 2000 force curves were collected for each condition.....	75
4.7 Frequency histogram followed by gaussian fit for shScrambled, shCltc1, shCltc3 and retinoic acid, respectively.....	76
4.8 Young's modulus of shScrambled, shCltc1 and shCltc3 mESCs treated with acting polymerizing inhibitors LatA and CytoD. Significance calculated with respect to the corresponding untreated samples. *p<0.05; ***p<0.0001 by Student's T-test. The error bars denote SE over 17-20 cells with 100 measurements on each cell.....	79
4.9 Frequency histogram followed by gaussian fit for LatA treated shScrambled, shCltc1 and shCltc3 cells respectively.....	80
4.10 Frequency histogram followed by gaussian fit for CytoD treated shScrambled, shCltc1 and shCltc3 cells respectively.....	82
5.1 The domain structure of PTEN protein consisting of 403 amino acids with five functional domains-PBD, phosphatase, C2, C-terminal tail and PDZ-BD.....	85
5.2 Crystal structure of PTEN protein (PDB -1D5R).....	85
5.3 Crystal structure of T4 Lysozyme (PDB -1B6I).....	86
5.4 Agarose gel of PTEN and T4 Lysozyme protein.....	92
5.5 SDS-PAGE gel for IPTG optimization at 15 °C and 10 h incubation time, where M stands for marker, S for supernatant, P for pallet and Un for Uninduced.....	93
5.6 SDS-PAGE gel for IPTG optimization at 15 °C and 16 h incubation time where M stands for marker, S for supernatant, P for pallet and Un for Uninduced.....	93
5.7 SDS-PAGE gel for IPTG optimization at 15 °C and 18 h incubation time where M stands for marker, S for supernatant, P for pallet and Un for Uninduced.....	94
5.8 SDS-PAGE gel for IPTG optimization at 18 °C and 18 h incubation time where M stands for marker, S for supernatant, P for pallet and Un for Uninduced.....	94

5.9 SDS-PAGE gel for WT-PTEN purification at 18 °C and 18 h incubation time with 2 L culture where M stands for marker.....	95
5.10 SDS-PAGE gel for Mu-PTEN at 18 °C and 18 h incubation time where M stands for marker.....	96
5.11 SDS-PAGE gel for T4 Lysozyme mutant at 37 °C and 3 h incubation time (transformation done with pLysS cells), where Un stands for uninduced, In for induced, 1- 4 for single isolated colony respectively, S for supernatant and P for pallet.....	97
5.12 SDS-PAGE gel image of T4 Lysozyme mutant in a) 8 M urea at 37 °C and 5 h incubation time, b) 20 mM Tris-HCl buffer pH 8.0 (transformation done with pLysS cells) where M stands for marker.....	98
5.13 MALDI of T4 Lysozyme mutant in DAHC and DHAP matrix.....	99
5.14 MALDI of T4 Lysozyme mutant in DAHC and DHAP matrix after providing atmospheric oxygen with balloon for 6-7 h at room temperature.....	100
5.15 SDS-PAGE gel for T4 Lysozyme mutant after purging atmospheric oxygen for 6-7 h, where M stands for marker.....	101

List of tables

1.1 Table 1 showing the spatial, temporal resolution, applications as well as limitations of the force spectroscopy techniques.....	9
4.1 The table shows the apparent Young's modulus (E) of cells under the mentioned conditions (n denotes the number of cells analysed).....	76
4.2 The table shows Young's modulus of shScrambled, shCltc1 and shCltc3 treated with LatA and CytoD (n denotes the no. of cells analysed for each type).....	79

Abstract

Understanding mechanical properties of biological elements such as cells, proteins, and deoxyribonucleic acid (DNA) is very important in order to understand their function. Various techniques such as nanoindentation, Optical Tweezers (OT), Magnetic Tweezers (MT) and Atomic Force Microscope (AFM) are widely used for studying the mechanical properties of biomaterials. AFM has been used previously for imaging of cells, bacteria and proteins as well as for protein-protein interaction, antigen-antibody interaction, ligand-receptor interaction and protein-drug interaction. Protein-drug interaction is very well studied using fluorescence, Ultraviolet-Visible (UV-Vis) absorption, and circular dichroism techniques. We have studied interaction of Chloramphenicol with titin I27 protein using Fluorescence and AFM. It has been found out from the fluorescence study that the drug binds to the protein resulting in the formation of protein-drug complex. Alteration in mechanical properties of proteins at different drug concentrations is studied using AFM. AFM data shows that the drug binds to the protein at 40 μM of drug concentration thereby resulting in an increment of unfolding force (by 25 pN) and decrease in persistence length. Therefore, the drug is mechanically stabilizing the protein. However, chemical stability of the protein is checked by equilibrium denaturation experiment. The denaturation experiment shows the increase in free energy of stabilization for the protein-drug complex with respect to protein only. Therefore, the drug stabilizes the protein mechanically and chemically.

In another study, mechanical properties of mouse embryonic stem cells (mESCs) is also studied. Previously, it was shown that loss of clathrin heavy chain results in loss of clathrin mediated endocytosis (CME) and thereby shows loss of pluripotency. However, the mechanical properties on loss of clathrin heavy chain was not known. The results shows that the mESCs lacking clathrin shows greater cellular stiffness in comparison to wild type cells. Also, treatment of mESCs with actin depolymerizing agents shows similar values of cellular stiffness as that of wild type cells.

Abbreviations used

DNA - Deoxyribonucleic Acid

nm- nanometer

μm - micrometer

AFM- Atomic Force Microscope

CLM – Chloramphenicol

mESCs - Mouse Embryonic Stem Cells

TNX-Tenascin-X

Fn-Fibronectin

PADC - Pyruvoyl-Dependent Arginine Decarboxylase

pN-piconewton

DLS - Dynamic Light Scattering

Sec-second

kPa-kilo pascal

iPSC - Induced Pluripotent Stem Cells

hASCS - Human Adipose-Derived Stromal Cells

hESC - Human Embryonic Stem Cell

nN – Nanonewton

GPa – Giga pascal

pN – piconewton

μN - micronewton

xx

mN – millinewton

TFM - Traction Force Microscopy

HPAC – High Performance Affinity Chromatography

UV – Ultraviolet

CD - Circular dichroism

UV-Vis- Ultraviolet Visible

NMR- Nuclear magnetic resonance

IR – Infrared

ITC- Isothermal calorimetry

DSC - Differential scanning calorimetry

SMFS - Single molecule force spectroscopy

ESCs – Embryonic Stem cells

HMSCs - Human Mesenchymal Stem Cells

WLC – Worm-Like chain

Trp – Tryptophan

WT – Wild Type

PL – Persistence Length

Cltc - Clathrin heavy chain

CME – Clathrin Mediated Endocytosis

SEM - Scanning Electron Microscopy

TEM - Transmission Electron Microscopy

STM - Scanning Tunnelling Microscopy

Å – Angstrom

SHG - Second Harmonic Generation

SFM - Scanning Force Microscope

Si – Silicon

Si₃N₄- Silicon Nitride

HOPG - Highly Ordered Pyrolytic Graphite

EtBr - Ethylene Bromide

dsDNA - Double Stranded DNA

h - Hour

pI - Isoelectric Point

FRET - Fluorescence Resonance Energy Transfer

SNase - Staphylococcal Nuclease

MBP - Maltose Binding Protein

DHFR - Dihydrofolate Reductase

NADP - Nicotinamide Adenine Dihydrogen Phosphate

Ig – Immunoglobulin

EDTA - Ethylenediamine tetraacetic acid

Tyr- Tyrosine

Phe – phenylalanine

kDa - kilodalton

PDB – Protein Data Bank

RMSD - Root Mean Square Deviation

HSA - Human Serum Albumin

IPTG - Isopropyl β -D-1-thiogalactopyranoside

xxii

mg – milligram

mL - millilitre

PMSF - Phenylmethylsulfonyl Fluoride

SDS-PAGE - Sodium Dodecyl Sulfate Polyacrylamide Gel Electrophoresis

mM – millimolar

μ M – micromolar

M - molar

GdmCl - Guanidinium Chloride

PBS – Phosphate Buffer Saline

λ_{ex} – Excitation wavelength

λ_{em} – Emission wavelength

BSA - Bovine Serum Albumin

KD – Knockdown

E-CAD – E-Cadherin

TGF β - Transcription Growth Factor β

ERK - Extracellular Signal Regulated Kinase

Lat A - Latrunculin A

Cyto D - Cytochalasin D

RA – Retinoic Acid

Pfn1 - Profilin1

PTEN - Phosphatase and Tensin Homolog Deleted On Chromosome 10

AA – Amino Acid

PBD - Phosphatase Binding Domain

PIP3 – Phosphatidylinositol 3,4,5-triphosphate

PIP2 – Phosphatidylinositol 4,5-bisphosphate

Mu - mutant

Kan – Kanamycin

Mu – Mutant

RPM - Revolutions per Minute

DTT – Dithiothreitol

Amp – Ampicillin

DAHC - Diammonium Hydrogen Citrate

DHAP - Dihydroxyacetone Phosphate

MALDI - Matrix-Assisted Laser Desorption/Ionization

Chapter 1

Introduction

Biological components which are involved in various physiological processes in living organisms are known as biomaterials such as proteins, cells, and deoxyribonucleic acid (DNA). Mechanical properties such as elasticity, force resistance, tensile strength etc. of these materials play crucial role in their functions [1–3]. So, the study of mechanics of biomaterials are essential to understand their functions and hence relevant physiological processes. Various techniques have been developed to study mechanical properties of biomaterials from nanometer (nm) to micrometer (μm) length scale. Atomic Force Microscope (AFM), Optical tweezer (OT), Magnetic tweezer (MT), and Nanoindentation are the popular techniques. Among them, AFM has been recognized to be one of the powerful techniques for such studies. The discussion will be focused on AFM based investigations as I have extensively used it for my studies.

In the present thesis, I have studied the interaction of chloramphenicol (CLM) with titin I27 protein and the mechanical properties of mouse embryonic stem cells (mESCs). I have mainly used AFM for my experiments. Fluorescence study has been done for studying the binding mechanism of CLM and I27 protein and for checking the chemical stability on protein-drug binding. The experiments are discussed in detail in upcoming chapters.

1.1 Mechanics of Biomaterials

Biomaterials are biological elements which are essential for performing various functions in living organisms. It can be cells, proteins, DNA, vesicles etc. My discussion will be focused on proteins

and cells. It is important to understand the mechanical properties of biomaterials in order to understand their function [4, 5].

1.1.1 Mechanical properties of proteins

Mechanical properties of proteins play crucial role in their functions such as passive elasticity generated by giant muscle protein titin [6]. Mechanics of proteins helps in understanding the folding/unfolding behavior, viscoelasticity, various biomolecular interactions such as protein-protein interaction, protein-ligand interaction and protein-drug interaction.

Proteins are essential part of our life. These are one of the essential building blocks which perform various biological functions in our body such as building tissues, muscles, act as enzymes, hormones, catalyst that are involved in transport of some molecules like oxygen. Each protein has a unique 3D shape in order to perform its function. If anything binds to a protein, its function and 3D structure changes. So, the study of interaction of proteins with small molecules such as drugs and dyes is crucial to understand various biological processes [7]. It is known that binding of calcium molecule with I27 protein alters the mechanical strength of I27 protein [8].

Since the 3D structure of protein is held together by various interactions such as hydrogen bonds, disulfide bonds and ionic interactions. So, the force required to break these bonds determines the mechanical strength of a protein. Mechanical strength of the protein tells about the flexibility of the protein. Dong et al. (2009) have studied the structural flexibility of bacteriorhodopsin protein. Measurements were done on the two sides of the purple membrane. The effective force constants for the extracellular matrix was found to be three fold greater than the cytoplasmic ones. This difference is attributed to the flexibility in conformational changes in the cytoplasmic side [9]. Rico et al. have studied the flexibility of bacteriorhodopsin protein and correlated with the crystal structure. They have found that the α -helices provides the molecular stability whereas interhelical loops shows structural flexibility [10]. Martinez-Martin et al. (2011) have measured the structural flexibility of pentameric IgM antibody using dynamic force microscopy. In order to do that, they have combined bimodal excitation with frequency modulation AFM. The combination of both provides the topography as well as elastic modulus of proteins. The elastic modulus was found to

be in the range of $8.2\text{-}19.0 \pm 0.1$ MPa and a correlation between structure and elasticity has been found out [11]. Cecconi et al. have studied the mechanical unfolding of *E. Coli* Ribonuclease H protein and the energy landscape was determined. It has been found that it unfolds in a two state manner and refolding of the protein occurs through an intermediate [12]. Ashlee Jollymore et al. have studied the folding-unfolding behavior of full length Tenascin-X (TNX) as well as its fibronectin III (FnIII) domains. They have found the mechanical properties of TNXFnIII exhibits similarity with the FnIII domains and Tenascin is an elastic protein and undergoes reversible folding-unfolding transition [13, 14]. Miklos et al. have studied the folding-unfolding behavior of titin and found out that unfolding occurs at 20-30 pN force regime whereas folding occurs at 2.5 pN force regime [15]. Wang et al. have studied the folding-unfolding of slipknotted protein pyruvoyl-dependent arginine decarboxylase (PADC). It has been found that unfolding occurs in a two state manner and unfolded and untied PADC refolded back into its native state. Folding occurs thereby showing complex behavior and misfolding [16]. Vazquez et al. have studied mechanical and chemical unfolding pathways of titin I27 protein and found out that the unfolding rates obtained by both the methods are same [17]. However, it was not clear that both of these follow the same pathway. To study that, free energy was calculated for different mutants of I27 protein and it has been found out that both the techniques follow different unfolding pathways as the rate constant obtained from the chemical denaturation method was five-fold faster [2]. Matthias Rief et al. have studied unfolding of titin I27 at different pulling speeds and found that protein was getting refolded on relaxation [18]. **The effect of temperature on the mechanical unfolding of titin I27 on its native as well as intermediate state has been studied by Yukinori Taniguchi et al. and they found out that the force for which native state unfolds into an intermediate state does not depend on temperature whereas unfolding force from the intermediate depends on temperature [19].** Unfolding pathways of T4 Lysozyme protein was studied by Qing Peng et al. and it has been found out that multiple pathways are obtained on stretching either from its N-terminus or C-terminus end [20] whereas Guoliang Yang et al. have studied unfolding and refolding of T4 lysozyme polymers and found out that the unfolding force is 64 ± 16 pN and relaxation occurred within 1 sec of relaxation [21].

Various measurement techniques such as dynamic light scattering (DLS), nano-rheology and AFM has been used to measure the viscoelastic properties of proteins [22–25]. Previously, viscoelasticity of bacteriorhodopsin protein has been studied using AM-AFM measurements in dynamic mode of AFM [26]. Izhar D. Medalsy et al. have studied viscoelasticity of

bacteriorhodopsin at different loading rates (0.0005 - 0.1 mN/s). It has been found that the mechanical stiffness of the protein as well as membrane increases [27]. In another study, viscoelastic response of single (I27)₅ protein has been studied using dynamic force spectroscopy and decrease in peak unfolding force was found [22]. In another study, small amplitude and low frequency has been used to study viscoelastic nature of I27 protein [28]. Viscoelasticity of single molecule such as dextran has been determined at millisecond timescale using AFM [29]. Power spectral density has been used to study the viscoelastic behavior of (I27)₈ protein [30]. Further, the quantification of viscoelasticity of polyprotein has been studied using two methods- deflection detection and displacement detection (interferometer based) and found that the dissipation in single molecule is below the AFM detection limit. However, the stiffness was accurately determined [31].

Chunbo Yuan et al. (2000) have studied unfolding dynamics of streptavidin-biotin complex. In this study, that Biotin was immobilized on the cantilever tip and streptavidin was immobilized on the substrate. Experiments were performed with various loading rates between 100 and 5000 pN/sec. It has been found that with the increase in the loading rate, unfolding force increased [32]. Jurgen Fritz et al. have studied the kinetics of P-selectin ligand complexes. P-selectin was immobilized on glass coverslip whereas P-selectin glycoprotein ligand-1 was immobilized on the tip. It has been found that the complex was able to withstand at 165 pN of rupture force [33]. Interaction between three structurally different proteins (α -synuclein, amyloid β -peptide, and lysozyme) has been studied as a function of pH. It has been found that the interaction between homologous pairs is minimal at physiological pH and it increases towards acidic pH [34].

1.1.2 Mechanical properties of cells

Mechanics of cells determine its functions such as migration, adhesion, differentiation and cell-cell interaction. Mechanical properties of cells are regulated by actin cytoskeleton and actin cytoskeleton regulates cell function [35–37]. Actin cytoskeleton is a network of actin and actin binding proteins. It combines with other cytoskeleton parts and mediates various cellular processes. Mechanics of cells helps in understanding the stiffness and cell-cell adhesion.

Emad A-Hassan et al. (1998) have studied the elasticity of living Madine-Darby canine kidney cells. For that, an experimental approach, force integration to equal limits mapping has been used. Force-distance curves were collected at time scales where contribution from viscous components are negligible and only elastic contribution is there [38]. Interaction between fibronectin and Staphylococcus epidermis has been studied by Yasser Bustanji. This interaction was compared with the biotin/avidin and L-selectin/P-selectin glycoprotein ligand-1 interactions. They found that the fibronectin case shows the high energy binding mode and sustain large deformations for longer times than the selectin case [39]. Ahmed Touhami et al. (2003) have measured the elasticity of yeast cells. Here, regions of different elasticity were distinguished on a single yeast cell using AFM and nanoindentation technique [40]. Measurements were done on the bud scar region and surrounding cell surface. Hertz model was used to measure the cellular stiffness of cells. It has been found out that bud scar region was 10 times stiffer than the surrounding surface. Viscoelastic properties of agarose gel as well as living A549 alveolar epithelial cells was measured by Félix Rico et al. (2005). For that spherical and blunted pyramidal tips were used. It has been found that agarose gel shows the elastic behavior. The Young's modulus varied by a factor of 2 in the linear regime by the two tips. The cell shows the viscoelastic behavior [41]. Michael J. Rosenbluth et al. (2008) have studied the deformability of non-adherent cells (human myeloid and lymphoid leukemia cells and neutrophils). The cells were adhered on the microfabricated wells and hertz model was used to study the cellular stiffness of these cells. The cellular stiffness was found to be 855 ± 670 Pa for myeloid cells, 48 ± 35 Pa for lymphoid leukemia cells, 156 ± 87 Pa for neutrophils [42]. M. Lekka et al. have measured the elastic properties of normal (Hu609) and cancerous cells (T24). It has been found that normal cells are stiffer than the cancerous cells. The young's modulus was found to be in the range of 1-10 kPa. Elsa Correia Faria et al. have studied the elastic properties of prostate cancer cells using pyramidal tip and three different cell lines named as 52 LNCaP, 53 PC-3 and 47 BPH cells were used. Young's modulus was found to be 287 ± 52 N m⁻², 1401 ± 162 N m⁻² and 2797 ± 491 N m⁻² for LNCaP, PC-3 and BPH cells, respectively [43]. Kyle E. Hammerick et al. have determined the elastic properties of induced pluripotent stem cells (iPSC). They have used two cell lines- fibroblast iPSC and human adipose-derived stromal cells (hASCs). For measuring the difference between the two, cell stiffness was measured. Young's modulus was found to be of the order of hASC-iPSC < human embryonic stem cell (hESC) < fibroblast-iPSC < fibroblasts < hASC [44]. Anand Pillarisetti et al. have measured the elastic properties of

undifferentiated and differentiated mouse embryonic stem cells. Elastic properties were measured for live and fixed cells using pyramidal tip as well as spherical tip. It has been found that the differentiated cells are more stiffer as compared to the undifferentiated cells [45]. Audrey Beaussart et al. have studied the cell-cell adhesion between *Lactobacillus plantarum* and biotic (lectin monolayer) and abiotic surfaces (hydrophobic monolayer). *Lactobacillus plantarum* was adhered on the cantilever with colloidal probe and biotic-abiotic surfaces were cured on the substrate. A strong adhesion was shown by *Lactobacillus plantarum* cells towards both biotic and abiotic surfaces [46].

There are various techniques such as AFM, OT, nanoindentation etc. that can be used to study the mechanical properties of biomaterials such as proteins and cells. These techniques characterize the mechanical properties of materials from atomic to macro level. AFM meets these essential criteria and it has been extensively used for such studies. It is capable of imaging and quantifying the material properties at the sub nanometers to several micrometers spatial resolution. It can measure forces ranging from ~10 pN to several nanonewtons (nN) and elastic modulus from kPa to GPa [47–51].

1.1.3 Techniques used

1.1.3.1 Nanoindentation

It is a good tool for probing cellular and molecular mechanics. For harder materials the deformation is too small. Since applying higher forces can result in deformation of the biological samples e.g. hard bones. Nanoindentation can measure force in the range of μN to mN and displacements from nm to μm .

The loading cycle usually consists of elastoplastic deformation whereas elastic portion is conserved during unloading. Elastic modulus and hardness is usually calculated by load-displacement curve. Analysis of initial unloading curve can give information about elastic modulus whereas reduced modulus is given by the equation:

$$E_r = \frac{1}{2} \frac{\sqrt{\pi}}{\sqrt{A}} S \quad (1.1)$$

where S is the stiffness and A is the contact area at maximum load.

Then elastic modulus is calculated by the following equation:

$$\frac{1}{E_r} = \frac{(1 - \gamma_m^2)}{E_m} + \frac{(1 - \gamma_i^2)}{E_i} \quad (1.2)$$

where E_i and γ_i are the elastic modulus and poisson's ratio of the indenter tip, E_m and γ_m are the elastic modulus and poisson's ratio of the material which is to be indented.

Usually elastic modulus and poisson's ratio of the indenter tip is known. So, for the material elastic modulus and poisson's ratio can be calculated. Hardness is usually calculated by dividing maximum load with the contact area.

Nanoindentation technique is used to measure mechanical properties of cells, tissues, organs etc. For measuring mechanical properties of individual cell, indentation tip with small radius is used while for tissues and organs, indentation tip with large radius (micron sized) is to be used. Sharp pyramidal tips are generally used for higher resolution types whereas three sided pyramidal tip is used to measure mechanical properties at precise locations whereas pyramidal tips can damage the biological sample since these tips penetrates into the sample. In order to avoid this problem, spherical glass beads and flat punch are generally used.

Mechanical properties of biological samples depend on the hydration level. In their natural state cells, tissues and organs are hydrated. So, nanoindentation samples are prepared by using epoxy followed by surface dehydration. Soft biological samples are challenging samples for nanoindentation technique [52]. This technique is useful for studying the nanomechanics of polymers, gelatin, bone etc. [53].

1.1.3.2 Traction Force Microscopy (TFM)

This technique measures traction forces generated by objects on which they are adhered. Here, the object of interest is attached to an elastic substrate and the deformation is calculated. This technique is widely accessible over a large length and force scale [54]. TFM has been widely used for the traction of single cell [55, 56]. Xavier Trepate et al has used TFM to measure intercellular forces to detect how cells move at the edge of epithelial cell sheets and they have

found out that collective motion is not from the leader cells but from the cells which are distributed on the sheet [57].

1.1.3.3 Biomembrane Force probe

This technique is used for quantification of single molecular bonds. This technique was invented by E. Evans et al. [58]. This is used for single molecule force spectroscopy and experiments to probe molecular adhesion and structures of biological interfaces. This works in a wide range of forces (0.1 pN to 1 nN). It can be used for measuring the interaction between ligand-receptor pairs. C. Gourier et al. has determined the energy landscape of streptavidin-biotin pair and cell-cell interactions are measured for mammalian gamet interactions [59].

1.1.3.4 Optical Tweezers (OT)

Optical tweezers is a single molecule manipulation technique used for the application of calibrated forces and measurement of displacement of the particles.

It consists of high numerical aperture microscope which focuses the laser to trap the particles. For biological applications, Nd-Yag laser with a wavelength of 1064 nm is generally used. Micrometer sized polystyrene beads are attached to the molecules of interest and then trapped by optical tweezer. These polystyrene beads acts as spherical indentor and the young's modulus (E) can be calculated by the following equation:

$$E = \frac{3(1-\gamma^2)}{4\delta\sqrt{r}}F \quad (1.3)$$

Where F is the indentation load, δ is the displacement load, γ is the poisson ratio and r is the bead radius.

Optical tweezers have been used to study virus-cell adhesion, unfold single RNA molecules, to obtain binding strength of fibrinogen-integrin pairs [60]. It has been used previously to study folding unfolding behavior of titin molecules and hysteresis curve was generated [15].

Thalhammer and co-workers developed macrotweezers capable of trapping active swimming organisms upto 70 μm length [61]. Macrotweezers has broadened the use of this technique for taxonomic identification, collection and tagging of micro-organisms.

1.1.3.5 Hybrid nanomechanical investigation technique

Magnetic tweezers is a technique for nanomechanical investigation of biological sample.

Micronanoelectromechanical systems (MNEMS) are also used for nanomechanical manipulation.

Nanomechanical cantilevers have been used for the detection of complex diseases. This is basically based on the concept of beam deflection due to interaction with biological molecules. This deflection of beam is due to adsorption induced deflection, change in resonant frequency due to mass loading. Huber et al. investigated the binding of two proteins, transcription factors SP1 and NF_B with DNA oligonucleotides [62]. Since mutation of binding sites leads to diseases, therefore the analysis of transcription factor at early stage is possible. The diagnosis of prostate cancer was also done where two forms of prostate specific antigen are detected using microcantilever system. Nanomechanics of cells was also determined using nanopatterns. Nanomechanical differences between normal and cancer cells can also be determined using nanopatterns with varying spread areas [63] [52].

The below attached table (Table 1) contains the resolution, application and limitation of force spectroscopy techniques.

Table 1 showing the spatial, temporal resolution, applications as well as limitations of the force spectroscopy techniques.

Technique	Optical tweezer	AFM	Nanoindentation	Traction Force Microscopy	Biomembrane force probe
Spatial resolution (nm)	0.1-2	0.5-1	1-10 ⁴	10 ³	5

Temporal resolution (s)	10^{-4}	10^{-3}	1	Depends on the field of view	10^{-3}
Applications	3D manipulation, tethered assay, interaction	Nanoscale imaging, force pulling and interaction (inter- and intra-molecular)	Mechanical properties of cells, tissues, organs, scaffolds and implants	Traction of individual cell, collective behavior of multicellular system	Single molecular bonds, Ligand-receptor interaction
Limitations	Photodamage, sample heating, non-specific interactions	Large high-stiffness of cantilever, non-specific interactions [64]	Modulation of elasticity is limited to linear and isotropic materials [53]	Fine variations in local cellular traction [65]	Resolution not good as AFM

Since most of my research work is related to AFM, so I will discuss about AFM in detail.

1.2 Protein-drug interaction

1.2.1 Proteins

Proteins are one of the essential building blocks which are made up of amino acids. They perform various functions in our body such as building muscles, energy production, involved in metabolism, immune system, energy buffer, maintaining pH etc. Our body needs proteins in larger amount. There are 20 amino acids among which there are nine essential amino acids which the human body does not synthesize so they actually come from the diet. Proteins can be of two types- complete or incomplete. Complete proteins contain all the essential amino acids whereas

incomplete proteins do not contain all the essential amino acids. It is necessary to understand the structure of proteins. Sequence of amino acids is described by the primary structure. Secondary structure is described by α -helix and β - sheets. Tertiary structure refers to the three dimensional structure of protein. Secondary structure folds into compact globular structure as a result of hydrogen bond. Quaternary structure is a three dimensional structure formed as a result of aggregation of polypeptide chains. When proteins fold, it undergoes a variety of conformational changes before it reaches the final form. It does not randomly go into any conformation. In a unique 3D shape it performs its function. Each protein is in the form of a random coil first, then it is translated by messenger ribonucleic acid to a linear chain of amino acids. When the polypeptide chain is being synthesized by ribosome, then the linear chain of amino acids folds into a three dimensional structure. When the protein does not fold into a particular 3D shape, then the protein can be misfolded. Misfolded protein can lead to several diseases such as neurodegenerative diseases, alzheimer's disease, allergy etc. **The folded form of the protein is the energetically favorable one i.e. functional and operative [66].**

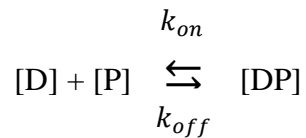
1.2.2 Drug

A drug is any substance that causes a change in physiology when it is consumed. Drugs can be consumed in the body via injection, smoking, inhalation etc. They can be pharmacological or pharmaceutical. A pharmacological drug produces biological effects when they are consumed in the body whereas pharmaceutical drug is used to cure, diagnose or prevent the body from diseases. Pharmacology means the study of body's reaction to drugs whereas pharmaceutical drug relates to medicinal drugs.

Since a major part of this thesis is focused on the study of protein-drug interaction, I will discuss it in detail.

1.2.3 Methods to study protein-drug interaction

The binding of a drug to a protein can be reversible and equilibrium process. If we assume that there is only one binding site on a protein per drug molecule, then the equilibrium process can be defined as



Where [D] is the concentration of free drug, [P] is the concentration of free protein and [DP] is the drug protein-complex concentration. k_{on} and k_{off} are the associated and dissociated rate constants. At equilibrium, the rate of association is equal to the rate of dissociation and is given by

$$k_{eq} = \frac{k_{on}}{k_{off}} \quad (1.4)$$

The dissociation constant is the reciprocal of the association constant.

Also the total number of drugs bound per protein can be calculated by the following equation

$$r = \frac{[DP]}{[P]+[DP]} = \frac{n \cdot k_a \cdot [D]}{1 + k_a \cdot [D]} \quad (1.5)$$

where n is the number of binding sites on protein.

Protein-drug interaction can be studied by direct or non-separation methods and indirect techniques or separation method. Separation method involves separation of free ligand from the bound species whereas non-separation method involves the changes in the physicochemical properties of the ligand or protein when drug molecules bound to them [67].

Separative methods

Various methods such as equilibrium dialysis, ultrafiltration, ultracentrifugation etc. have been characterized under separative methods. A brief discussion about these methods is given below.

Equilibrium dialysis method depends on the difference in molecular size of the drug and protein. It consists of two compartments that are basically separated by a semipermeable membrane. The semi permeable membrane will only allow smaller molecules to pass through it. Basically it will

allow only drug molecules to pass through it and will not allow the protein molecules and drug-protein complex to pass through it. In one compartment, there will be protein and the other contains the drug. After few hours, equilibrium will be reached and the concentration of free drug can be found. However, this method has some limitations. Since it takes longer time to reach the equilibrium, first thing is to determine the equilibration time for any protein-drug complex formation. Second thing is that volume shift occurs because of semi permeable membrane and the presence of proteins. Non-specific adsorption also occurs on the cell walls and on the permeable membrane.

Ultrafiltration is very much similar to previous one except here high pressure is applied to force the solution to pass through the membrane. In this case also, non-specific binding and protein leakage can occur.

In case of ultracentrifugation, a solution of drug and protein is mixed together and is allowed to pass through centrifugal field. Since the sedimentation coefficient of drug is very small, so it will remain in supernatant, protein and the protein-drug complex will settle down at the bottom. This method has the advantage of eliminating problems associated with the membrane effects. However, this equipment is quite expensive in comparison to ultrafiltration and electro dialysis.

Lazaro et al. have used Poly methyl methacrylate technique to measure the kinetics of permeation through hexadecane or 1-octanol membrane in presence or absence of protein in the donor compartment [68]. The free drug concentration in the acceptor compartment can be measured at different times and the difference can be used to estimate the binding constant. This method has several advantage that the absence of equilibration time, non-specific adsorption is also occurred and there is no volume change due to oncotic pressure.

Liquid chromatographic method used to access drug-protein binding can be divided in two categories- whether both interacting species are free in solution or one component generally the protein. In size exclusion chromatography, molecules are basically separated on the basis of their size. Here, protein and the mixture of protein-drug complex elute first since they are large in size and hence does not penetrate. However, drug molecules elute later on, because they are small in size. This method has some disadvantages because of poor protein recovery and low column efficiency. High performance affinity chromatography (HPAC) is based on the immobilization of

a protein on the support while drug is injected into the column. High affinity drugs will interact with the protein and elute later while low affinity one will come first.

Capillary electrophoretic technique has several advantages such as high efficiency, separation selectivity, low sample and reagent consumption, high speed of analysis and the ability to work under physiological conditions. It has several disadvantages because of non-specific adsorption on the capillary walls, low detection limits of commonly used ultraviolet (UV) High performance affinity chromatography (HPAC) detectors.

Non-separative methods

There are various spectroscopic methods that can be used in order to study protein-drug binding such as fluorescence, circular dichroism (CD), UV-Visible (UV-Vis), nuclear magnetic resonance (NMR) etc.

Fluorescence spectroscopy is used for studying protein-drug interaction, number of binding sites, the mechanism of binding and the binding distance between the protein and the drug.

Changes in UV- Vis absorption spectra may be interpreted in terms of change in the polarity. CD spectroscopy also tells the change in three dimensional structure of protein when the drug binds to it. Infrared (IR) spectroscopy is an excellent tool to study the secondary structure of protein whereas NMR tells the groups which are involved in the binding process. Molecular docking is also done in order to determine the binding of protein and drug.

Isothermal calorimetry (ITC) and differential scanning calorimetry (DSC) are also used to study the protein-drug interaction. ITC is basically used to study the biomolecular interaction. In this technique, successive amount of drug is added to the protein solution. Each addition of drug will result in some specific amount of protein-drug complex formation which is dictated by heat release. Sometimes large amount of protein sample is needed and very high and low affinity processes cannot be studied by this process. The sample should be highly purified. For DSC, reaction cell basically contains the protein and drug. The sample is heated and the transition mid-point where 50 % of the protein is in native state and 50 % is in denatured state whereas in absence

of ligand the transition mid-point occurs at higher value. DSC is basically used to measure the large binding constants (upto 10^{15} mol⁻¹L) which cannot be measured by other techniques. The main disadvantage is low throughput and large sample consumption. Using calorimetric methods, it is possible to calculate enthalpy change (ΔH), gibbs free energy change (ΔG) and entropy change (ΔS).

Surface plasmon resonance based assays has the capability to characterize the binding reactions in real time, small amount of sample is required etc. This technique involves immobilizing the protein on the surface and the drug flows in the solution over the surface. It basically monitors changes in refractive index. This method is interesting because of lack of labeling [69].

1.2.4 Atomic Force Microscope (AFM)

AFM can also be used in order to study protein-drug interaction [70]. Protein-drug sample is mixed together in a vial and then dropcasted on a freshly gold coated coverslip [71]. The system is allowed to incubate for half an hour. After 30 minutes, sample is rinsed three times with deionized water in order to remove the unbound protein. Some amount of buffer is filled in the liquid cell and force spectroscopy is done. There are some studies of protein –ligand interaction where first protein is incubated on gold coated coverslip for 30 minutes, washed three times with DI water and then ligand is added in the buffer solution. The force spectroscopy is done after that.

AFM can be used to measure the protein- drug interaction, protein-protein interaction, protein-ligand interaction [70–74]. Protein-drug interaction can also be studied by using fluorescence measurement, CD, UV-Vis absorption, synchronous fluorescence spectroscopy etc. [75, 76, 85, 77–84].

In the present thesis, we have measured the interaction of titin I27 protein with CLM drug. Single molecule force spectroscopy (SMFS) is studied by AFM. WLC model is being used for measuring the change in persistence length.

In another work, mechanical properties of stem cells are measured by AFM. Hertz-model is used to determine Young's modulus of stem cells.

1.3 Stem cells

Stem cells are the cells which divide into different cell types. These are basically of two types: embryonic stem cells (ESCs) and adult stem cells. Embryonic stem cells come from the 3 to 5 days old embryo only and these cells are pluripotent i.e. they can differentiate into more than one type of cell whereas adult stem cells have limited ability to divide into different cell types.

As we know that ESCs have the ability to divide into different cell types and the mechanical properties vary at different stages of differentiation. So, it is very important to understand the mechanical properties of stem cells as it affects cellular composition, cell-cell and cell surface interactions [45, 86].

AFM appears to be a very good tool in understanding the structural and mechanical properties of single cell [87]. Use of AFM for mechanics of stem cells provides useful insights in understanding the progress of certain disease such as cancer [88]. It also appears to be very good technique for measuring the viscoelasticity of cells [89]. Previously, it has been used to study the topographic and morphometric features of human mesenchymal stem cells (hMSCs) [90]. In another study, biomechanical properties of hMSC was determined using AFM and membrane tether length was determined using optical tweezers [91]. Also, fluorescence spectroscopy and AFM have been used to study the nanomechanobiology of hMSC [92]. It has also been used to study the mechanical properties of differentiated and undifferentiated mouse embryonic stem cells (mESCs) [45]. Andreas has studied mechanics of human bone marrow mesenchymal stem cells and they have compared the mechanical properties of cell nuclei at different stages [86].

In the present thesis, I have studied the mechanics of mESCs lacking clathrin mediated endocytosis (CME) using AFM.

1.4 Organization of the thesis

In chapter 2, the working principle of AFM, its applications are discussed. For my research work, Worm-like chain (WLC) model and hertz model are used for checking the effect of CLM drug on titin I27 protein and for checking the mechanical properties of stem cells, respectively.

In chapter 3, interaction of titin I27 with CLM was studied by using single molecule and bulk measurements. In order to check whether CLM is binding to titin I27 or not, first fluorescence spectroscopy is done. Fluorescence spectra shows that fluorescence intensity decreases with the addition of drug. This process is called fluorescence quenching. Mechanism of quenching is also studied. It shows that CLM binds to titin I27 resulting in the formation of complex between the two. The proximity of CLM to Tryptophan (Trp) was further confirmed with the help of molecular docking studies. Using PatchDock, we identified the residues involved in the interaction of I27 with CLM. We found that the distance between the CLM and Trp (Trp34) in the selected model is less than 5 Å. This explains the quenching of the Trp fluorescence which we observed in our previous results. When the drug molecule binds to protein, there can be change in the mechanical properties of the protein. So, the change in mechanical properties was studied by AFM. Force spectroscopy was done for I27- WT and I27 with varying concentrations of CLM. It has been found that unfolding force increases by 25 pN in the presence of 40 µM drug concentration with respect to I27-WT and persistence length (PL) decreases for I27 with 40 µM drug concentration. That means protein is getting mechanically stabilized when 40 µM drug is added to the protein. In order to check whether binding is happening at 40 µM drug concentration or the stability at 40 µM drug concentration, equilibrium denaturation experiments were performed. These experiments also shows the increase in free energy of stabilization for 40 µM drug concentration. The results showed a direct effect of the broad-spectrum antibiotic CLM on the passive elasticity of muscle protein titin. The I27 is stabilized both mechanically and chemically by CLM [93].

In chapter 4, mechanical properties of stem cells is determined by AFM. It has been found out that, mESCs lacking clathrin shows less cellular stiffness in comparison to differentiated cells. It has been shown previously that clathrin heavy chain (*Cltc*) is responsible for maintaining pluripotency of mESCs. However, mechanical properties such as cellular stiffness was not known in absence of *Cltc*. Here, young's modulus of mESCs in presence of *Cltc* has been calculated. It has been found out that mESCs lacking clathrin shows higher Young's modulus i.e. cells becomes stiffer in comparison to wild type cells. However, cellular stiffness of *Cltc* knockdown mESCs with actin

polymerization inhibitors is also calculated. These treated cells shows cellular stiffness similar to WT mESCs cells [94].

In chapter 5, all the experiments which did not work have been discussed. Purification of PTEN, T4 Lysozyme proteins was tried by changing different parameters. We were able to purify PTEN protein, but we got very less amount of protein even with large amount of culture. That amount was not sufficient for our measurements. In case of T4 Lysozyme, to make polymers from monomers, we needed pure protein but we were not able to get pure protein. That's why in both the cases, we could not proceed further.

In chapter 6, I have concluded my thesis work and the future possibilities of this work. We have studied the interaction of titin I27 with CLM using AFM and fluorescence spectroscopy. These results show that CLM is stabilizing the I27 protein mechanically and chemically. This work has provided insight that will guide development of future pharmacological applications of CLM. We have not checked the effect of temperature as well as denaturants on the stability of CLM stabilizing the protein using AFM. It is known for the I27 protein that stability decreases with increase in temperature [19]. We can also take into account of stability check for native as well as intermediate state. Also, the interaction of CLM with other Immunoglobulin (Ig) domains can be checked using AFM and fluorescence studies. We can check the mechanical properties of PTEN as well as T4 Lysozyme protein.

Chapter 2

Methods

2.1 Introduction

In this chapter, I will discuss the experimental and theoretical methods that have been used for my studies. For studying the interaction of titin I27 with chloramphenicol (CLM), experimental methods such as fluorescence, equilibrium denaturation and Atomic Force Microscope (AFM) are discussed whereas for theoretical methods Worm-like chain (WLC), and molecular modelling techniques are discussed while for studying the mechanical properties of mouse embryonic stem cells (mESCs), AFM as an experimental method and Hertz model as theoretical model are discussed.

2.2 Experimental methods

2.2.1 Atomic Force Microscope (AFM)

AFM is a scanning probe microscope that measures interactions between a sharp probe (cantilever tip) and the sample. Now a days, it offers a large number of biological applications over other techniques. AFM can be used for imaging and force spectroscopy. AFM imaging can be used to find the structure of biological samples and their heterogeneity. However, force spectroscopy can be used to find out the interaction forces between cantilever tip and the substrate used. It can be the protein-ligand interaction, protein-protein interaction and it can also be used to measure the adhesion forces for the biological samples [95].

There are many microscopic techniques such as scanning electron microscopy (SEM), transmission electron microscopy (TEM), scanning tunnelling microscopy (STM), optical microscopy and confocal laser scanning microscopy, however, AFM provides several advantages over other microscopies. Electron microscope provides 2D images whereas AFM provides visualization of 3D surface profile [96, 97]. Also, samples which are to be analyzed do not require any special sample preparation. AFM gives accurate surface height information with precision of angstrom (\AA) and three dimensional topographs while other microscopic techniques only give topographic contrast. Further, Electron microscope requires a high vacuum environment whereas AFM works in all types conditions such as Ultra High Vacuum, air and liquids. AFM provides better resolution than SEM. AFM can perform imaging with true atomic resolution in ultrahigh vacuum. High resolution AFM is comparable to resolution of STM and TEM. AFM is cost-effective method for imaging of nanoparticles. In practical terms, it requires much less space in comparison to SEM/TEM. It can be operated in air, vacuum, low temperatures, aqueous conditions. Another noteworthy advantage of AFM is that it does not require samples to be labelled with fluorescent dyes. Procedure for sample preparation is simple. Mechanical, electrical, magnetic characterization of images captured by AFM can be easily done [98].

However, the main disadvantage of AFM is the maximum surface area it can scan. The area which is to be scanned is maximum of 150×150 microns whereas SEM can acquire image of size of the order of millimeters. The STM also has the disadvantage that it is only used for conducting or semiconducting surfaces.

2.2.1.1 Principle of Operation

Atomic force microscopy is one of the high resolution scanning probe microscopes. It has a sharp tip of radius 10 to 20 nm, generally made up of Si or Si_3N_4 . It is used to measure the forces between the tip and sample. The cantilever is attached to a substrate which is fixed at one end. When the cantilever is far away from the surface, then the force between the tip and sample is attractive and if the distance between the two is less, then the force between the two is repulsive. Depending on the type of force between the two (attractive and repulsive), the cantilever will show deflection towards or away from the sample surface. The deflection of the cantilever is detected and converted

into an electrical signal. The detection system uses a laser beam that falls on the back of the cantilever, laser light gets reflected, falls on the photodetector and the signal is measured (see Fig. 2.1). When the cantilever deflects, the angle of the deflected laser beam changes and the laser spot will fall on the different parts of the photodetector. Photodiode usually consists of four quadrants. The vertical deflection can be calculated by comparing the signal from top and bottom halves whereas lateral deflection can be calculated by comparing the signal from left and right halves of the detector.

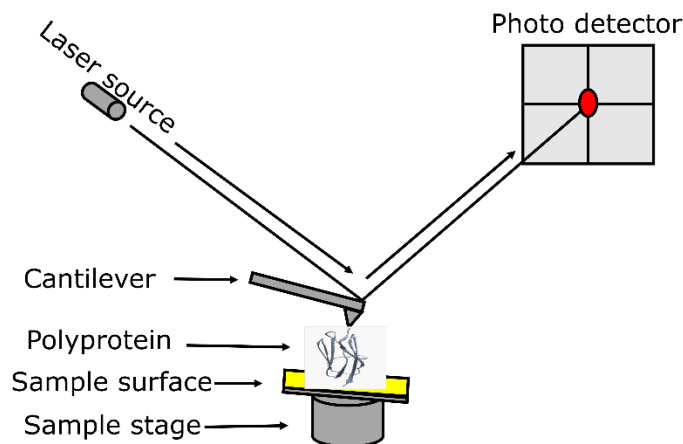


Fig. 2.1: Schematic of AFM where a laser beam is allowed to fall on the back of the cantilever. Laser beam reflects from the cantilever surface and falls on the photodetector. The photodetector gives the signal which is proportional to bending of the cantilever. A polyprotein is tethered between the sample surface and the cantilever tip.

AFM can be operated in two modes: static and dynamic mode.

In static mode, tip is always in contact with the sample. This is used for high resolution imaging and force spectroscopy. Here, setpoint is the deflection of the cantilever, so a lower value of setpoint gives the lower value of imaging force. Previously, AFM has been used to image

aquaporin, the water channel of *E. Coli* [99]. In another study, aquaporin crystals and surface topographs have been recorded [100]. Imaging of purple membranes was also done using AFM [101]. Molecular mechanisms of amyloid fibril formation and toxicity in Alzheimer's disease have been also studied by AFM [102].

In dynamic mode, cantilever is oscillated with a fixed frequency and tip is allowed to interact with the sample. Due to tip-sample interaction, tip amplitude and phase difference between the drive and tip changes. These changes can be recorded to further extract viscoelasticity. Stiffer cantilevers are used for intermittent contact mode generally stiffness more than 10 N/m. These cantilevers give stable imaging in air as these cantilevers are able to break the capillary forces. Soft cantilevers are used for doing tapping mode in liquid medium.

There are other tapping mode-based characterization such as kelvin probe and magnetic mode. For electrical characterizations kelvin force microscopy is used, basically a constant potential difference is measured between a conductive AFM probe and the sample, however, for magnetic characterization, a magnetic coated cantilever is used. Here, the oscillating probe scans the surface in order to get topographical features and then probe elevates off the surface by a small distance and the attraction/repulsion is recorded.

In the mechanical mapping mode, AFM measures Young's modulus values through the nano-indentation technique. After getting the force curves through nano-indentation, force curves are fitted with linear elastic models such as hertz model. In the multifrequency mode, AFM employs the detection of multiple cantilever frequencies which gives information about tip-sample non-linearity. Multiharmonic mode requires simultaneous mapping of young's modulus, the deformation and topography of the sample. Viscoelastic mapping is the other novel model that works as multifrequency and bimodal AFM. There cantilever is oscillated at two eigen mode frequencies-the first mode records surface features while second mode records frequency variations which is related to stiffness [103]. When AFM is combined with optical microscope it gives unique information from a single cell to a tissue level [104]. Combination of AFM with confocal microscope is used to measure the mechanical properties of soft heterogeneous three-dimensional samples [105]. Second harmonic generation (SHG) is also used in combination with AFM for the investigation of soft biological sample. SHG occurs usually when two photons of

frequency ω interacts with the non-linear medium and get converted to new photon with the frequency of 2ω . Since this is a non-linear process only non-centrosymmetric structures such as collagen are able to emit SHG signals. Stylianou et al. proposed use of AFM combined with SHG in order to understand non-linear optical properties of collagen and long term SHG is used as a non-destructive imaging modality to monitor collagen related diseases [106].

2.2.1.2 Sample preparation

Sample preparation can be different for different AFM measurements. A common requirement in all is the immobilization of the sample on substrate which can be achieved either by specific or non-specific interactions between sample and substrate.

For imaging generally muscovite mica is used as a substrate. Mica is negatively charged, positively charged particles can be easily adsorbed onto it. We can play with other things such as pH, ionic strength etc. If a protein is negatively charged, then it can be treated with divalent ions such as Mg^{2+} in order to have a good adsorption. Imaging can be done in air as well as in liquid solution. Before doing the measurement, mica is first cleaved by scotch tape, then sample is drop-cast on the mica surface and allowed to evaporate. However, one disadvantage of imaging the sample in air is that the sample gets squeezed i.e. we do not get the actual information about the sample. While doing imaging in liquid, we will have damping from the solution [107].

In typical single-molecule force spectroscopy measurements, protein is tethered between AFM tip and substrate. We can have events due to non-specific adsorption. A way to overcome this disadvantage is to make proteins with repeated domains. In such cases, repetitive force vs extension curves are obtained. For proteins that do not occur naturally, a protein of interest can be inserted into naturally occurring protein [108]. For force spectroscopy, freshly coated gold substrates can also be used for the measurement. If the substrates are not used immediately, then substrates get organic contamination i.e. hydrocarbons get deposited easily on the samples. Organic contamination can be removed by placing the substrates under UV irradiation.

2.2.1.3 Cantilevers

AFM cantilevers are usually made up of Silicon (Si) or silicon nitride (Si_3N_4). Cantilevers can be made with different materials to obtain high resolution [109]. Also, they can be modified for getting good quality data. Focused - ion beam (FIB) modification of cantilevers can be done to get good resolution [110–112]. For studying the electrical properties of sample, conductive cantilevers usually coated with gold, aluminium are used whereas for studying the magnetic field, magnetic materials are coated [113]. Cantilever stiffness determines force-sensitivity and the tip-radius determines the resolution of imaging. So, the choice of cantilevers may differ in various experiments. For soft samples, soft cantilevers having stiffness in the range of 10-30 mN/m should be used whereas for hard samples, cantilever with stiffness of 30-100 mN/m were used.

Choice of the indenter tip is another parameter which should be taken into account while doing the measurement. For soft biological samples, usually spherical tips are used. For inhomogeneous biological samples, large diameter tips ($\sim 20 \mu\text{m}$) are used, while for higher resolution, tips of smaller diameter ($\sim 10 \mu\text{m}$) are used. If we want to probe single cell, then sharp pyramidal tips can also be used. The problem with sharp tip is that it can penetrate into the sample and damage it [114].

2.2.1.4 Applications

AFM is used for imaging as well as force spectroscopy measurements [115].

1. Imaging

In biology, AFM has been widely used for imaging of biomolecules such as nucleic acids, supported membranes and proteins.

After the invention of AFM, DNA was the first biological sample used for studying the applications of AFM [107]. It has been used previously to measure the persistence length of DNA [116]. Also, imaging of single and double stranded DNA is done in propanol [117]. In a study, circular modules of DNA were imaged in air under various relative humidities using Scanning

force microscope (SFM). For doing this measurement, tips of radius of curvature 10 nm were used. Generally, SFM tips has the tendency to move DNA. This problem was overcome by Bustamante et al. where mica was treated with Mg^{2+} and circular modules of plasmid DNA was drop-cast onto it. However, they found wider width and lower height than expected. The wider width was attributed to the radius of the tip and lower height can be due to compression of DNA by the tip [118]. To overcome these problems, chemically modified mica surfaces were used [119, 120]. Further, imaging of DNA was also done in liquid environment where they have studied binding of unmodified DNA surface with modified mica substrate. With that, DNA was stable for 30 minutes and results were consistent. This success is attributed to the use of modified mica substrates [121].

AFM has been widely used for imaging of lipid monolayers and their interaction with enzymes. It provides direct microscopic information about their interaction. This also acts as novel technique for the investigation of enzyme kinetics and biological membranes. It looks at cytosol and extracellular space at a nanoscale level [122, 123].

Imaging of virus is also done using AFM. AFM has revealed the mechanism of formation of crystals in icosahedral plant virus, cucumber mosaic virus and structure of the herpes simplex virus. Its high resolution and its capability of in vivo imaging makes it more useful for study in virology and pathology [124].

AFM is a common tool to study the biophysical properties of proteins [125]. [Previously, it has been used for getting the structural information of individual bacteriorhodopsin at different pH in aqueous solution and it has been found that \$pH > 8\$ gives reproducible imaging \[101\].](#) In case of imaging, it is widely used for aggregation studies. Generally, muscovite mica is used as a substrate. But in some cases, proteins do not adsorb very well on mica. For that, highly ordered pyrolytic graphite (HOPG) is used as a substrate. For larger proteins, it is necessary to use substrate in the micrometer range having low roughness values. In such cases, template stripped gold substrates are used [126, 127].

Besides doing imaging, AFM has been widely used for force spectroscopy measurements.

2. Single-Molecule Force Spectroscopy (SMFS)

AFM is used to study folding-unfolding transitions, intermolecular interactions of proteins with ligands, drugs and other proteins.

Previously, binding of small drug molecules (cisplatin, ethylene bromide (EtBr) etc.) to DNA was studied and the results showed the behavior of native double stranded DNA (dsDNA) when force spectroscopy was done after the immediate addition of cisplatin to DNA and the measurements after 24 h showed the increase in force upto 73 pN [128]. AFM based method is also used for the detection of protein binding site on DNA molecule [129].

AFM is a very good tool for studying the dynamics of proteins. In a study, folding-unfolding dynamics of a GA protein was studied. For AFM measurements, a construct of (NuG2-GA)₄ was made where NuG2 serves as a fingerprint and acts as a caliper for the observed GA events. Two types of unfolding events-one at a contour length (ΔL_C) of ~18 nm and unfolding force of 60 pN while other at 20 pN were found. The events with ΔL_C of 18 nm shows the events for NUG2 whereas the other showing ΔL_C of 13.8 ± 0.5 nm corresponds to GA protein [130].

Unfolding pathways of bacteriorhodopsin has been studied. For that, protein molecules were first localized and extracted from the membrane. It has been found that the helices (G and F) and helices (E and D) unfolded pairwise whereas helices B and C unfolds one after the other [131].

In another study, mechanical stability of protein GB1 was checked with bi-his residues. Here, Ni²⁺ is used as a metal whereas Cu²⁺, Zn²⁺ or Co²⁺ can also be used. Ni²⁺-His and few mutations also showed enhancement in mechanical stability [132].

AFM can also be used for measuring isoelectric point (pI) of a protein. In a study, colloidal particle based method is used and adhesion forces were measured between AFM probe and substrate. pI is taken as that value where there is large gap in the adhesion forces. The advantage of using AFM technique for measuring pI is that very less amount of protein is needed for the measurement [133].

AFM experiments can explain the potential energy landscape. For that, force spectroscopy experiments should be performed at different pulling speeds. When an external force is applied on the molecule, the isolated bonds get ruptured and the energy landscape barrier gets lowered. Since force required to unfold the domains depends on the pulling speed, the energy landscape barrier diminishes in time. Measured forces are usually plotted on a scale of log (pulling rate).

Evans proposed that the unfolding force of a protein shows a linear dependence with the log of the loading rate [134]. The slope and intercept of linear fit to the force vs log (loading-rate) curve gives information of the position of the transition state along the reaction coordinate and the height of the energy barrier respectively. The reaction coordinate for AFM experiments is the protein's end-to-end distance. Eventually, these experiments can be analyzed to extract the energy landscape of protein unfolding with respect to the reaction coordinate [18, 135, 136].

This analysis is beyond the scope of the current thesis. However, it is important to notice that our all the experiments, Wild Type (WT) as well as I27 – CLM experiments were performed at a fixed speed (1500 nm/sec) to avoid the dependency of force on the loading rate. This assures that the rupture force of I27 increases due to the CLM binding instead of the variation in loading rate.

It is well known that interaction of proteins with ligands, drugs, dyes and other proteins is important to understand as they play important role in biotechnology. There are various methods which can be used to find out these interactions such as fluorescence, fluorescence resonance energy transfer (FRET) and refractive index. In a study, mechanical properties on binding of proteinG, NUG2 with IgG antibody is studied and the binding results shows there are very less conformational change upon binding but the unfolding force increased from 105 to 210 pN when proteinG binds to IgG. Also, AFM provides functional binding assay for protein-ligand systems. Protein-ligand binding is an equilibrium process and provides a way of directly calculating dissociation constant, K_D . However, protein-ligand unbinding is a non-equilibrium process and using AFM, K_D cannot be calculated directly. AFM provides a unique advantage for the protein-ligand systems for the quantitative analysis for measuring binding assays [70]. In a study, mechanical stability of Staphylococcal nuclease (SNase) and SNase inhibitor was determined. Unfolding force for SNase was found to be 26 pN while for SNase inhibitor unfolding force increased to 50 pN [137]. Also, the effect of E9 ligand on the mechanical stability of Im9 protein has been studied. Unfolding force increased by 10 pN with its complex [74].

Also, unfolding pathways of maltose binding protein (MBP) is studied. Binding of MBP to maltose or malotriose, results in an increase of unfolding force. However, unfolding of MBP happens via two parallel mechanical unfolding pathways resulting in the kinetic partitioning [71]. Mechanical stability of dihydrofolate reductase (DHFR) with different ligands such as methotrexate,

nicotinamide adenine dihydrogen phosphate (NADP) and dihydrofolate was also studied. DHFR unfolds at 27 pN without showing significant sawtooth pattern of unfolding. However, unfolding force increases to 82, 98 and 83 pN in the presence of different ligands such as methotrexate, NADP and dihydrofolate, respectively [73].

The titin is a well-studied protein for AFM measurements. It is a muscle protein and is made up of immunoglobulin (Ig) domains. It is a sarcomeric protein which is responsible for passive force elasticity. On stretching titin behaves as a molecular spring. In a study, mechanical properties of I27, I28 alone and I27-I28 is studied. It has been found out that I27 is thermodynamically more stable than I28, however, I28 is mechanically more stable than the I27. I27 unfolds at 200 pN whereas I28 unfolds at 260 pN i.e. at higher forces than the I27. This discrepancy occurs when mechanical unfolding is assumed to be kinetic process not an equilibrium process [138]. Effect of temperature on titin I27 at different temperatures and different speeds was also studied. It has been found out that the transition force and Gibbs free energy does not show any dependence on temperature at different pulling speeds. The unfolding force from transition force shows a consistent increase with different pulling speeds [19]. Mechanical and chemical unfolding of titin I27 was also studied in order to confirm whether both of them follow the same pathway. It has been found out that in these these techniques, proteins follow different unfolding pathways [17] and the rate constant obtained by chemical denaturation studies is five times faster. The effect of surrounding anions such as Cl^- , Br^- , I^- , ClO_4^- , SO_4^{2-} etc. on the mechanical stability of I27 was also studied. It has been found out that mechanical stability i.e. unfolding force decreases with increase in ionic radii [139]. Interaction of Titin I27 with calcium is also studied suggesting that binding can result into different mechanical properties of I27 protein. To check that, fluorescence and single molecule force spectroscopy was done. With increase in calcium concentration, fluorescence intensity decreases suggesting calcium is binding to I27 protein. When Ethylenediamine tetraacetic acid (EDTA) was added, a partial recovery of fluorescence intensity was obtained suggesting that EDTA was not able to unbind all the calciums bound to the protein. SMFS suggests an increase in the unfolding force of 40 pN for every peak and decrease in the persistence length [8].

Previously, investigation on mechanical protein fibronectin as well as membrane protein bacteriorhodopsin has been done. The studies have shown that small osmolytes enhance stability

of folded domains and reduce the PL of the unfolded chain [140–142]. It is argued that in presence of such small molecules, the protein chain tends to form coils and it reduces the PL [143]. The mechanical stability of the protein is enhanced in such situations due to an increase in chemical potential of denatured versus the folded state.

The interaction of CLM with titin I27 shows a similar result. For studying the interaction, SMFS and fluorescence measurements were done. Single-molecule measurements show that unfolding force is increased by 25 pN with 40 μM drug concentration, thereby stabilizing the protein. Further, stability is confirmed by equilibrium denaturation experiments. Denaturation experiments also show the stability at 40 μM drug concentration [93].

AFM has the capability to do measurement on living cells at single cell level. It can distinguish cancer cells from normal cells and also differentiated cells from stem cells [45, 144]. Morphological changes in cancer cells on treatment with anticancer agents have been also studied.

2.2.2 Fluorescence spectroscopy

When a molecule in the ground state absorbs energy, it gets excited to the excited singlet state and then it comes back to ground state with the emission of energy. This process is referred to as fluorescence (Fig. 2.2).

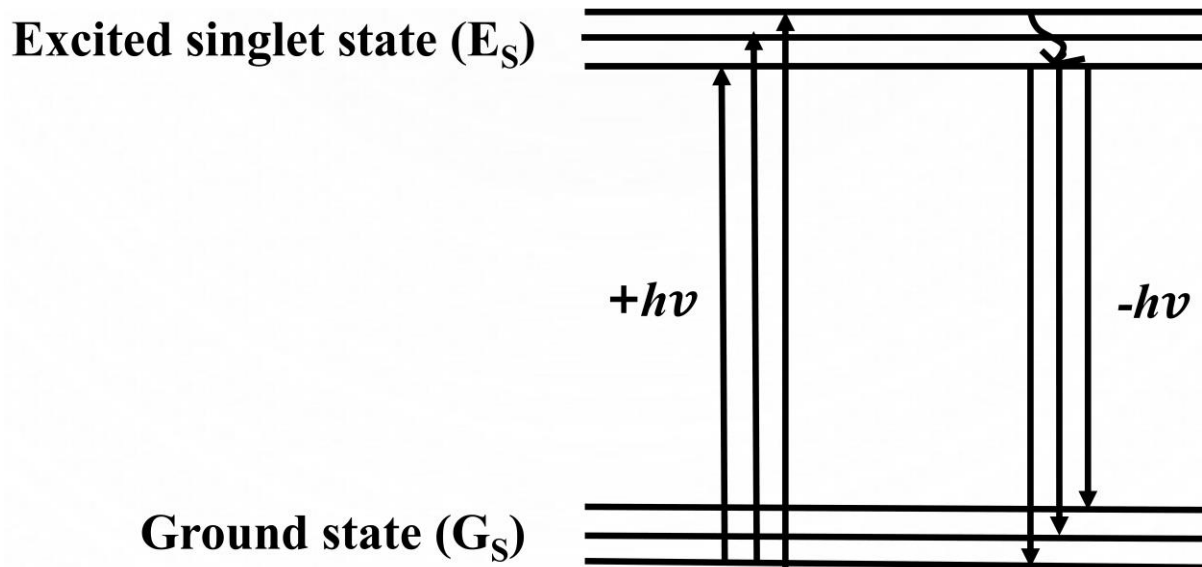


Fig. 2.2: Jablonski diagram showing the fluorescence emission spectrum.

2.2.2.1 Intrinsic Fluorescence in Proteins

Since proteins are made up of long chain of amino acids. There are 20 types of amino acids. Among these only 3 amino acids, Trp, Tyrosine (Tyr) and phenylalanine (Phe) acts as fluorophore. Generally, proteins are excited at 280 nm wavelength. Emission from Phe is almost negligible as it has low quantum yield and low absorption and emission wavelengths. The absorption at 280 nm is due to both Tyr and Trp, whereas absorption at 295-305 nm results in the excitation of Trp only [145].

The protein which we study in our laboratory extensively for mechanical stability experiments, I27 domain of titin contains one Trp and one Tyr. When a drug molecule binds to it, fluorescence intensity decreases with the addition of the drug. This decrease in fluorescence intensity is referred to as fluorescence quenching.

Fluorescence quenching has been widely used in investigating interactions between proteins and small drug molecules. The change of the microenvironment around a fluorophore changes the fluorescence intensity. Fluorescence quenching in a system is a result of energy transfer or complex-formation between the two molecules. The fluorescence quenching data is useful in

deciphering and quantifying the protein-drug binding. It is used in order to find the binding mechanism as well as the number of binding sites [75, 76, 79, 82, 146].

2.2.2.2 Mechanism of fluorescence quenching

The mechanism of quenching can be classified into two categories: static and dynamic quenching. Static quenching usually refers to the formation of a complex between the two molecules i.e. protein (fluorophore) and drug (quencher) molecule whereas dynamic quenching occurs when excited fluorophore interacts with other molecules and thereby results in non-radiative transition (Fig. 2.3) [147].

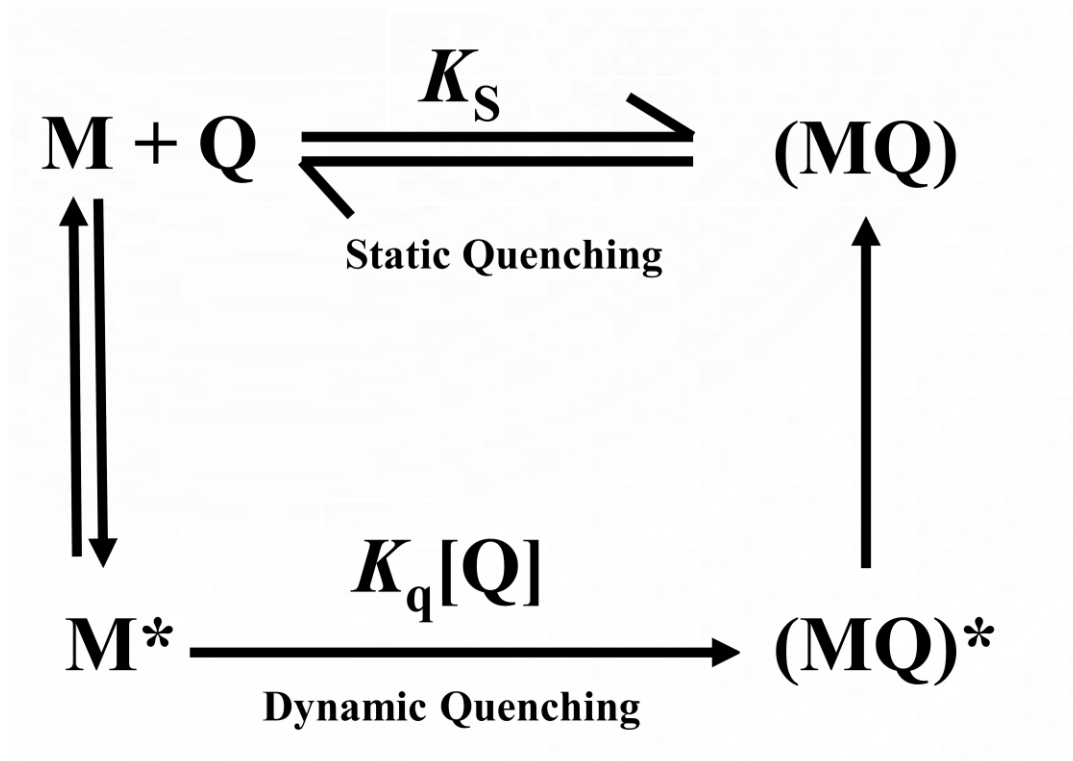


Fig. 2.3: Schematic showing static and dynamic quenching.

Generally, quenching data is analyzed using Stern-Volmer equation.

$$\frac{F_0}{F} = 1 + K_{SV}[Q] = 1 + k_q\tau_0 [Q] \quad (2.1)$$

Where F_0 and F are the fluorescence intensities in the absence and presence of quencher respectively. K_{SV} is the Stern-Volmer constant, $[Q]$ is the concentration of quencher, k_q is the quenching rate constant of biological molecule and τ_0 is the fluorescence lifetime of biological molecule.

Eq. 2.1 shows the linear plot of F_0/F vs $[Q]$. Sometimes there are two populations of fluorophores a) accessible and b) inaccessible to quenchers or buried. In such cases, non-linear curve is obtained and stern-volmer plot will show downward curvature. For that, modified stern-volmer equation is used [145, 148].

In the case of static quenching, fluorescence lifetime remains constant in the presence of quencher ($\tau_0/\tau=1$) while in case of collisional quenching, $\tau_0/\tau = F_0/F$.

The fluorescence lifetime of the biomolecule is 10^{-8} s [149], with a maximum dynamic quenching constant k_{max}^q for various quenchers known to be 2.0×10^{10} Lmol⁻¹s⁻¹ [150].

Also, quenching mechanism can be described using UV-absorption spectroscopy. Since dynamic quenching effects the excited state only, so no change in the absorption spectra is expected whereas in case of static quenching changes in the absorption spectra should be obtained [83, 151].

2.2.2.3 Equilibrium denaturation method

This method is used for checking the conformational stability of the protein i.e. by how much amount the native conformation is more stable than the denatured state.

It is used for comparing the conformational stability of the proteins which have slight difference in the amino acid sequence and folding mechanism can also be described using this method. If the denaturation curve has more than one step then that means it contains more than one domain.

For a two–state mechanism



Only native state (N) and the denatured state (D) are present.

The denaturation data obtained from the unfolding curve can be plotted in terms of denatured fraction (f_D), which can be written as

$$f_D = \frac{(Y - Y_N)}{(Y_D - Y_N)} \quad (2.3)$$

where Y is the observed parameter at a given urea concentration, Y_N and Y_D are the fluorescence intensity values obtained for the native and denatured states, respectively. These values can be obtained by extrapolations from the linear portions in the low and high denaturant concentration region.

The equilibrium denaturation data was analyzed using methods described previously [152, 153]. The equilibrium constant (K_D) between the native and denatured state can be calculated by

$$K_D = \frac{f_D}{(1 - f_D)} \quad (2.4)$$

The K_D values obtained can be used for calculation of free energy change, ΔG_D .

$$\Delta G_D = -RT \ln K_D \quad (2.5)$$

The free energy of stabilization i.e. $\Delta G_D(H_2O)$, can be calculated by

$$\Delta G_D = \Delta G_D(H_2O) + m(GdHCl) \quad (2.6)$$

where m is the slope of the line.

The free energy of stabilization can be calculated from the intercept of the line.

2.3 Theoretical methods

2.3.1 Worm-Like Chain (WLC) model

WLC model is used to describe the behavior of semi-flexible polymers and their intrinsic elasticity allow them to remain rigid even at smaller length scales. It is used to describe the elastic properties of single stranded DNA, double stranded DNA, ribonucleic acid etc. Discrete version of the WLC model was given by Kratky and Porod whereas continuous WLC model was given by Saito, Takahashi and Yunoki [154, 155].

Discrete WLC model assumes length and angle of bond length to be fixed. Continuous WLC model assumes total contour length of the polymer to be fixed and angle correlation between the polymer segments is determined by persistence length.

PL quantifies the bending stiffness of polymer. For pieces of polymer shorter than the PL, polymer behaves like a rigid rod whereas larger segments can be described on the basis of random walk model.

$$F(x) = \frac{k_B T}{P} \left[\frac{1}{4\left(1 - \frac{x}{L_C}\right)^2} - \frac{1}{4} + \frac{x}{L_C} \right] \quad (2.7)$$

where F is force, x is vertical tip position, k_B is Boltzmann constant, T is absolute temperature, P is PL and L_C is contour length of the polymer.

Fig. 2.4 shows the schematic to explain the parameters used for WLC model.

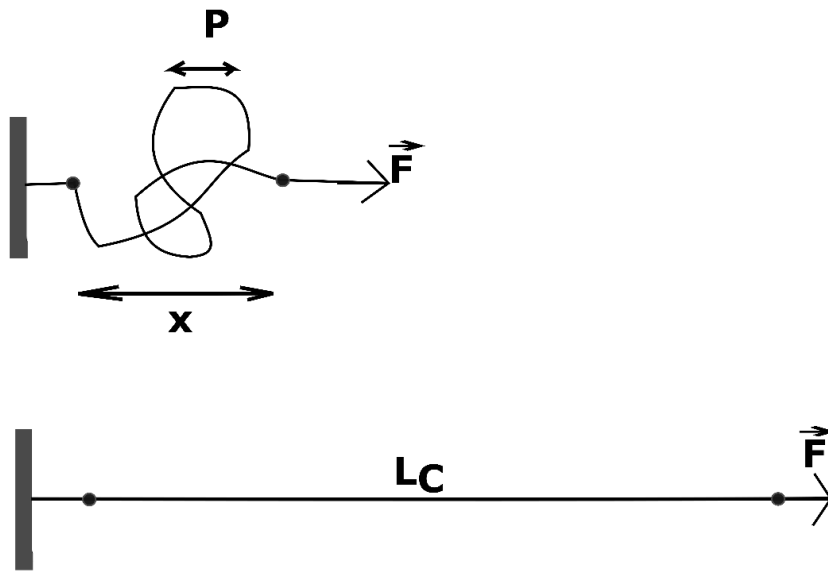


Fig. 2.4: Worm-like chain model is used to describe the entropic elasticity of polymer which basically describes the relationship between force (F) and extension (x) of protein using contour length (L_C) and persistence length (P), respectively.

The PL, which characterizes the entropic elasticity of the unfolded chain and contour length, which is the measure of maximum physical possible extension of the chain were used as fit parameters.

In another work of my research, mechanical properties of stem cells was studied. It has been found out that, mESCs lacking clathrin shows less cellular stiffness in comparison to differentiated cells. In order to study that, hertz model is used. A brief discussion about hertz model is described in detail here.

2.3.2 Hertz model

Hertz model is used to quantify the elastic contacts of biomolecules.

It assumes the sample to be isotropic, homogeneous and linear elastic. The indenter should not be deformable and there should not be any interaction between the indenter and the sample. If all these conditions are met, then Young's modulus can be extracted by fitting Hertz model to the force-indentation curve.

Material properties are determined by the poisson's ratio. For soft samples, poisson's ratio is 0.5. Indenter tip can have various geometries such as spherical, pyramidal etc. The geometry of the indenter tip decides which equation should be used.

The AFM cantilever and the cell can be modelled as two linear springs in series and as a result of which the force experienced by the cell can be represented as

$$F = kd \quad (2.8)$$

where k is the spring constant of the cantilever and d is the deflection of the cantilever.

A certain amount of known force is applied on the cell and the cell indentation value is recorded.

$$\delta = (z_1 - z_0) - (d_1 - d_0) \quad (2.9)$$

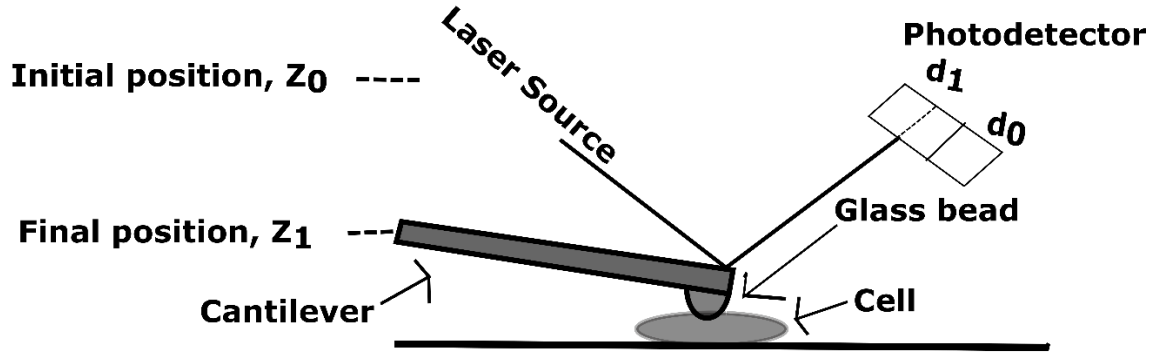
Where d_0 and z_0 represents the initial cantilever deflection and cantilever movement, d_1 and z_1 represents the final cantilever deflection and cantilever movement, respectively.

By substituting the actual cantilever deflection into the force formula, we get

$$F = k (d_1 - d_0) \quad (2.10)$$

The cell indentation and force can be used to determine the mechanical behavior of cell [156].

Fig. 2.5 shows the shows the schematic to explain the parameters of Hertz model.



Sample indentation

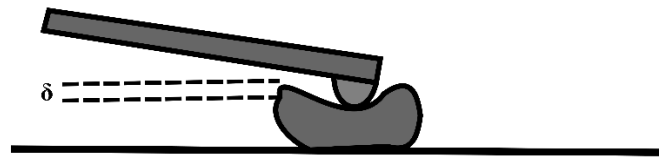


Fig. 2.5: AFM schematic showing the interaction of glass bead with the cell where d_0 and z_0 shows the initial cantilever deflection and the movement, and d_1 and z_1 shows the final cantilever deflection and the movement.

For spherical indenter tip:

$$F = \frac{E}{(1 - \nu^2)} \left[\frac{a^2 + R^2}{2} \ln \frac{R + a}{R - a} - aR \right] \quad (2.11)$$

$$\delta = \frac{a}{2} \ln \frac{(R+a)}{(R-a)} \quad (2.12)$$

Where F is measured by the cantilever possessing the bead, which is pressed against the cell, R is the bead radius, δ is the deformation in the cell, E is young's modulus, and ν is the poisson's ratio.

Hertz model is valid for small indentations i.e. upto 5-10 % of the height of the sample.

For calculating the Young's modulus, all the operations have to be applied on the extend curve. First, offset or tilt is removed, then baseline subtraction, contact point operations are to be performed and then hertz model is fitted on the extend curve [114].

2.3.3 Molecular modelling

Molecular docking is a computational modelling used to predict the preferred binding mode of a ligand to a protein, both of them basically bind to form a stable complex. It is used to check the orientation of a molecule and the binding conformation of ligands to the appropriate binding site. The main goal is to understand molecular recognition, binding free energy, binding affinity, binding constant of complexes and strength of association [157].

Docking is usually performed between a macromolecule and small molecule i.e. we can take the case of protein-drug interaction, protein-ligand interaction or protein-protein interaction. It has a wide variety of applications in drug discovery systems [158].

Molecular docking can be categorized into three ways as induced fit docking, lock and key binding and ensemble docking [159]. Induced fit docking considers both the ligand and receptor to be flexible. Ligand binds flexibly at the active site of the receptor in order to maximize the bonding forces between them while in case of lock and key binding, both the ligand and receptor are considered to be rigid and it shows tight binding. Ensemble docking explains flexibility and complexity of conformational states of protein [160]. Various servers are also available for molecular docking such as PatchDock, Swiss Dock, UCSF-Dock etc [161].

We have used PatchDock for studying the interaction of titin I27 with CLM.

PatchDock

PatchDock is a freely available software for prediction of protein-protein and protein small molecule complexes. This method was verified on antigen-antibody and enzyme-inhibitor complexes [162].

A very simple and intuitive web interface for PatchDock is available at <http://bioinfo3d.cs.tau.ac.il/PatchDock/>.

For input, we need two molecules either uploaded to the server or retrieved from protein data bank. We can directly enter the Protein Data Bank (PDB) IDs to the server also. There are basically four optional fields:

1) Clustering Root Mean Square Deviation (RMSD)

This specifies the radius of RMSD clustering in Å that means the output molecules should be atleast separated by that distance.

2) Complex type

For protein-small ligand molecule complexes, this algorithm uses a parameter optimized for small size molecules. If this parameter is not set, then it will take default configuration.

3) Potential binding sites for ligand and receptor

This information is supplied as an uploaded file that lists the residues of the potential binding site or sites.

We need to submit the email ID also. Once the docking is done, we get notification on email.

We usually get top 20 solutions. We get geometric score, desolvation energy, interface area size, actual transformation of molecules [163].

For our work, PDB of protein (1TIT) and CLM (separated from PDB - 4CLA) was given.

Chapter 3

Interaction of Chloramphenicol with titin I27 using single-molecule force spectroscopy

3.1 Introduction

In this chapter, interaction of Chloramphenicol (CLM) with titin I27 probed using single-molecule force spectroscopy is described. For studying this interaction, various experimental and theoretical methods are used. Experimental methods includes fluorescence, equilibrium denaturation and Atomic Force Microscope (AFM) whereas for theoretical methods Worm-Like Chain (WLC), and molecular modelling techniques are used. All the methods have been discussed in chapter 2 in detail. I will discuss the results obtained from these methods in detail. Our results show that CLM binds to I27 resulting in the formation of complex between the two. PatchDock results shows that Trp comes in the vicinity of I27 and fluorescence quenching occurs as a result of binding between the two. AFM result shows that CLM mechanically stabilizes the protein at 40 μM concentration. In order to confirm this stability, equilibrium denaturation experiments were performed. Denaturation experiments also confirms the stability at 40 μM CLM concentration. Therefore, CLM stabilizes the I27 protein mechanically and chemically.

The binding of small molecules such as drugs and dyes to biological macromolecules is active area of investigation [7]. It is important to understand the efficacy as well as side-effects of some broad spectrum drugs such as CLM and aureomycin [164, 165]. This investigation of protein-drug

interaction is important for pharmacology and pharmacokinetics [166]. Each drug has a therapeutic window for treatment of various diseases. For instance, it has been shown that the inhibitory concentration of CLM for various organisms is 4-12.5 mg/L (12-38 μ M). The peak serum concentration for CLM is in the range of 15-25 mg/L (46-77 μ M) and the trough concentration is found to be around 5-10 mg/L (15-30 μ M) [167]. The toxicity is reported to increase when concentration rises above 25 mg/L [168]. This demands a proper understanding of drug-protein interaction at various concentrations and how concentration of drug molecules affects the functioning of a protein.

Protein-drug interaction can be studied by direct or non-separation methods such as ultraviolet-visible absorption spectroscopy and fluorescence spectroscopy and indirect techniques or separation methods such as gel filtration, ultracentrifugation and equilibrium dialysis [67, 69, 169]. It is also extensively investigated using fluorescence quenching [75, 77, 82, 170]. Recently, there are reports of the effect of a drug on the mechanical properties of single molecules of proteins [142]. Single molecule techniques wherein a force is applied on single molecule to produce mechanical unfolding can be used to investigate the drug-protein interaction at the level of single molecules [70]. In this work, we report the effects of CLM drug on elasticity of I27, one of the Ig domains of muscle protein titin using AFM.

Titin is a giant muscle protein and contains two types of domains. One of them is Fibronectin type III (Fn(III)) and the other domains are Immunoglobulin (Ig) [171]. Further, these domains are arranged in an array of N-terminal I-band consisting of Ig domains and C-terminal A-band that consists of alternating fibronectin and Ig domains. Titin is also known as connectin and acts as a molecular spring which is responsible for passive force (elasticity) in muscle sarcomere and stability of myosin filaments [6]. The mechanical response of the single octamer of I27, one of the Ig domains from the I-band is measured using AFM [18, 172]. The interaction of titin I27 with calcium and its effect on the mechanical properties were investigated using fluorescence and AFM [8].

CLM is a broad spectrum antibiotic which is used for treatment of bacterial infections and it is also a muscle relaxant. It is known to have a direct impact on muscles which is concentration-dependent

[173]. The myocardial effects of CLM on rat heart muscle have been investigated and are reported to cause depressed isometric contraction to some extent [174].

The effect of certain antibiotics such as CLM, kanamycin and streptomycin was investigated on rat heart muscles and were shown to have a direct negative inotropic effect on isolated rat heart muscles [175].

The chick embryos were found to have a significantly reduced heart-rate at large concentrations (250 $\mu\text{g}/\text{mL}$) of CLM [176]. This has led to reports on interaction of CLM with many proteins such as Human Serum Albumin (HSA) [78, 79] and Lysozyme [83]. However, there is no understanding if CLM binds to titin, and its effect on elasticity of titin which is a major part of the muscle sarcomere.

In this work, we first investigated protein-drug interaction in the bulk using fluorescence quenching. We found that fluorescence intensity decreases with an increase in the concentration of the drug providing evidence of CLM binding to I27. Further, using single-molecule force spectroscopy we unraveled the effect of drug on mechanical stability of I27 polyprotein at various concentrations. We found that the unfolding force increases when CLM binds. It is maximum at a concentration of 40 μM . The increase in unfolding force at this concentration is ~ 25 pN. The entropic stiffness of the unfolded chain is also increased due to this binding. The mechanical stability seen at 40 μM , is also seen in equilibrium chemical denaturation experiments which were performed with monomers of I27.

3.2 Methods

3.2.1 Protein

Titin is a giant protein and is encoded by TTN gene. It is the third most abundant protein in muscle. We have used titin I27 (PDB -1TIT) for measurements. It is made up of 89 amino acids and has molecular weight of 10.9 kDa. It consists of one Trp and one Tyr. It consists of seven β -strands. Fig. 3.1 shows the crystal structure of titin I27 (PDB - 1TIT).



Fig. 3.1: Crystal structure of titin I27 (PDB - 1TIT).

3.2.2 Protein expression and purification of I27 monomer (I27)₁ and I27 octamer (I27)₈

Plasmid pET-23a containing the human I27 gene with an ampicillin resistance marker was transformed into *Escherichia coli* BL21(DE3) chemical competent cells. One isolated colony was selected and grown in LB medium at 37 °C until OD600 reached 0.6. Once OD600 reached 0.6, then the culture was induced with 1 mM isopropyl β-D-1-thiogalactopyranoside (IPTG) and incubated at 37 °C, 180 rpm for 6 hr. The cells thus obtained were lysed with lysis buffer containing 50 mM Tris-HCl pH 8.0, 300 mM NaCl, 20 mM imidazole, 0.1 mM phenylmethylsulfonyl fluoride (PMSF), and 0.25% β-Mercaptoethanol using ultrasonication. The clarified lysate obtained after cell lysis was loaded on a pre-equilibrated 5 mL HiPrep Ni-NTA affinity column (GE Healthcare).

The composition of equilibration buffer was 50 mM Tris-HCl pH 8.0 and 300 mM NaCl. Finally, the protein was eluted with an equilibration buffer containing 250 mM imidazole. Fractions containing desired proteins were checked on 15% sodium dodecyl sulfate polyacrylamide gel electrophoresis (SDS-PAGE) and pooled together. Imidazole was removed by buffer exchange (10 mM PBS pH 7.4) using amicon tubes (Merck, MWCO: 10 kDa). Protein was flash frozen in liquid nitrogen with 10% glycerol and stored at -80°C for further use. The concentration of protein was checked on nanodrop each time before the experiment. The yield of I27 monomer was found to be 0.9 mg/mL. The I27 octamer was also purified using a similar procedure. The yield of I27 monomer was found to be 3 mg/mL.

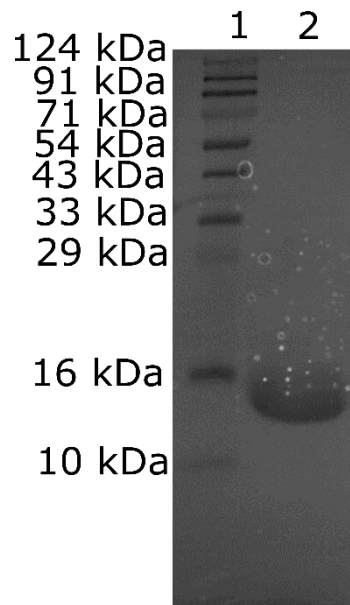


Fig. 3.2: 15% SDS-PAGE gel image of titin I27 monomer. Lane 1 shows marker and Lane 2 shows monomer of I27.

Fig. 3.2 shows the SDS-PAGE gel image of I27 monomer. Since we got pure protein for I27 monomer, so we directly used this protein for fluorescence and equilibrium denaturation experiments. Before doing the experiment, each time the protein was dialyzed in 10 mM PBS buffer pH 7.4 for 10-12 h. Fig. 3.3 shows SDS-PAGE gel image for octamer of I27.

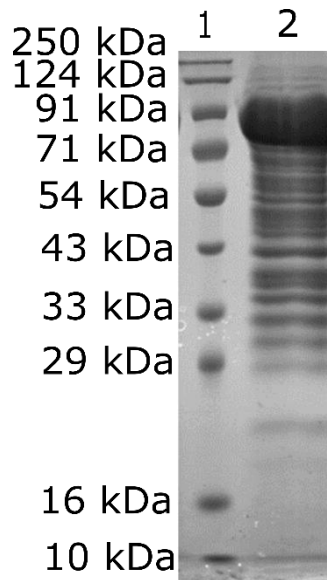


Fig. 3.3: SDS-PAGE gel for titin I27 octamer. Lane 1 shows the marker and Lane 2 shows the octamer of I27.

(I27)₈ was used for AFM experiments. So, we did not need too much pure sample. We proceeded with this sample only for AFM experiments.

3.3 Fluorescence spectroscopy

3.3.1 Sample preparation

1 mM stock solution of CLM was prepared in 10 mM PBS pH 7.4. I27 monomer was dialyzed in 10 mM PBS pH 7.4 for 10-12 h and the concentration of protein was measured on nanodrop. A stock solution of I27 monomer of concentration 200 μ M was made. Samples of different concentrations of CLM (0, 10, 20, 30, 40, 50, 75 and 100 μ M) with a constant protein concentration of 40 μ M were made in 10 mM PBS pH 7.4 and the total volume of each solution was made upto 100 μ L with 10 mM PBS buffer pH 7.4 only. Fluorescence measurement was done in 96 well plate at room temperature with excitation wavelength, λ_{ex} : 295 nm and emission scan range between

315-600 nm. All the fluorescence measurements were done on Perkin Elmer Enspire multimode reader (IISER Pune).

3.4 Docking studies

The available crystal structure of I27 (PDB : 1TIT) was docked with CLM using the PatchDock server [163]. Out of the ten models provided by the server, we chose the best fit model considering the docking score. Chimera was used for graphical analysis and figure generation.

3.5 Atomic force spectroscopy

In the past, AFM has been used to study the mechanical properties of single biomolecules such as proteins, unstructured polymers, etc. In typical AFM experiments on the proteins, a polyprotein (multidomain) is attached between a microcantilever tip and substrate (Fig. 3.4).

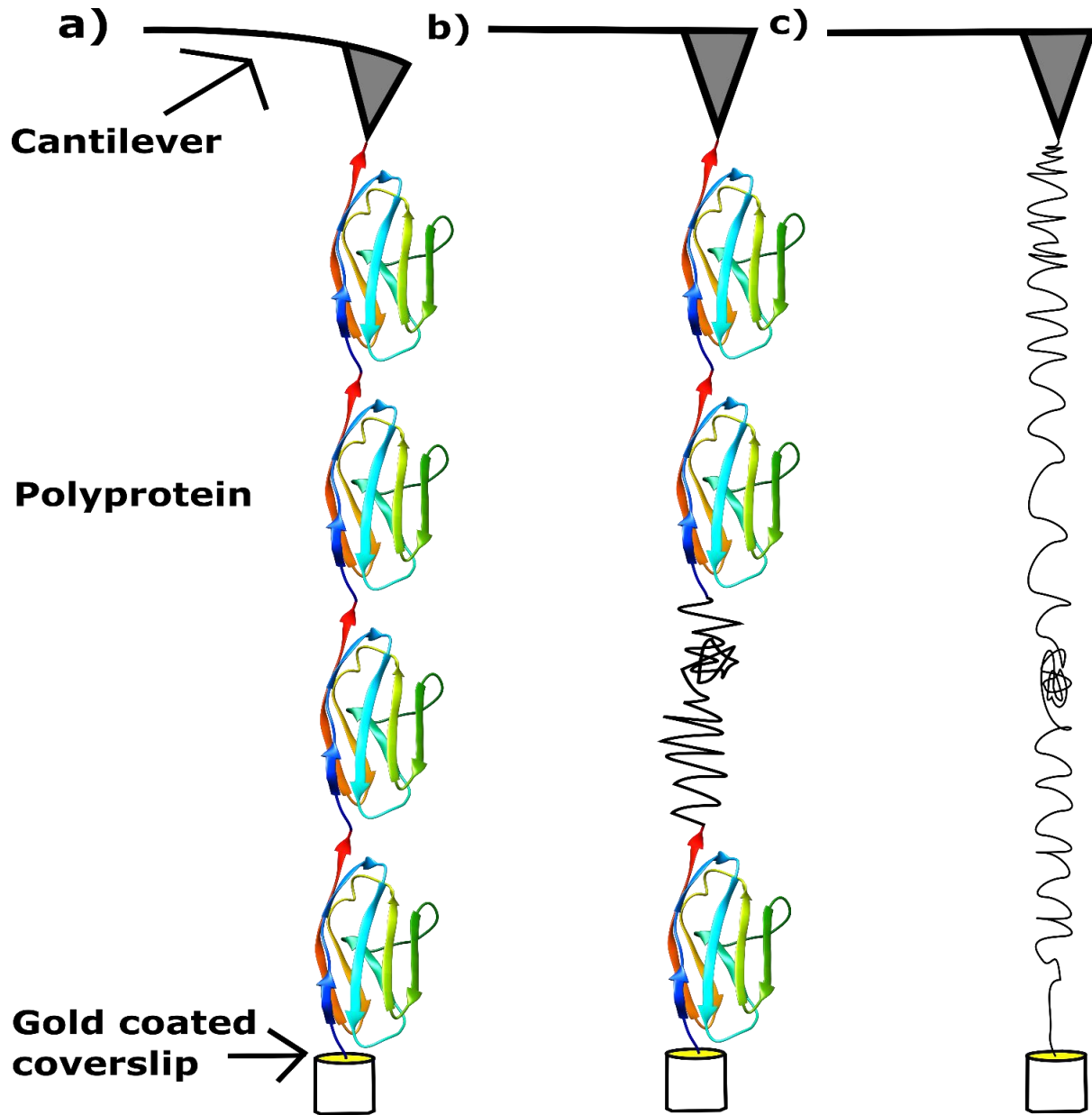


Fig. 3.4: a) Schematic of I27 octamer tethered between AFM cantilever and gold coated coverslip, b) One of the domains gets unfolded when the applied force reaches a critical value resulting in relaxation of cantilever to its equilibrium position, c) Unfolding of last domain. Further pulling will result in the stretch of the unfolded domain followed by the tip-molecule detachment.

When the relative distance of cantilever-substrate is changed with a constant speed along the perpendicular direction to the substrate, domains sequentially unfolds. Each peak in the pattern

represents the force required to unfold a domain which can be associated with the mechanical stability of the domain along the direction of pulling (Fig. 3.5).

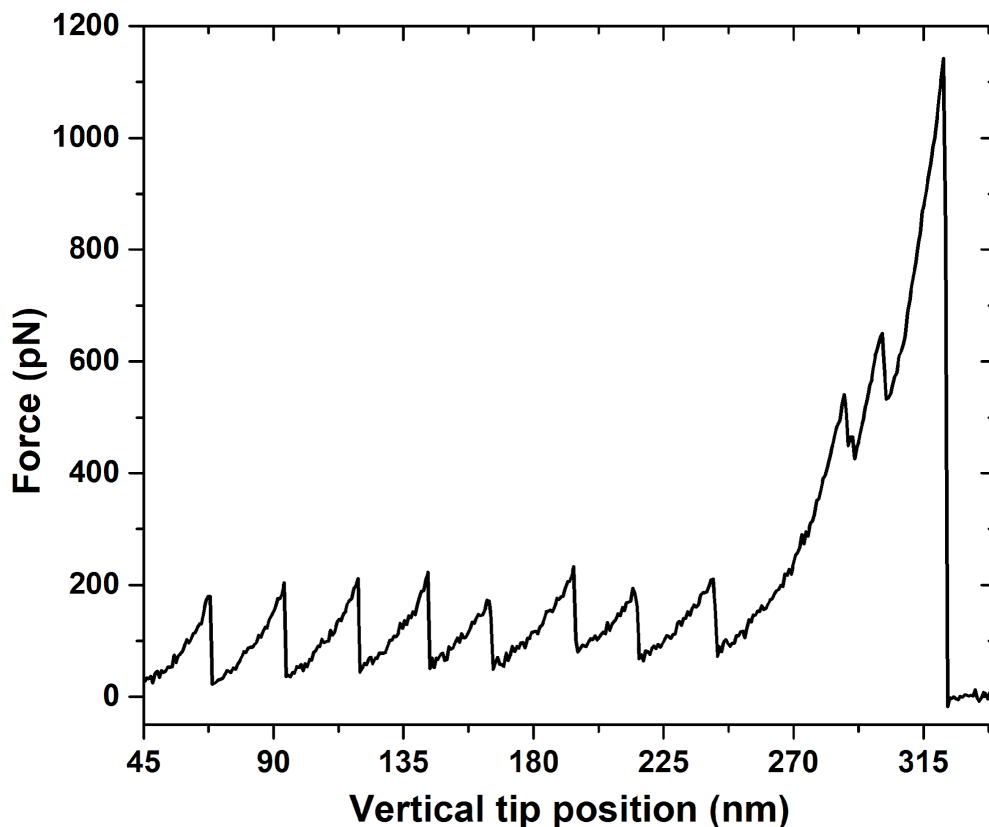


Fig. 3.5: Force extension curve of (I27)₈ at room temperature at 1500 nm/sec. The characteristic sawtooth pattern showing 7 unfolding events.

In the present chapter, we have investigated the mechanical stability of I27 polyprotein with 8 identical repeats in presence of CLM.

3.5.1 Calibration of the cantilever

Some amount of milli-Q (500-600 μL) was taken in a liquid cell, cantilever is brought down through nanopositioner. When cantilever gets dipped into the liquid and we have done the calibration in air, the sum signal gets zero, then mirror is rotated in order to have maximum sum signal.

When cantilever touches the glass coverslip surface, then force curve is taken. From there, we get the sensitivity and when we retract the cantilever by some distance and oscillate it, we get the spring constant of the cantilever. This method is known as thermal noise method. [The method is based on the equipartition theorem which states that the energy stored in the spring is equal to the thermal energy](#)

$$\frac{1}{2} k \langle x^2 \rangle = \frac{1}{2} k_B T$$

where k is the spring constant, $\langle x^2 \rangle$ is the mean square displacement of the cantilever deflection, k_B is the Boltzmann constant and T is the temperature.

The amplitude measured by thermal noise depends on the temperature, the spring constant of the cantilever and the method by which cantilever deflection is detected [177, 178].

The experiments were performed in a commercial AFM (JPK Nanowizard-II, Berlin, Germany). Rectangular silicon-nitride cantilevers from micromasch (Micromasch, Bulgaria) with stiffness 0.05 N/m were used for I27 measurements.

3.5.2 Sample preparation

For protein-drug sample preparation, an appropriate amount of drug was added to the protein sample. The sample was mixed properly and then incubated on a freshly gold-coated coverslip for 30 minutes. While for (I27)₈ without drug, only I27 protein (2-5 μM , 40 μL) was incubated on a gold-coated coverslip for 30 min. After incubation, the sample was washed with 10 mM PBS pH 7.4 to remove unbound protein. After 2-3 washing, 600 μL of PBS pH 7.4 was taken in a liquid cell and force spectroscopy was done.

3.5.3 Analysis

Sawtooth pattern with minimum of 5 events and the force curves in which the last event show high force in comparison to the forgoing ones are only used for the analysis. First and last event should be neglected for analysis because first one can show the non-specific binding and the last one shows the detachment from the sample.

3.6 Equilibrium denaturation of (I27)₁

3.6.1 Sample preparation

A stock solution of 8 M Guanidinium chloride (GdmCl) with 10 mM PBS buffer pH 7.4 was prepared in milli-Q. The solution was filtered and kept at room temperature for further use. 1 mM stock solution of CLM was prepared in 10 mM PBS buffer pH 7.4. 200 μ M stock solution of protein (I27 monomer) was made and kept in ice. Three different sets of experiments with varying concentrations of CLM were performed. In one set of experiment, the concentration of protein (40 μ M) and CLM (30 μ M) were kept constant while the concentration of Guanidinium hydrochloride (GdmCl) was varied. All the samples with varying GdmCl concentrations were gently mixed and incubated overnight at 28 °C in a water bath. The total volume of each solution was made upto 100 μ L with 10 mM PBS buffer pH 7.4 only. The same protocol was followed for the rest two different concentrations of CLM, 40 and 50 μ M. The samples were pipetted and kept in 96 well plate at 28 °C for fluorescence measurement with excitation wavelength, λ_{ex} at 295 nm and emission scan range between 315-600 nm. All the fluorescence measurements were performed on Perkin Elmer Enspire multimode reader (IISER Pune).

3.7 Results

3.7.1 Fluorescence

Effect of CLM on tryptophan fluorescence quenching

Fluorescence quenching has been widely used in investigating interactions between proteins and small drug molecules. The change of the microenvironment around a fluorophore changes the fluorescence intensity. Fluorescence quenching in a system is a result of energy transfer or complex-formation between the two molecules. The fluorescence quenching data is useful in deciphering and quantifying the protein-drug binding.

Here, we checked the binding of CLM by monitoring the tryptophan (Trp) fluorescence (λ_{ex} : 295 nm; λ_{em} : 330 nm) in I27 protein. Titin I27 has one Trp and one tyrosine (Tyr). When excited at 280 nm, we will have contribution from both Trp and Tyr, whereas when excited at 295 nm, Trp gets excited selectively. Fluorescence in Trp is due to the presence of indole chromophore. Since the measurements are done at pH 7.4, so the fluorescence quenching can be due to the proton exchange at C2, C4 or C7 position. As a result of which proton donor should contact the C2, C4 or C7 position of the indole ring [179]. Chloramphenicol has 3 hydrogen bond donors [180]. That's why, we observed that with an increase in CLM concentration, the intensity of fluorescence emission of (I27)₁ decreased without a shift in the emission maxima (330 nm). These quenching experiments suggest that CLM interacts with I27 and its binding site is close to Trp (Fig. 3.6).

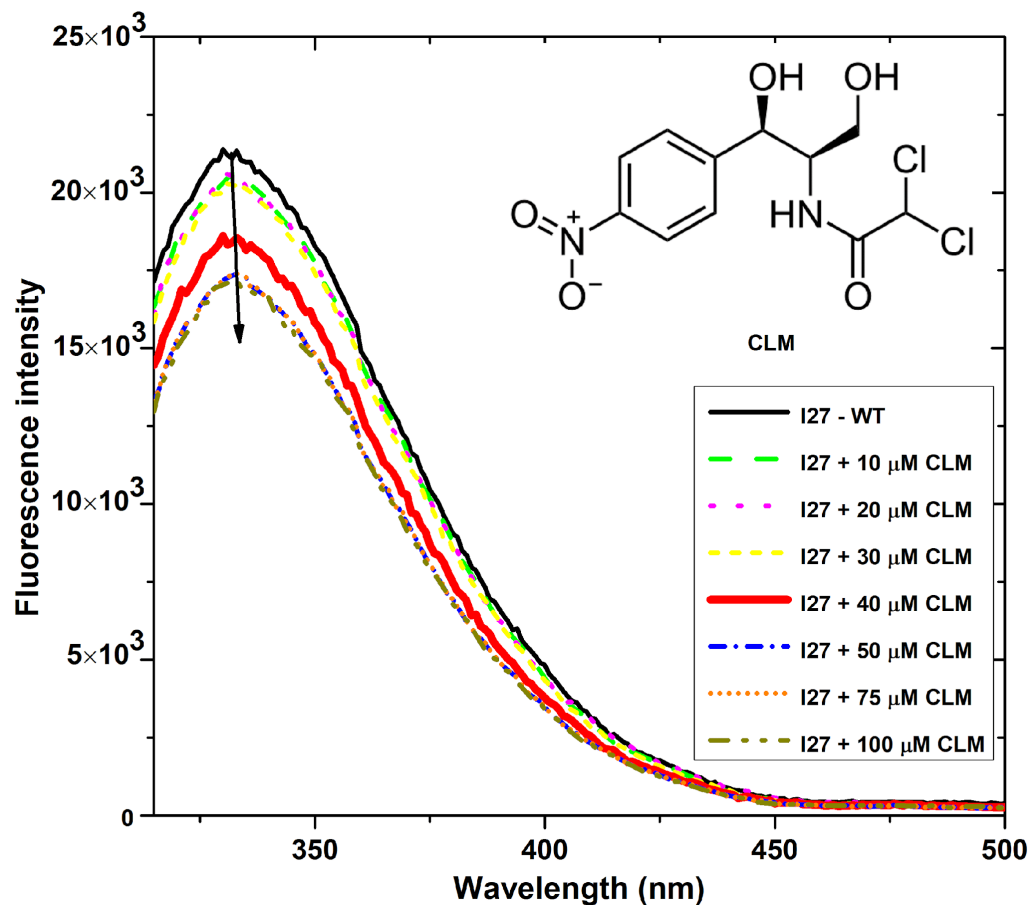


Fig. 3.6: The Trp fluorescence emission spectra of I27 excited with 295 nm wavelength after the addition of CLM to the solution. The arrow indicates increasing concentrations of CLM (0, 10, 20, 30, 40, 50, 75 and $100 \times 10^{-6} \text{ molL}^{-1}$). We observed that the fluorescence is quenched with the addition of CLM to the solution. 10 mM PBS (pH 7.4) buffer is used for the protein as well as for CLM solution.

The proximity of CLM to Trp was further confirmed by molecular docking studies. Using PatchDock, we identified the residues involved in the interaction of I27 with CLM. We found that the distance between the CLM and Trp34 in the selected model is less than 5 \AA (Fig. 3.7). This explains the quenching of the Trp fluorescence which we observed in our previous results.

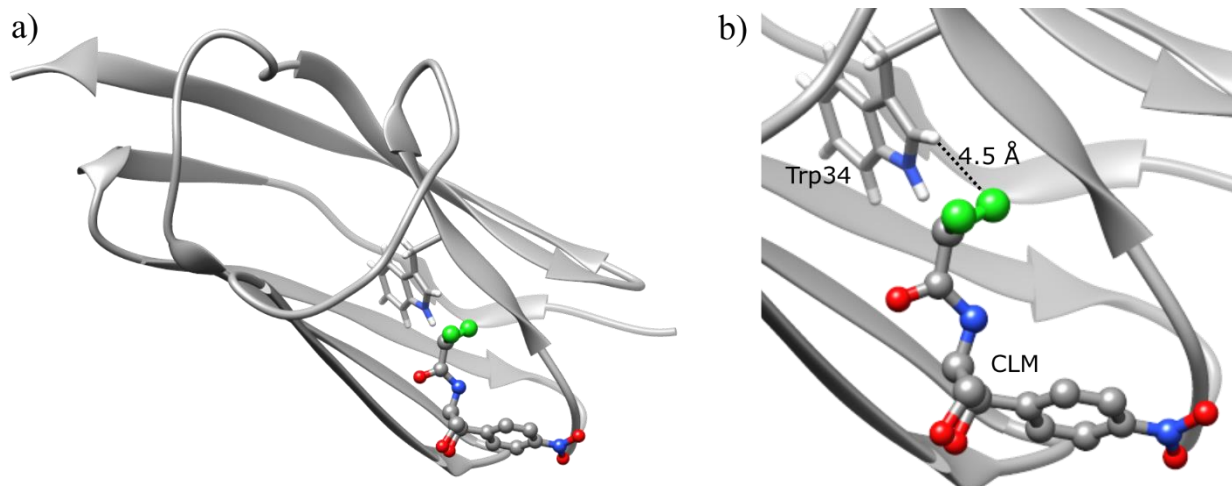


Fig. 3.7: Docking studies to check the proximity of CLM to Trp34 of titin I27 protein. a) I27 (PDB : 1TIT) docked with CLM using PatchDock, b) Interaction of CLM with Trp34 within 5 Å. It suggests that the fluorescence quenching is due to attachment of CLM to the protein in vicinity of Trp.

Mechanism of fluorescence quenching

Generally, quenching data is analyzed using Stern-Volmer equation.

$$\frac{F_0}{F} = 1 + K_{SV}[Q] = 1 + k_q\tau_0 \quad (3.1)$$

Where F_0 and F are the fluorescence intensities in the absence and presence of quencher respectively. K_{SV} is the Stern-Volmer constant, $[Q]$ is the concentration of quencher, k_q is the quenching rate constant of biological molecule and τ_0 is the fluorescence lifetime of biological molecule.

Fig. 3.8 shows the Stern-Volmer plot for the quenching of I27 fluorescence due to binding of CLM. The fluorescence lifetime of the biomolecule is 10^{-8} s [149], with a maximum dynamic quenching

constant k_{max}^q for various quenchers known to be $2.0 \times 10^{10} \text{ Lmol}^{-1}\text{s}^{-1}$ [150].

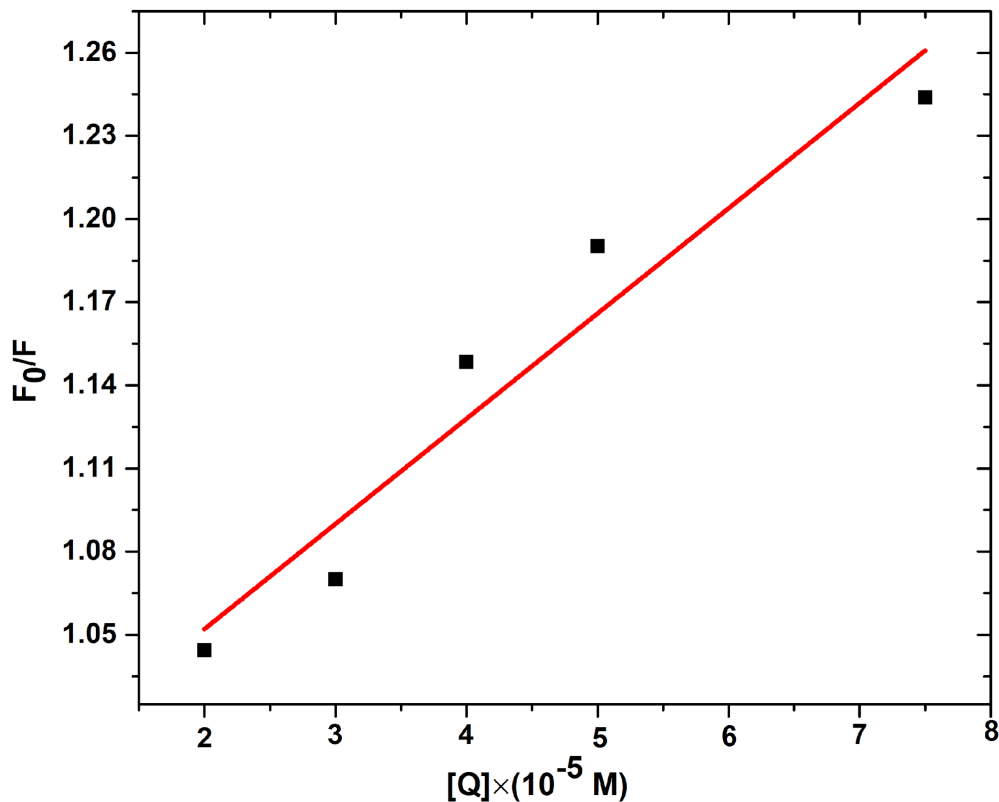


Fig. 3.8: Stern-Volmer plot for quenching of I27 at different drug concentrations (pH is 7.4, the excitation wavelength, $\lambda_{ex} = 295 \text{ nm}$). The concentration of I27, $[I27] = 40 \times 10^{-6} \text{ M}$, the drug concentration is varied, $[Q] = 20, 30, 40, 50, \text{ and } 75 \times 10^{-6} \text{ M}$.

The value of the quenching constant (K_{SV}) here is found to be $3.795 \times 10^3 \text{ Lmol}^{-1}$. This corresponds to a dynamic k_q of order $10^{11} \text{ Lmol}^{-1}\text{s}^{-1}$, which is larger than k_q^{max} , indicating that quenching here is predominantly static. These results demonstrate that the interaction between I27 and CLM molecules results in the formation of a complex.

3.7.2 Atomic force spectroscopy

Fig. 3.9 a) and b) show representative force curves of the unfolding of I27 without and with CLM molecule attached, respectively. We see 8 unfolding events of the octamer of I27. The unfolding force was measured for I27 and I27 in presence of 40 μM CLM. We observed that the force required to unfold the domains of I27-WT (wild type) is 218 ± 2 pN. On the other hand, the force needed to unfold the domain of I27 in presence of 40 μM CLM is 242 ± 2 pN. The unfolding force for I27 with 40 μM CLM is 25% higher than the I27-WT.

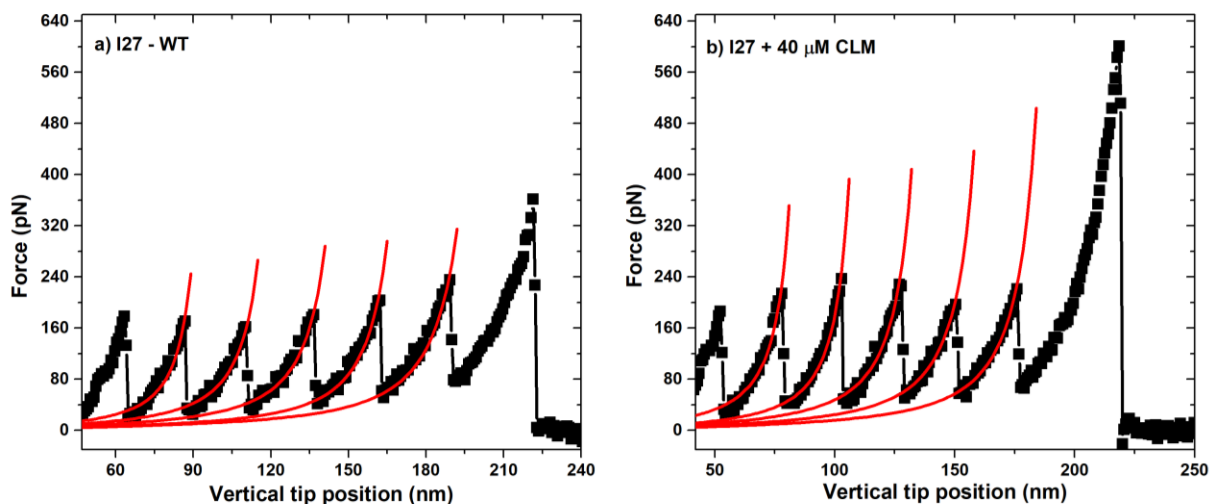


Fig. 3.9: Representative measurements for the unfolding of polyprotein without and with the drug a) I27-WT, and b) I27 with 40 μM CLM. The force required to unfold the domain is more for I27 with 40 μM CLM compared to I27-WT. Solid red line represent the WLC model fitted to the force versus extension curve.

One can see from the below Gaussian fits that there are two distinct peaks, one at ~ 200 pN while other at ~ 360 pN. For 40 μM of CLM concentration, more events are observed at higher peak force as compared to I27 only while for higher concentrations, the 2nd peak slowly diminishes (Fig. 3.10).

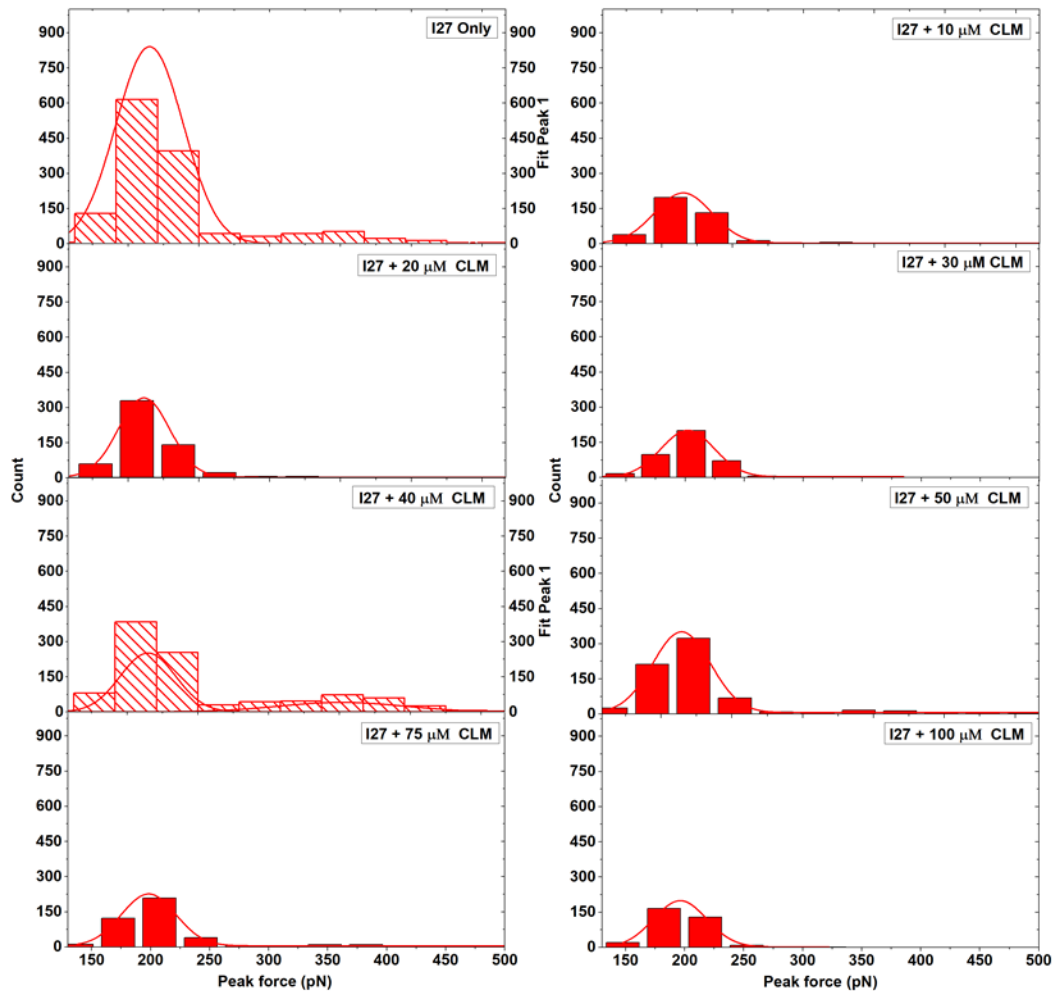


Fig. 3.10: Unfolding force frequency histograms followed by Gaussian fit for I27 only and I27 with different drug concentrations.

Fig. 3.11 represents the unfolding forces of I27 at different concentrations of CLM. Fig.3.11 represents the persistence length for I27-WT and I27 with 40 μM CLM. The peak number corresponds to total number of domains which still remains **unfolded** at this particular unfolding event. For instance, for a I27-octamer, the peak number 6 specifies that there are only 2 folded domains remaining since there are total 8 domains in the polyprotein. The fluorescence quenching data suggests that at 40 μM concentration, CLM attaches to the I27 near Trp. The enhancement in force required to mechanically unfold the protein in the presence of CLM with 40 μM indicates that the CLM mechanically stabilizes titin's individual domains.

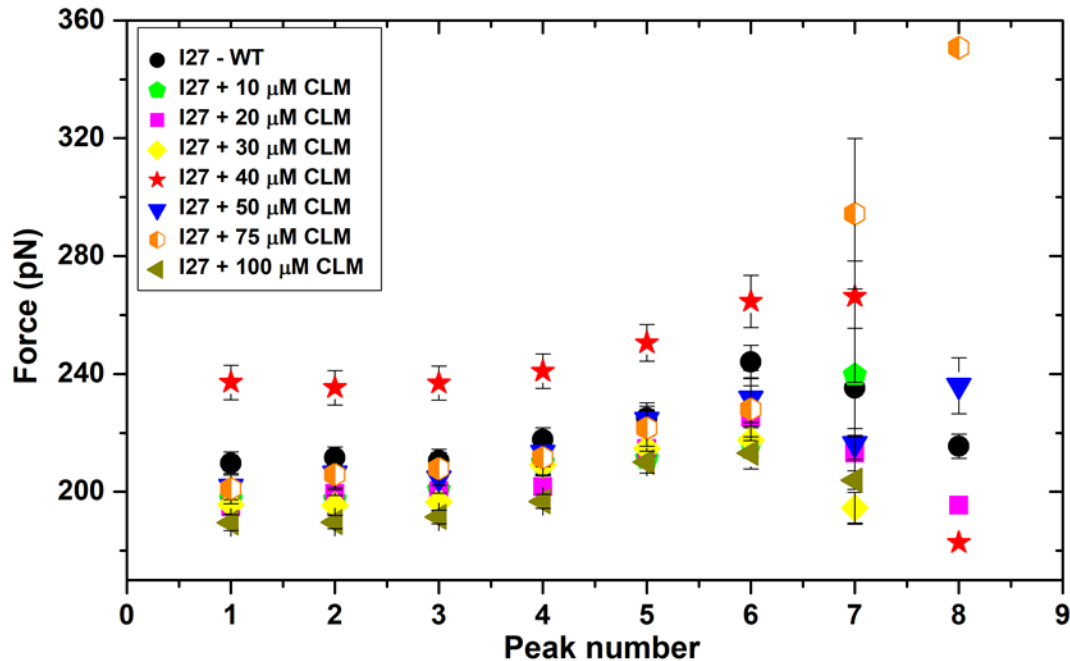


Fig. 3.11: The graph shows the domain-wise unfolding force after the addition of the drug at various concentrations. The peak number suggests the number of unfolded domains. The sample size is 160 and 98 for the I27-WT and I27 with 40 μM CLM respectively. The unfolding force is higher for 40 μM CLM concentration. The difference is of ~ 25 pN for each domain, the error bars are standard errors which is standard deviation divided by square root number of measurements.

Further, we fitted Worm-Like Chain (WLC) model to the force extension data of the unfolded domains of I27. A brief discussion about WLC model is described in section 2.2.1.

The force curves with more than 6 events were considered for the analysis. We analyzed 160 force curves for I27-WT and 98 curves for I27 with 40 μM CLM concentration. Fig. 3.12 shows the persistence length change on the addition of 40 μM CLM to the I27 protein. The graph shows that persistence length decreases with the addition of CLM for each unfolding domain. It suggests softening of the chain. Such softening could also be the result of enthalpic contribution to the chain elasticity due to binding of CLM molecule to the chain. This indicates that the CLM remains bound to the chain even after the domain is unfolded.

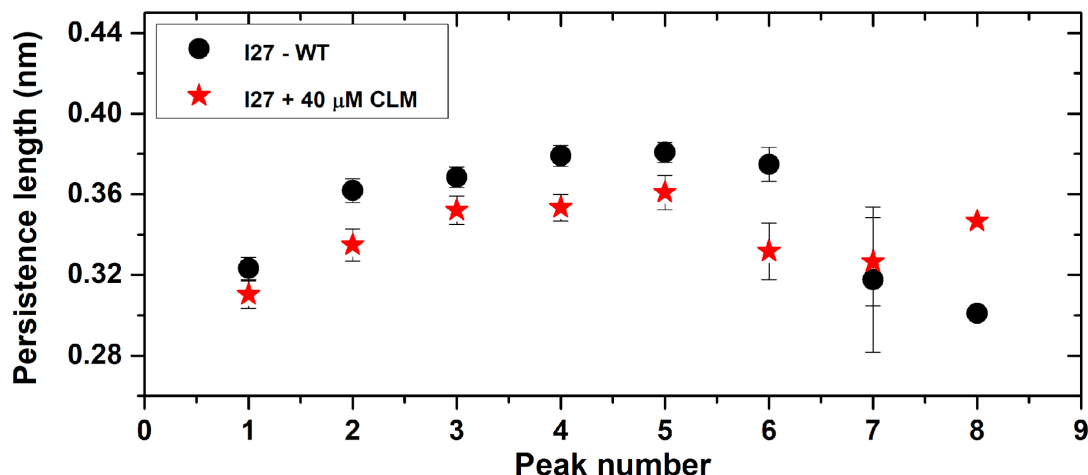


Fig. 3.12: The domain-wise persistence length of I27-WT and I27 with 40 μ M CLM. The error bars are standard errors.

3.7.3 Equilibrium denaturation experiment

We performed the equilibrium denaturation experiments at a fixed protein concentration (40 μ M) with increasing GdmCl concentrations and monitored the denaturation of protein with varying CLM concentration. A detailed description of equilibrium denaturation experiment is described in the section 3.6.1.

The equilibrium denaturation data was analyzed using methods described previously [152, 153].

Fig. 3.13 a) shows the denatured fraction at a particular denaturant concentration. The curves represent unfolded fractions as a function of denaturant concentration. There is a shift in the GdmCl concentration when 40 μ M CLM is added to I27 protein (Fig. 3.13 b) whereas there is no shift for I27 with 30 and 50 μ M CLM concentration. This shift is towards the higher GdmCl concentration. This indicates that the chemical stability of the protein is enhanced at 40 μ M drug concentration.

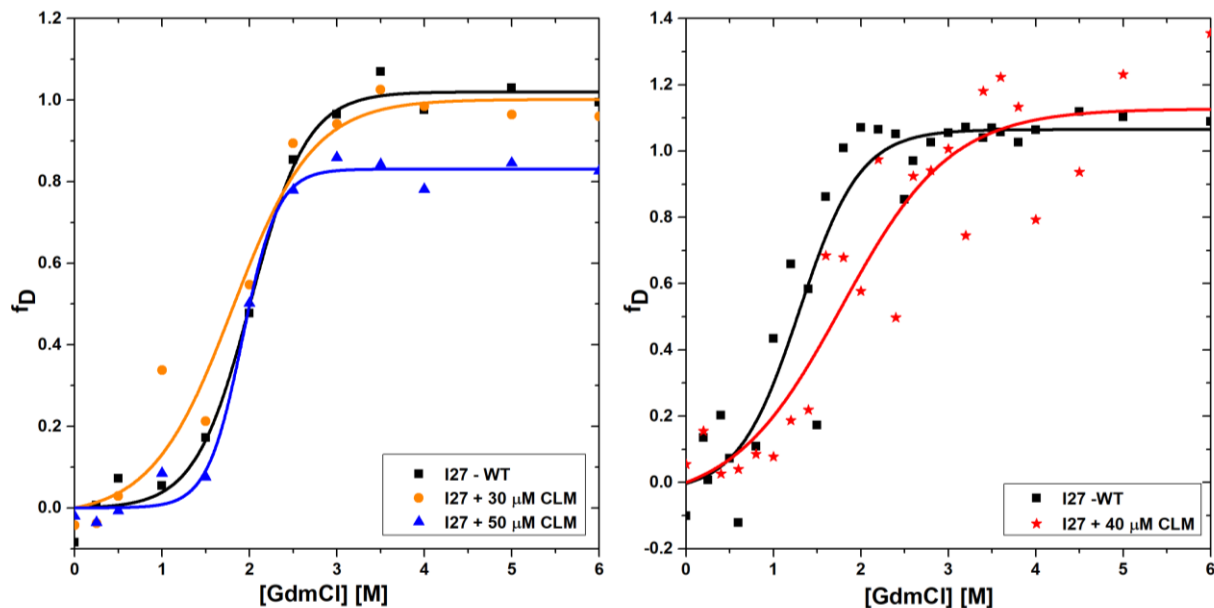


Fig. 3.13: Equilibrium denaturation experiments on monomers of I27-WT and I27 with different drug concentrations followed by Trp emission fluorescence spectroscopy. The denaturation data is plotted in terms of denatured fraction. a) The data in black filled squares are I27-WT, orange filled circles are I27 with 30 μ M CLM concentration and filled blue triangles are of I27 with 50 μ M CLM concentration, b) The data in black filled squares are I27-WT, red filled stars are I27 with 40 μ M CLM concentration. Solid lines are fit to a two-state model.

Free energy of stabilization was also calculated for all the three CLM concentrations.

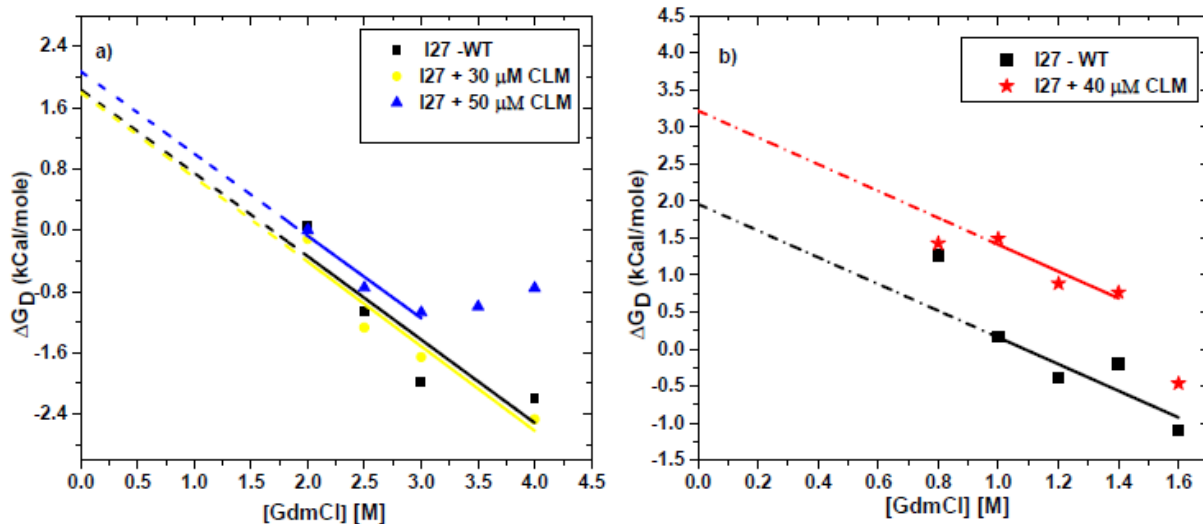


Fig. 3.14: Plot of ΔG_D versus GdmCl molarity for calculation of ΔG_D (H_2O). a) The data in black filled squares are I27-WT, yellow filled circles are I27 with 30 μ M CLM concentration and filled blue triangles are of I27 with 50 μ M CLM concentration, b) The data in black filled squares are I27-WT and red filled stars are I27 with 40 μ M CLM concentration.

Fig. 3.14 a) shows the free energy of stabilization for I27 – WT, I27 with 30 and 50 μ M CLM concentrations, respectively whereas Fig. 3.14 b) shows the free energy of stabilization for I27 – WT and I27 with 40 μ M CLM, respectively.

The value of ΔG_D (H_2O) for I27-WT is found to be 1.95 ± 0.93 kcal/mole, while for I27 with 30, 40 and 50 μ M is 1.79 ± 0.67 kcal/mole, 3.25 ± 0.63 kcal/mole and 2.07 ± 0.62 kcal/mole respectively. This indicates that at 40 μ M drug concentration the stability of I27 domains is enhanced.

3.8 Discussion

Previously, protein-drug interaction was investigated by various methods such as UV-visible absorption spectroscopy, fluorescence, circular dichroism (CD), isothermal calorimetry (ITC) and 3D fluorescence spectroscopy. Interaction of CLM with serum albumin proteins (both HSA and

BSA-Bovine Serum Albumin), lysozyme, hemoglobin and bovine pancreatic system was studied by these methods [76, 78, 79, 81, 83, 181]. We investigated the binding of CLM with titin in the current work. The fluorescence data and the PatchDock results suggest that quenching is due to binding of CLM near Trp. The mechanism of fluorescence quenching was also studied. The results show that quenching is due to the formation of the I27-CLM complex.

The mechanical properties of I27 in the presence of calcium were studied previously which shows an increment of unfolding force by 40 pN and stiffness of unfolded domain is inferred through persistence length [8]. Another investigation on mechanical protein Fibronectin as well as membrane protein bacteriorhodopsin has shown that small osmolytes enhance stability of folded domains and reduce the persistence length of the unfolded chain [140–142]. It is argued that in presence of such small molecules, the protein chain tends to form coils and it reduces the persistence length [143]. The mechanical stability of the protein is enhanced in such situations due to increase in chemical potential of denatured versus the folded state. The interaction of CLM with I27 shows a similar result. However, it is unclear if such effects are working in case of CLM stabilizing the protein since we see this effect at much lower concentration of CLM compared to these osmolytes. Our single-molecule measurements show that unfolding force is increased by 25 pN with 40 μM drug thereby stabilizing the protein. Further, stability is confirmed by equilibrium denaturation experiments. Denaturation experiments also show the stability at 40 μM drug concentration.

One of the limitations of the AFM based pulling experiments is the validity of WLC model to infer persistence length. WLC is successful in situations wherein the enthalpic contribution to the free energy is negligibly small. This is true in cases such as homopolymers in good solvents. The measurements of persistence length is thus likely to be riddled with errors if enthalpy is significant. However, the mechanical stability of individual domains is reported accurately by AFM pulling experiments. The stabilization of I27 with CLM in our study is also corroborated with ensemble studies of single monomers. We note here that in order to probe changes in mechanical properties with such drug molecules at low concentrations, it is important to provide evidence of binding of drug molecules with complementary methods such as fluorescence quenching.

Besides performing antibacterial activities, CLM acts as a muscle relaxant too [173]. Its effect is found to be direct on muscles and it is concentration dependent. Fluorescence quenching experiments show that the drug is binding to I27 protein in the vicinity of Trp. AFM and equilibrium denaturation experiments suggest that binding results in both chemical and mechanical stabilization of the protein. Physiologically, it may affect the muscle function in a significant way. Our results are a step forward in terms of understanding the effect of CLM on muscle sarcomere at molecular level.

3.9 Conclusion

In this study, single-molecule and bulk measurements were performed to study the interaction of CLM with I27. The Stern-Volmer plot shows that protein-drug complex forms in a certain range of drug concentration. The increase in unfolding force in single-molecule study also shows that binding takes place at a particular concentration (40 μM). However, there was no change in average unfolding force for other drug concentrations. Binding of protein with drug results in increasing the unfolding force of 25 pN. Chemical denaturation experiments show that the drug enhances chemical stability at this concentration. The higher unfolding force indicates that protein at 40 μM of drug concentration does not yield easily to external forces.

Chapter 4

Assessment of the mechanical properties of mouse embryonic stem cells lacking clathrin heavy chain using AFM

4.1 Introduction

Embryonic stem cells (ESCs) are the cells obtained from the undifferentiated inner cell mass of the mammalian embryo. These cells have the ability to grow and differentiate into all the three germ layers namely ectoderm, endoderm and mesoderm. On the other hand, adult stem cells can only generate a limited number of cells.

It has been shown previously that the clathrin heavy chain (*Cltc*) is responsible for maintaining the pluripotent state of the ESCs. Knockdown (KD) of clathrin results in decrease in E-Cadherin (E-CAD) levels and an increase in the transforming growth factor β (TGF β) and extracellular signal regulated kinase (ERK) signaling pathway. It has been found that the decreased pluripotency upon clathrin mediated endocytosis (CME) loss can be rescued by inhibiting TGF- β R, MEK, and GSK3 β , or overexpressing E-CAD [182].

Previously, cell stiffness of cancer cells was also measured using AFM [183]. It was also shown that mouse embryonic stem cells (mESCs) show low cellular stiffness in comparison to differentiated cells [45]. However, the mechanical properties such as cellular stiffness upon loss

of *Cltc* are not studied. Atomic force spectroscopy is used to find out the changes in mechanical properties of shScrambled (shScrambled refers to wild-type embryonic stem cells), shCltc1, shCltc3 (shCltc1 and shCltc3 refers to the *Cltc* knockdown which was done in mESCs using two shRNAs) cells, such as Young's modulus (E). mESCs lacking *Cltc* show higher Young's modulus in comparison to wild type (WT) stem cells. The increase in stiffness of stem cells is attributed to the presence of actin stress fibres and the accumulation of inactive, phosphorylated actin binding protein, COFILIN. COFILIN is an actin regulatory protein. COFILIN binds to G- and F-actin. The actin assembly dynamics can be accelerated by increase in number of actin filaments ends on which the monomers can be added or dissociated [184]. Young's modulus of stem cells on treatment with actin polymerizing inhibitors such as Latrunculin A (LatA) and Cytochalasin D (CytoD) was also determined. LatA is the most widely used reagent for depolymerization of actin filaments for live cells. LatA has the strong affinity for monomers. Depolymerization is attributed to sequestering of actin monomers and it dissociates phosphate from its ends [185]. CytoD binds to G-actin and inhibits G-actin-cofilin interaction [186]. It has been found out that Young's modulus of shScrambled, shCltc1 and shCltc3 decreases when treated with LatA and CytoD. Their stiffness values are similar as we obtained for WT mESCs.

4.2 Materials and methods

4.2.1 Bead attachment on cantilever

A tipless cantilever with stiffness of 0.07 N/m was used for AFM measurement. 2 μ L of spherical glass beads (size-5 μ m) was drop-casted on a clean glass slide. Beads were allowed to get dried for 5 minutes. An approximate equal amount of araldite adhesive (locally sourced) and hardener glue was taken and mixed properly. With the help of a sharp toothpick, small dots were made on a clean glass slide. Using the servo control of AFM, the cantilever was brought down on the araldite glue. Since the bead was of very small size, a very small amount of glue was picked up on the cantilever, and the cantilever was again lowered down on the glass slide in order to remove the excess glue. After that, the cantilever was lowered down onto the bead. Cantilever was maintained under positive load. After 5 minutes, the cantilever was pulled back along with the bead. Fig 4.1 shows the schematic of 5 μ m spherical glass bead attached on the cantilever. Before measurements,

the cantilever was calibrated each time on the glass coverslip in milli-Q as described in section 3.5.1.

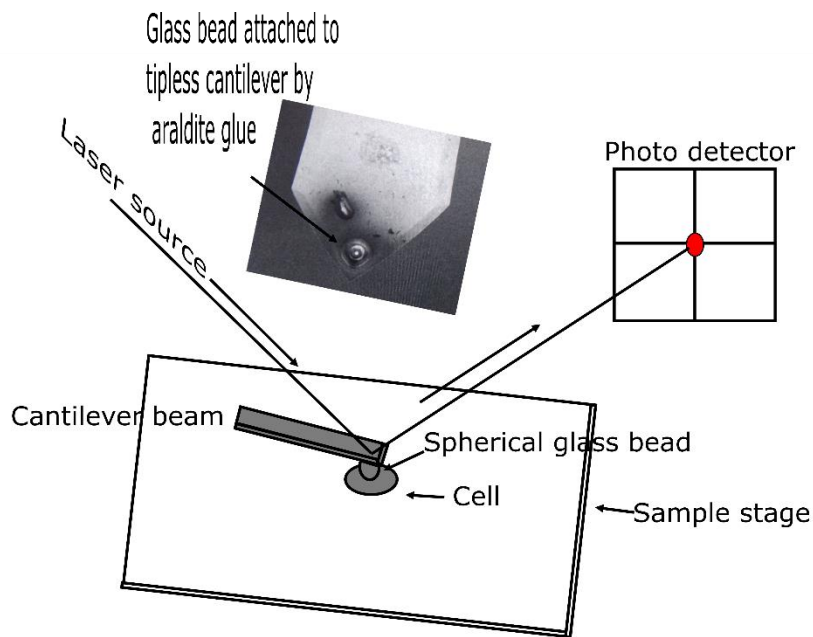


Fig. 4.1: Schematic of AFM where a spherical glass bead of diameter $5\ \mu\text{m}$ is attached on the tipless cantilever. The inset shows the SEM image of the glass bead attached on the cantilever.

4.2.2 Cell mechanics using AFM

A thin layer of matrigel was coated on 22 mm glass coverslips. To measure the young's modulus of matrigel, a $3\ \mu\text{m} \times 3\ \mu\text{m}$ area was selected and measurements were taken over 10×10 grid. Cells were plated on 22 mm glass coverslip and were deformed under a glass microsphere attached to the cantilever which is of similar size as the cell. For each cell, a $3\ \mu\text{m} \times 3\ \mu\text{m}$ area was selected and 100 force curves were taken in a 10×10 grid at different locations on a single cell. All the measurements were done on live cells only and at the middle of the cell. Indentation studies were performed on more than 20 control (undifferentiated) mESCs and treated cells (Cltc KD or RA-treated). The approach velocity was $2\ \mu\text{m}/\text{sec}$ with sampling rate of 2048 data points per second.

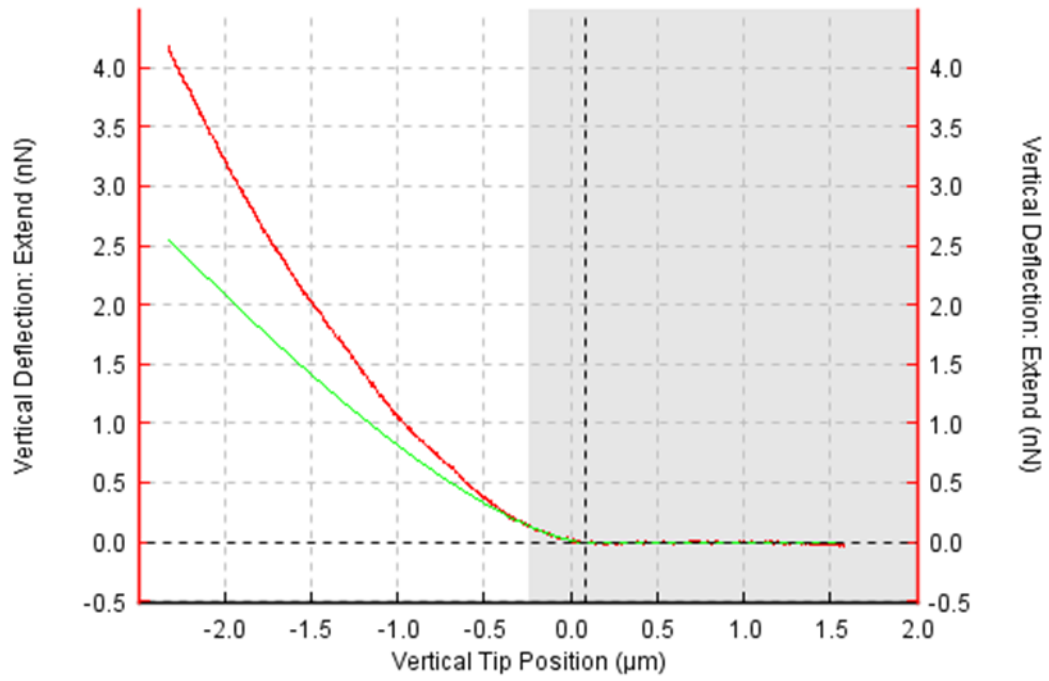
4.2.3 AFM analysis

Assuming the glass-glass contact to be infinitely stiff compared to the glass-cell contact - a reasonable assumption since it is 10,000 times stiffer, the slope of the curve in the contact region for glass is one implying no deformation (Fig. 4.5). The slope of the curve on cells is much less suggesting a certain amount of deformation.

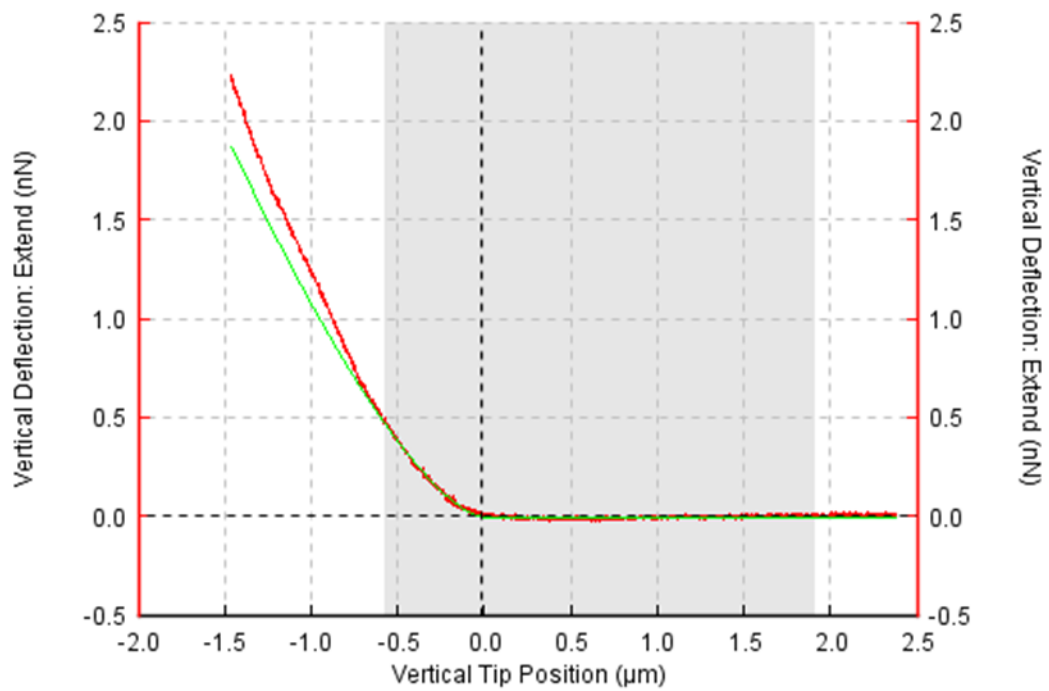
We used glass-glass contact for calibration of deflection sensitivity, and the subtraction of cantilever deflection from the push given by the piezo extension yields deformation in the tissue. The force is calculated by multiplying the cantilever deflections by its stiffness. The force versus deformation curve is then fitted with Hertz model (see section 2.2.2). In order to fit the Hertz model, 1st baseline correction is done. For doing that, the part of the curve which is away from the surface should be flat. Since in that region there is no force between the two and this gives the force baseline. After the baseline correction, contact point is determined. This function determines the point where the force curve crosses zero force line. Then, tip-sample separation is determined and hertz model is fitted. Since we have used spherical glass bead with 5 μm diameter, so tip radius of 2.5 μm and poisson ratio of 0.5 is used as fitting parameter.

Fig. 4.2 shows the Force vs indentation curves fitted with Hertz model for a) shScrambled, b) shCltc1, c) shCltc3, d) retinoic acid respectively.

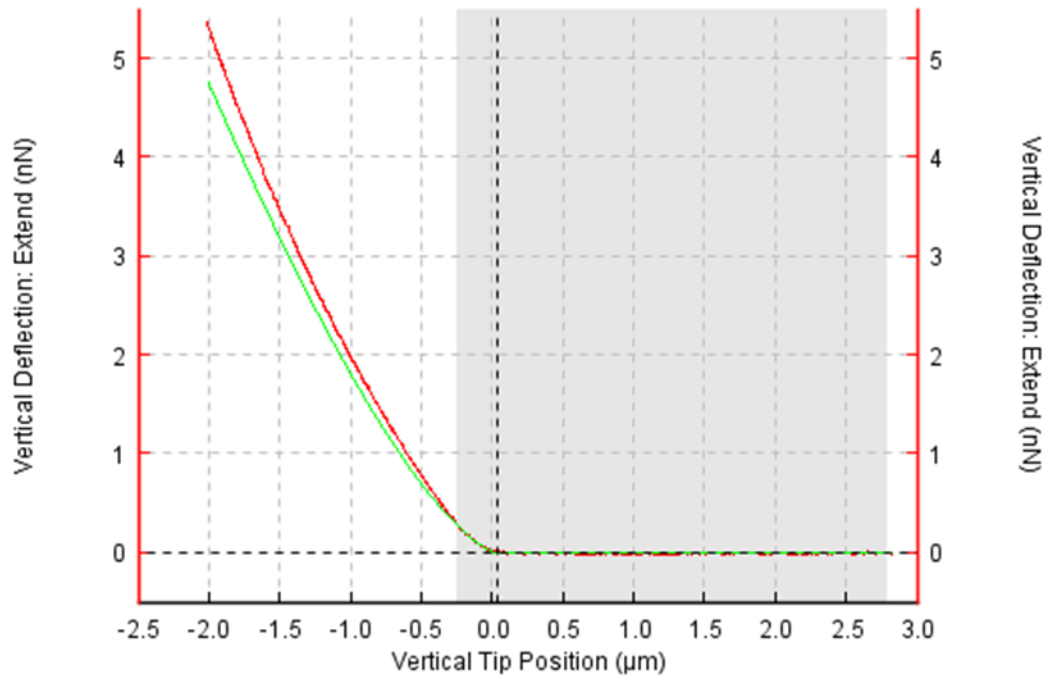
a)



b)



c)



d)

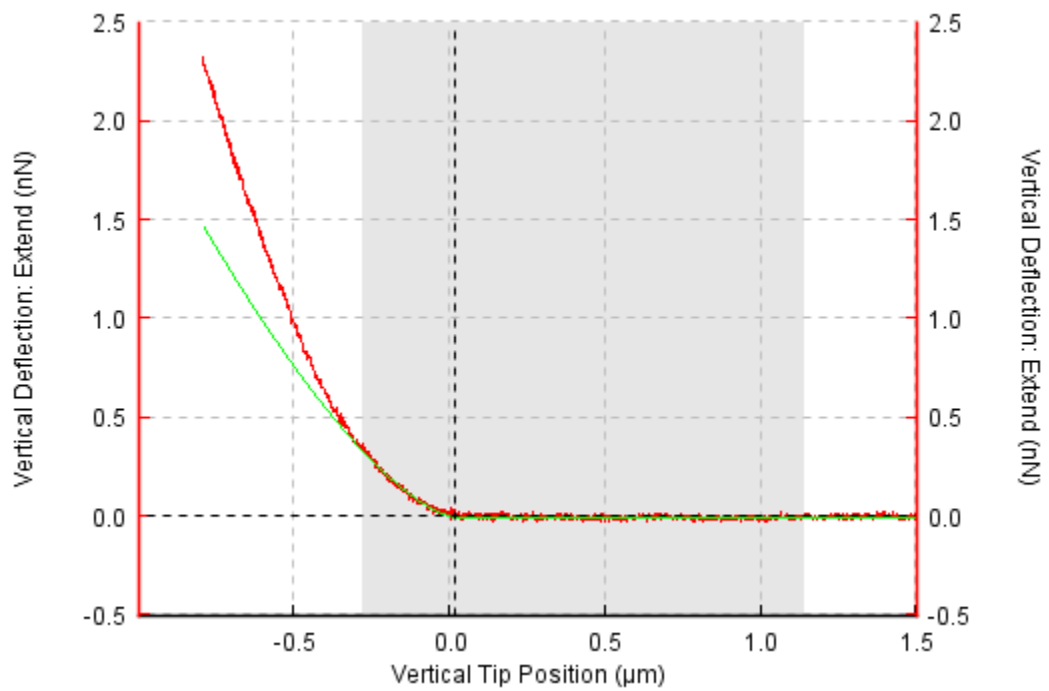
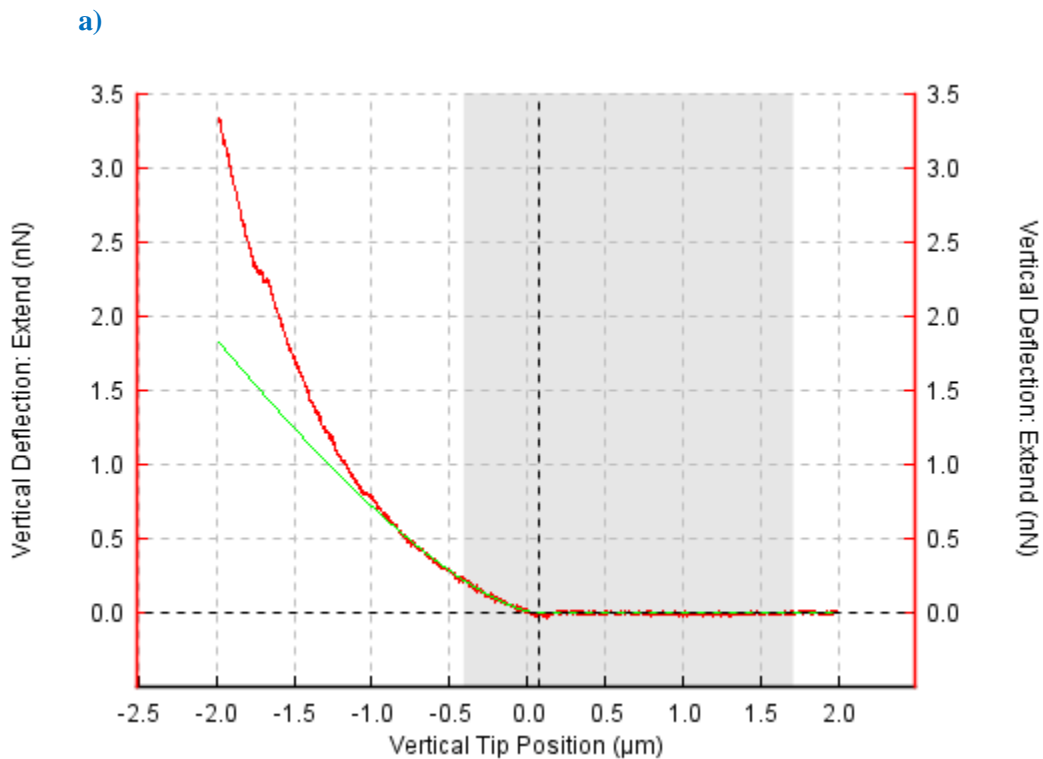


Fig. 4.2: Force vs indentation curves fitted with Hertz model for a) shScrambled, b) shCltc1, c) shCltc3, d) retinoic acid respectively. The grey area shows the region over which the hertz model is fitted, that area describes the region where the cell is elastically deformed. The E value describes the stiffness of the cell 269 Pa, 627.5 Pa, 405.7 Pa, 745 Pa, respectively.

The below attached graphs show the force vs indentation curves for the mESCs treated with LatA (Fig. 4.3).



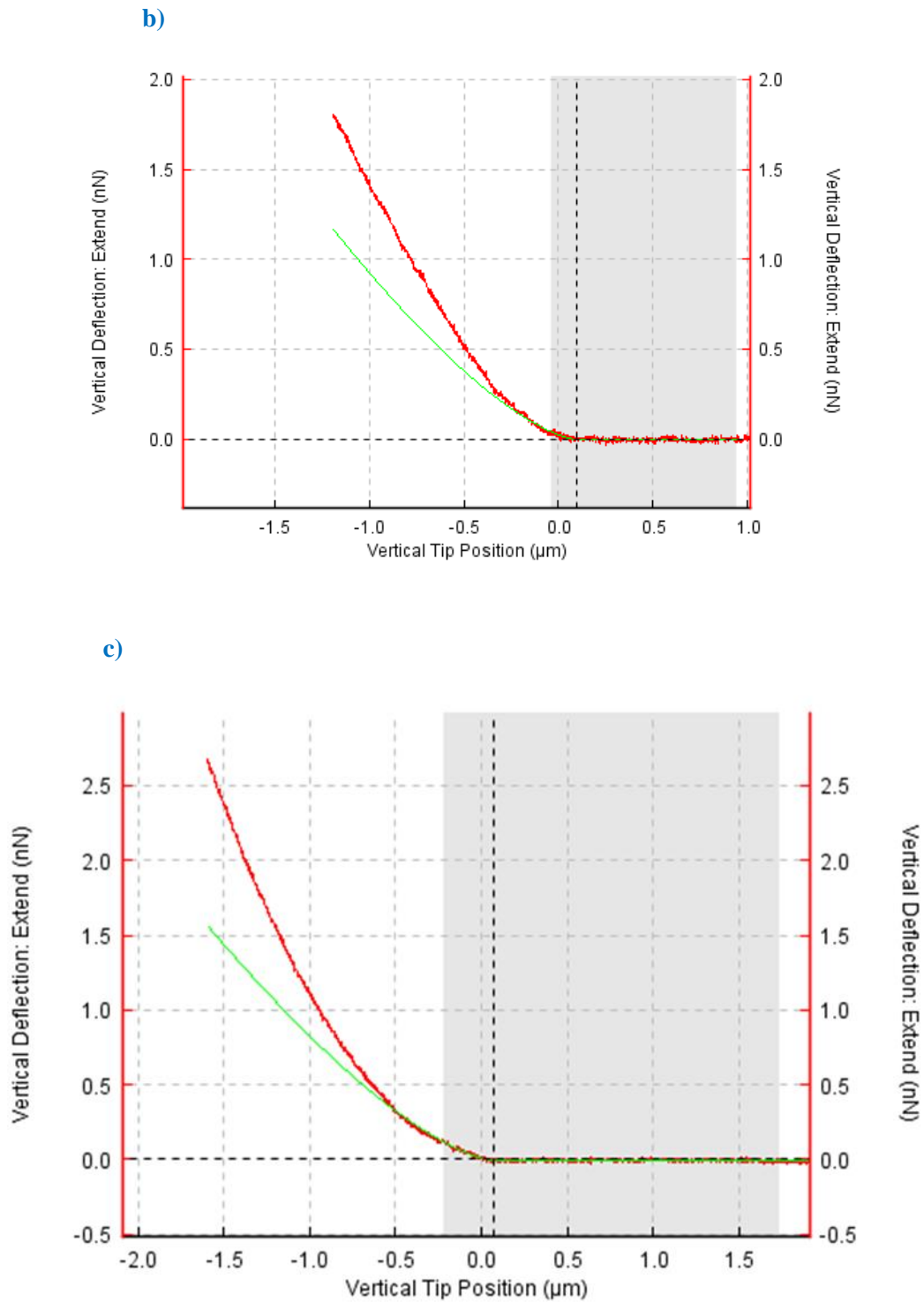
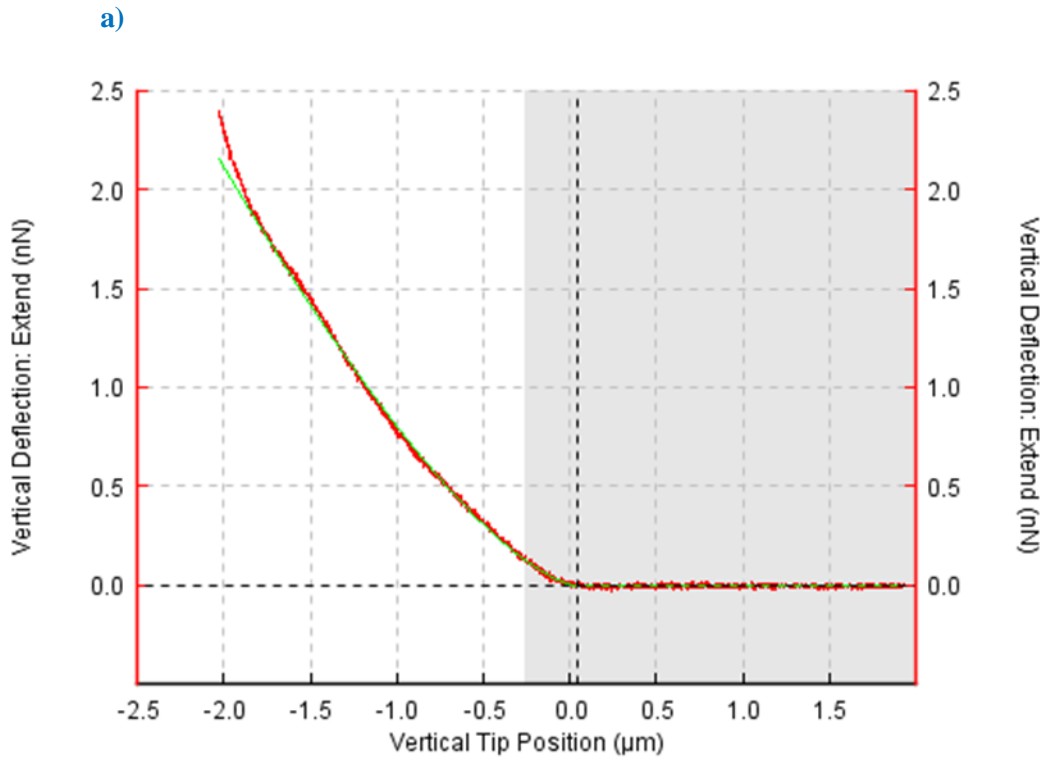


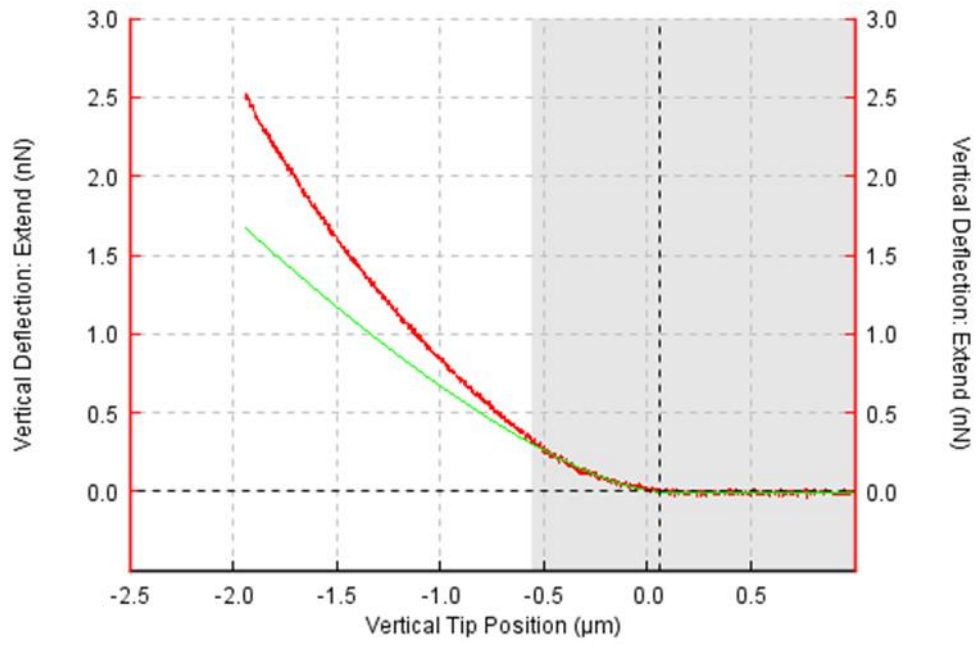
Fig. 4.3: Force vs indentation curves fitted with Hertz model for a) shScrambled, b) shCltc1, c) shCltc3 cells treated with LatA, respectively. The grey area shows the region over which the hertz model is fitted,

that area describes the region where the cell is elastically deformed. The E value describes the stiffness of the cell 240 Pa, 298.9 Pa and 277.3 Pa, respectively.

Similarly, the below attached graphs show the force vs indentation curves for the mESCs treated with CytoD (Fig. 4.4).



b)



c)

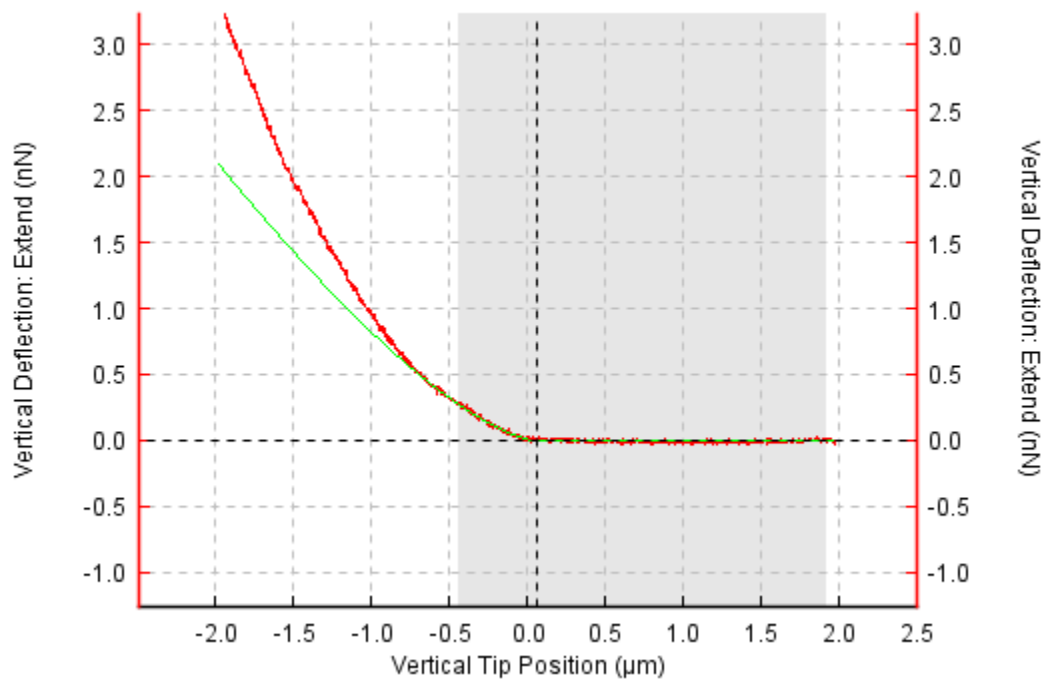


Fig. 4.4: Force vs indentation curves fitted with Hertz model for a) shScrambled, b) shCltc1, c) shCltc3 treated with CytoD, respectively. The grey area shows the region over which the hertz model is fitted, that area describes the region where the cell is elastically deformed. The E value describes the stiffness of the cell 280.8 Pa, 228.5 Pa and 276.8 Pa, respectively.

4.3 Results

4.3.1 *Cltc* knockdown results in increase in cell stiffness

A tipless cantilever with stiffness of ~ 0.07 N/m, with a spherical glass bead of diameter $5 \mu\text{m}$ attached to the end was used for all AFM measurements (Fig. 4.1) (see Materials and methods). In AFM investigations, the spatial resolution depends on sharpness of the tip. Sharp pyramidal tips are generally used for measurements of mechanical response at a subcellular level on components such as the cytoplasm and nucleus, combined with high resolution imaging. Tipless cantilevers with a spherical bead attached to one end (Fig. 4.1) are used to measure deformations and resulting stress of inhomogeneous surfaces and are used to investigate the response of the cell as a whole [41, 114]. The spherical tips also provide more contact area for measurement and prevent cell damage by avoiding membrane rupture.

The approximation in all these studies is that the glass-tip contact is assumed to be non-deformable and hence has infinite stiffness. As a result of that, all the stiffness values may have systematic error in their absolute values. This assumption is largely valid for cells and tissues which has stiffness values in the range of a few kPa. The below figure shows force curves on cells with respect to glass and matrigel (Fig. 4.5).

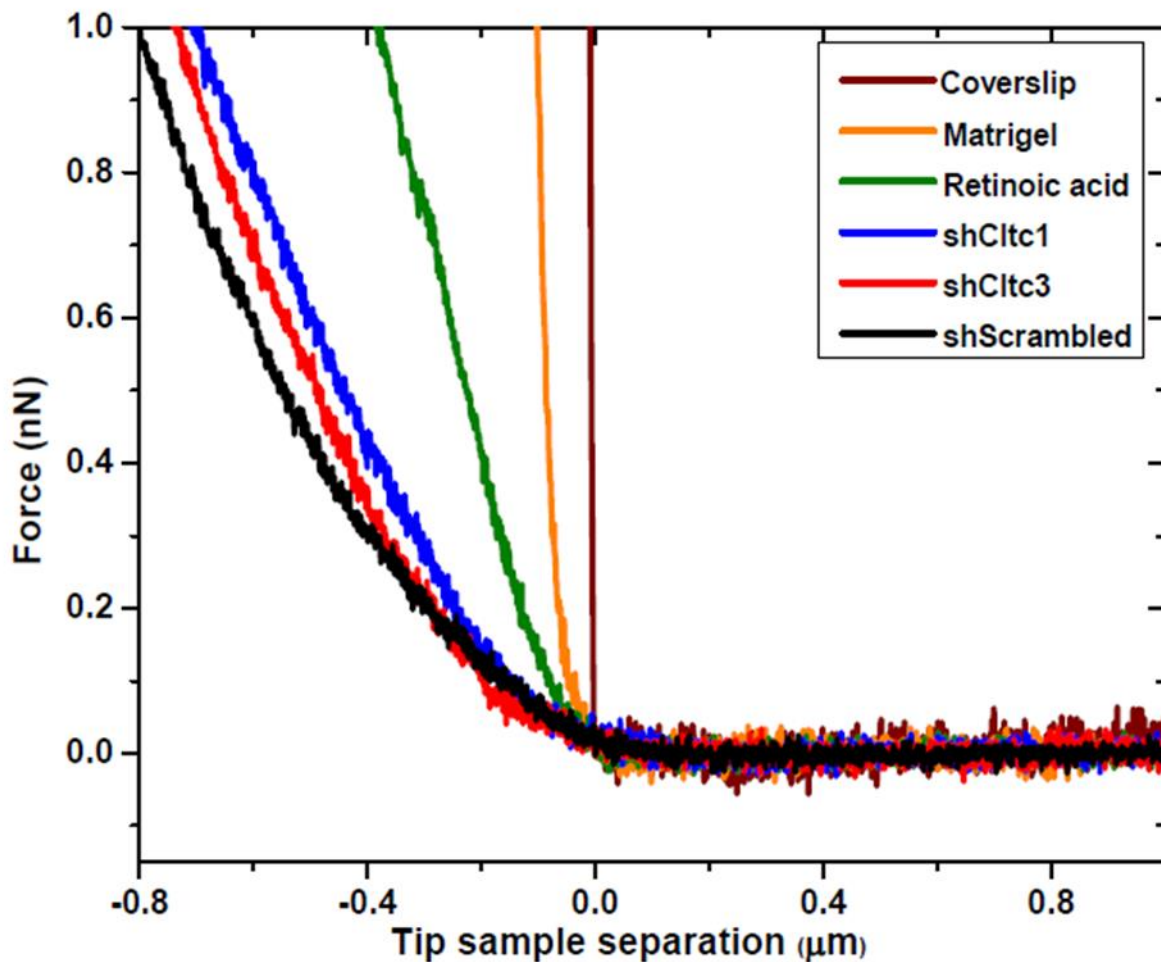


Fig. 4.5: Representative force curves on samples: Representative force curves on all samples plotted together. This data is used to estimate the Young's modulus reported in Fig. 1 and Fig. 2. Raw data clearly reveals variation in stiffness in mESCs after various treatments and KDs. Glass cover-slip is a reference and the tip-glass contact is assumed to be non-deforming.

To measure the Young's modulus of matrigel, a $3 \mu\text{m} \times 3 \mu\text{m}$ area was selected and measurements were taken over a (10×10) grid. The Young's modulus of matrigel was found to be in the range of 2-3 kPa. These values are higher than those reported earlier [187, 188] and can be attributed to differences in protocols adopted for preparing the gel and also the size of the microspheres used in the AFM measurement.

Young's modulus (E) for mESCs expressing Scrambled shRNA was 0.278 ± 0.029 kPa whereas E for cells expressing shCltc1 was 0.625 ± 0.037 kPa, and for shCltc3 was 0.465 ± 0.025 kPa,

indicating higher stiffness in Cltc KD mESCs (Fig. 4.6, table 4.1). The raw data clearly revealed a variation in relative stiffness of cells under different knock-down conditions. The stiffness difference between shCltc1 and shCltc3 was also statistically significant with confidence level of 95% (p-value 0.02). Measurements were also made from mESCs treated with retinoic acid (RA) for 48 hrs to induce differentiation (Young's modulus 0.773 ± 0.071 kPa), indicating greater stiffness (Fig. 4.6, table 4.1). Our results demonstrate that the Young's modulus increased by 2.2 fold in shCltc1, 1.7 fold in shCltc3, and by 2.8 fold in RA-treated mESCs compared to shScrambled mESCs, indicating an increase in cellular stiffness upon loss of CME and/or subsequent differentiation.

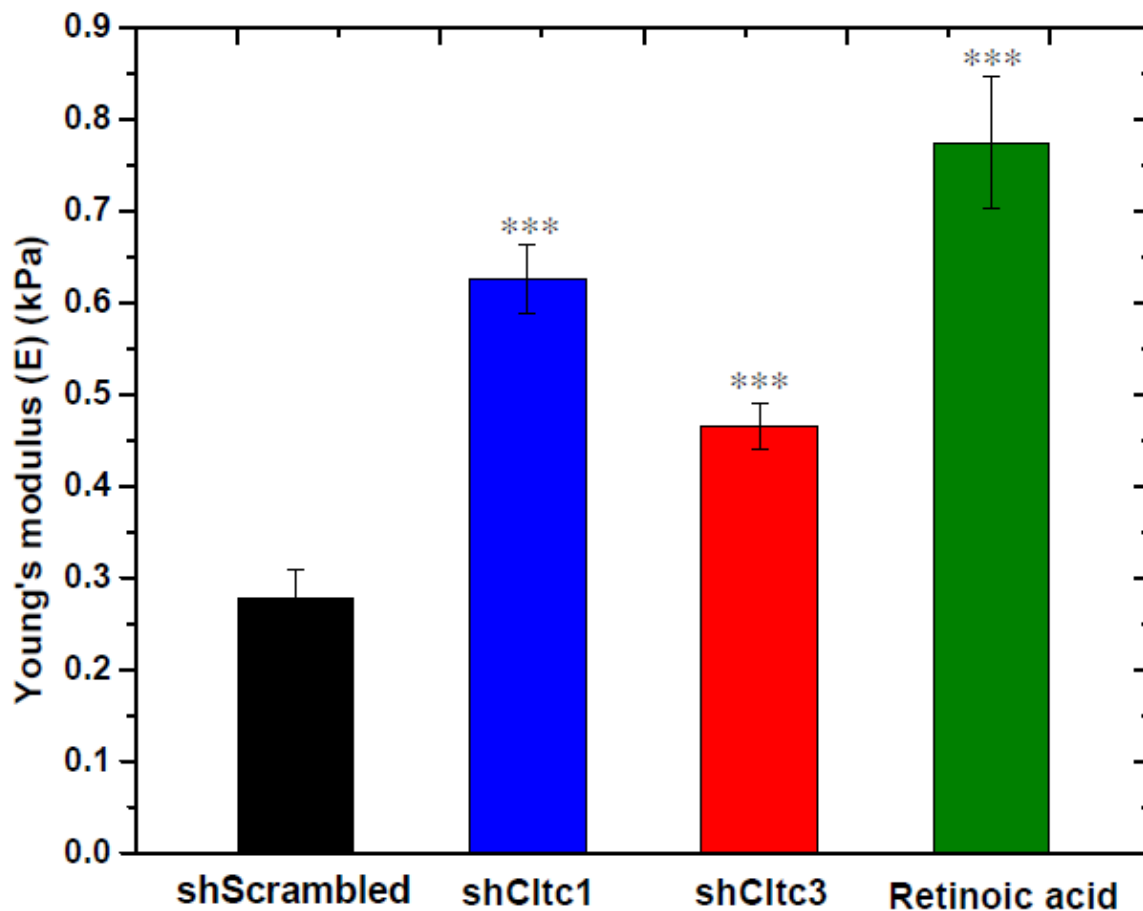


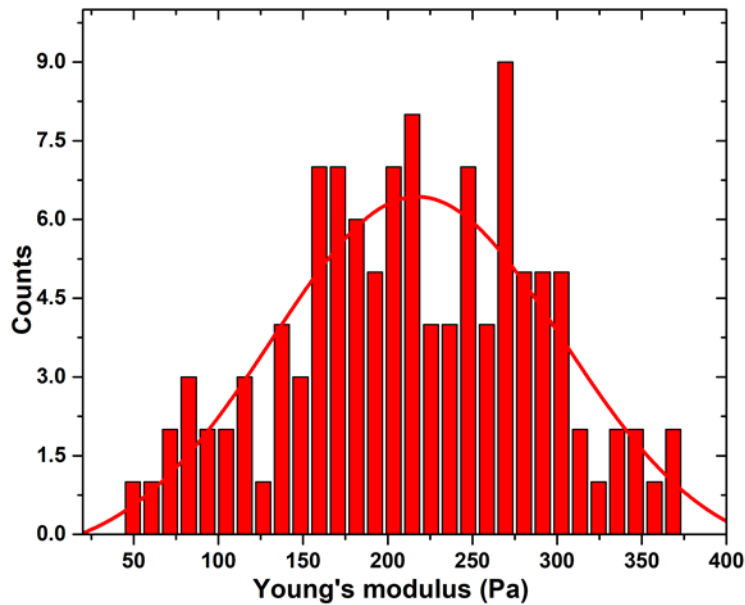
Fig. 4.6: Young's modulus (E) of shScrambled, shCltc1, shCltc3 and RA treated mESCs. *** $p < 0.0001$ by Student's T-test. The error bars denote standard error over 22-25 cells with 100 measurements on each cell with $3 \mu\text{m} \times 3 \mu\text{m}$ grid. ~ 2000 force curves were collected for each condition.

Table 4.1: The table shows the apparent Young's modulus (E) of cells under the mentioned conditions (n denotes the number of cells analysed).

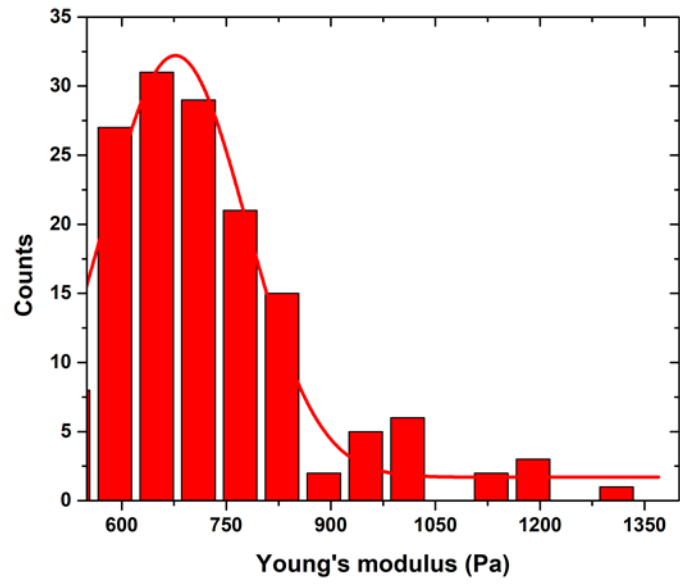
Cell type	Young's modulus (kPa \pm SE)	Fold change with respect to shScrambled
shScrambled	0.278 \pm 0.029 (n=25)	
shCltc1	0.625 \pm 0.037 (n=25)	2.2
shCltc3	0.465 \pm 0.025 (n=23)	1.7
Retinoic acid	0.773 \pm 0.071 (n=22)	2.8

Fig. 4.7 shows the histogram followed by Gaussian fit for shScrambled, shCltc1, shCltc3 and retinoic acid respectively.

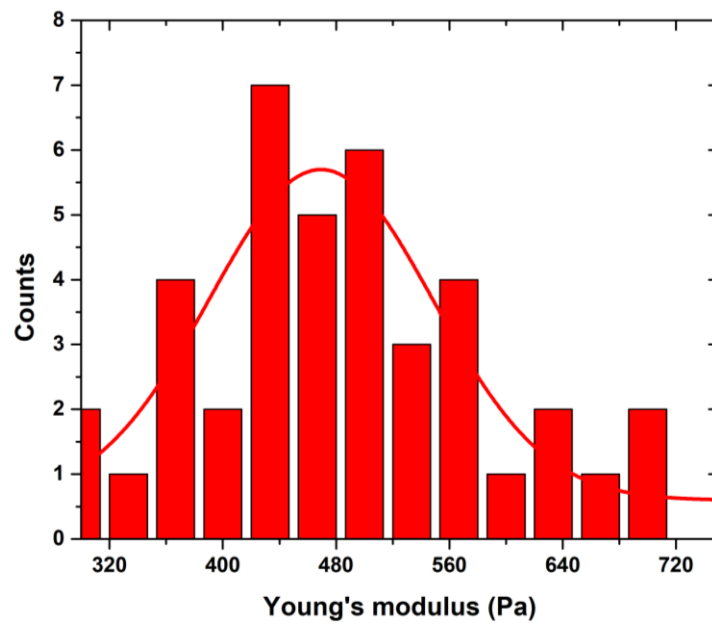
a)



b)



c)



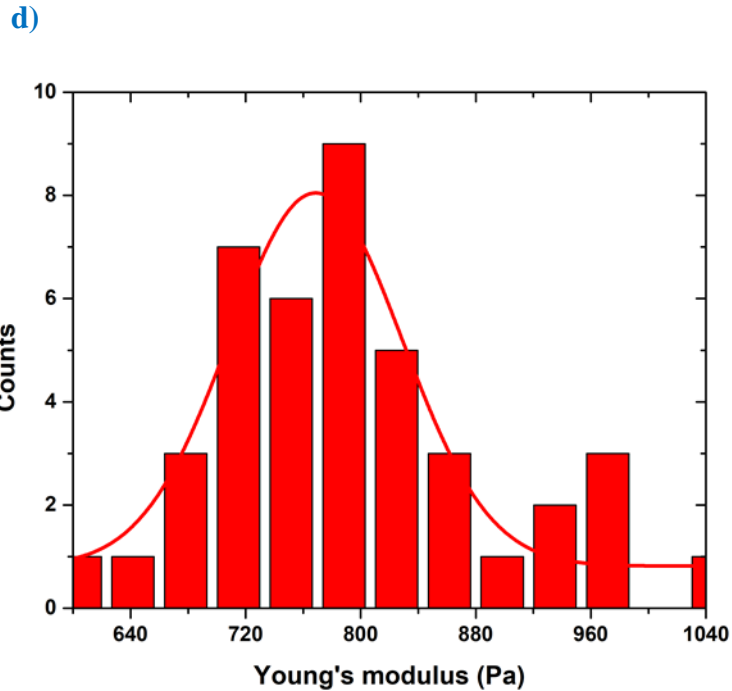


Fig. 4.7: Frequency histogram followed by gaussian fit for shScrambled, shCltc1, shCltc3 and retinoic acid, respectively.

4.3.2 F-actin depolymerizing agents reduce the stiffness of *Cltc* deficient mESCs

It is seen that the treatment of *Cltc* KD mESCs with actin depolymerizing agents, LatA or KD of the actin polymerizing protein, Profilin1 (Pfn1), resulted in a discernible loss of actin fibres, which indicates that the reorganization of the actin cytoskeleton in *Cltc* KD can be reversed by the action of LatA or KD of Pfn1. To confirm whether the actin cytoskeleton was the major regulator of cellular stiffness and differentiation observed in *Cltc* deficient mESCs, shScrambled and shCltc mESCs were treated with actin polymerizing inhibitors such as, LatA and CytoD. Upon treatment with LatA, the Young's modulus for shScrambled mESCs was 0.206 ± 0.014 kPa (Fig. 4.8, table 4.2), indicating a decrease in stiffness compared to untreated shScrambled mESCs (Fig. 4.6, table 4.1) and similar to what has been previously reported [189]. When mESCs were treated with LatA, a reduction in the Young's modulus was observed for shCltc1 (0.218 ± 0.017 kPa) and for shCltc3 (0.218 ± 0.024 kPa) mESCs (Fig. 4.8, table 4.2). Similarly upon treatment with CytoD, the Young's modulus for shCltc1 and shCltc3 reduced to 0.197 ± 0.019 kPa and 0.258 ± 0.017 kPa,

respectively, and was comparable to that of shScrambled mESCs (0.195 ± 0.018 kPa) (Fig. 4.8, table 4.2).

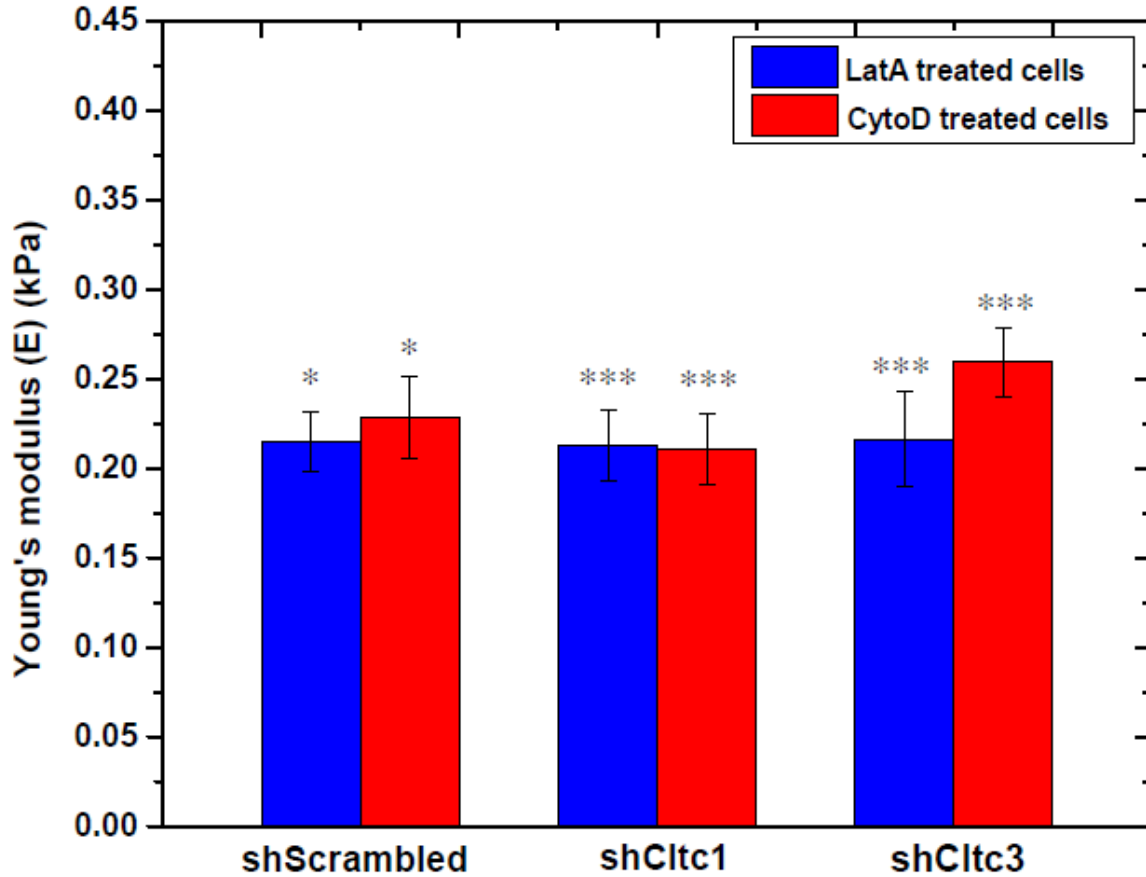


Fig. 4.8: Young's modulus of shScrambled, shCltc1 and shCltc3 mESCs treated with acting polymerizing inhibitors LatA and CytoD. Significance calculated with respect to the corresponding untreated samples. * $p < 0.05$; *** $p < 0.0001$ by Student's T-test. The error bars denote SE over 17-20 cells with 100 measurements on each cell.

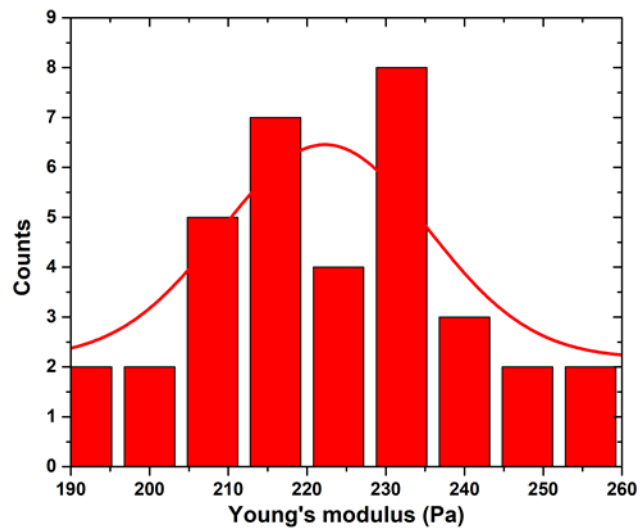
Table 4.2: The table shows Young's modulus of shScrambled, shCltc1 and shCltc3 treated with LatA and CytoD (n denotes the no. of cells analysed for each type).

	Young's modulus (kPa \pm SE) of cells treated with LatA	Young's modulus (kPa \pm SE) of cells treated with CytoD

Cell type		
shScrambled	0.206 ± 0.014 (n=20)	0.195 ± 0.018 (n=17)
shCltc1	0.218 ± 0.017 (n=19)	0.197 ± 0.019 (n=19)
shCltc3	0.218 ± 0.024 (n=18)	0.258 ± 0.017 (n=18)

Fig. 4.9 shows the frequency histogram followed by gaussian fit for LatA treated shScrambled, shCltc1 and shCltc3 cells, respectively.

a)



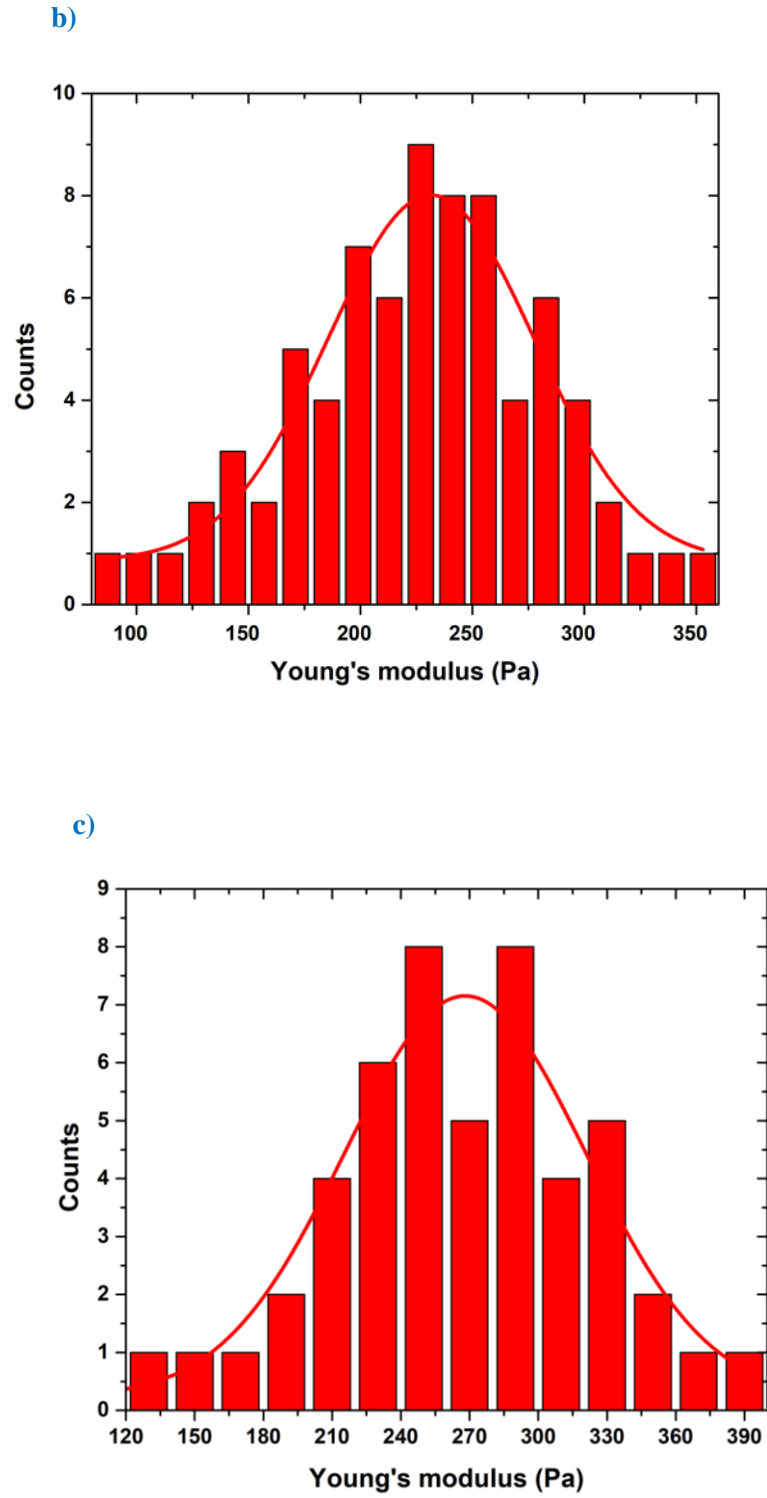
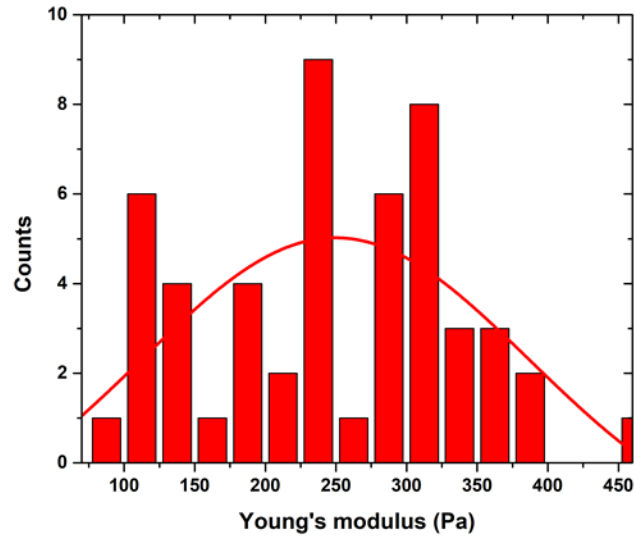


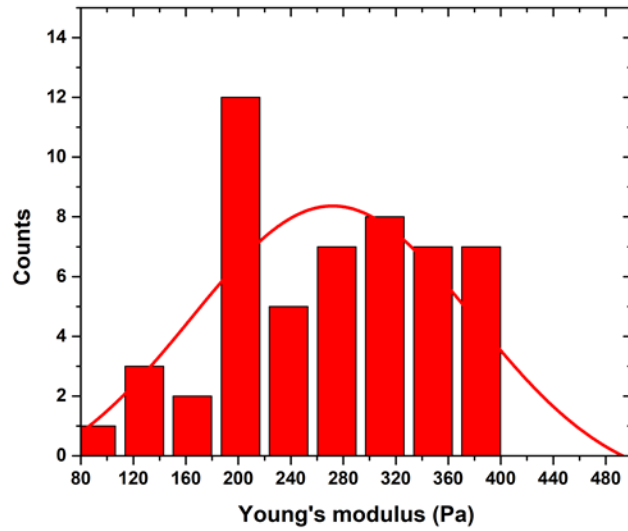
Fig. 4.9: Frequency histogram followed by gaussian fit for LatA treated shScrambled, shCltc1 and shCltc3 cells respectively.

Similarly, Fig. 4.10 shows the frequency histogram followed by gaussian fit for CytoD treated shScrambled, shCltc1 and shCltc3 cells, respectively.

a)



b)



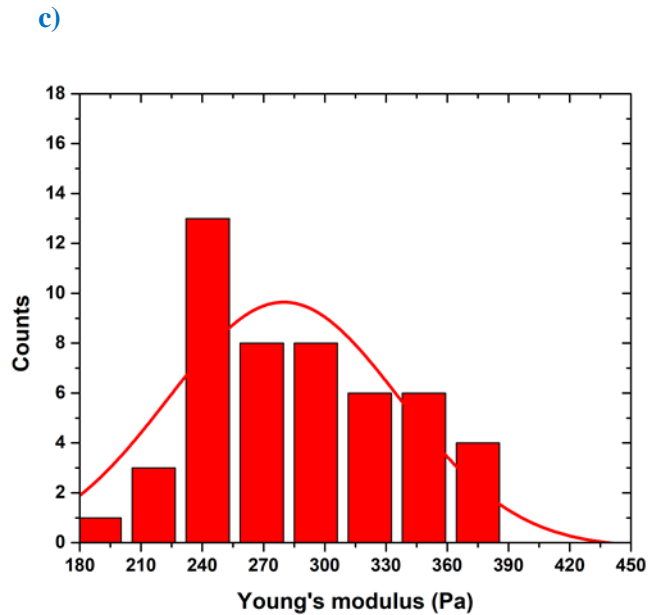


Fig. 4.10: Frequency histogram followed by gaussian fit for CytoD treated shScrambled, shCltc1 and shCltc3 cells respectively.

4.4 Conclusion

In this study, we have found out that mESCs lacking CME show greater cellular stiffness in comparison to WT cells (Fig. 4.3). It has been shown previously that the stiffness of early differentiating ESCs is higher as compared to undifferentiated ESCs [45].

We also found out that the treatment of mESCs with actin depolymerizing agents such as LatA and CytoD results in decrease in cell stiffness, with their stiffness values coming closer to WT cells (Fig. 4.4).

Chapter 5

Expression and purification of PTEN and T4 Lysozyme mutant protein

5.1 Introduction

Since proteins are an essential building block which perform various biological functions such as growth and repair of cells, act as catalyst and transport of molecules from one place to other and the 3D structure of the protein determines its function. It is stabilized by multiple interactions such as hydrophobic interactions, hydrogen bonds and covalent bonds. Therefore, it becomes very important to understand the mechanical properties of proteins (flexibility, viscoelasticity, elastic modulus, friction and adhesion) as it helps in understanding energy landscape of protein folding/unfolding. We were interested in measuring the mechanics of PTEN and T4 lysozyme protein.

5.1.1 PTEN protein

PTEN is a protein encoded by the PTEN gene. Protein encoded by this gene is phosphatidylinositol 3, 4, 5- triphosphate-3-phosphatase. PTEN is phosphatase and tensin homolog deleted on chromosome 10. It acts as a tumor suppressor protein through its phosphatase activity. This protein specifically catalyzes the dephosphorylation of Phosphatidylinositol 3,4,5- triphosphate (PIP3) to Phosphatidylinositol 4,5-bisphosphate (PIP2) [190, 191]. It is a 403 amino acid (AA) protein and consists of an N-terminal PIP2 binding domain (180 AAs), C2 domain (165 AAs), and a C-terminal tail (50 AAs) (Fig. 5.1). N-terminal PIP2 binding domain is rich in

α -helix and is phosphatase binding domain (PBD), C2 domain is rich in β -sheet and a C-terminal tail has several phosphorylation sites (Fig. 5.2). Molecular weight of WT-PTEN was found to be 65-70 kDa whereas mutant PTEN (Mu-PTEN) is N-terminal extended form of PTEN. Molecular weight of Mu-PTEN is 72 kDa. It is a cytosolic protein and it binds to the membrane. On doing several mutations, it has been found out that both the phosphatase and C2 domain play important roles in membrane binding. Genetic alterations of PTEN causes neurological defects and various human cancers [192].

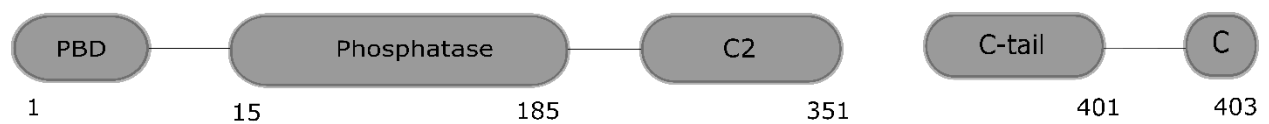


Fig. 5.1: The domain structure of PTEN protein consisting of 403 amino acids with five functional domains- PBD, phosphatase, C2, C-terminal tail and PDZ-BD.

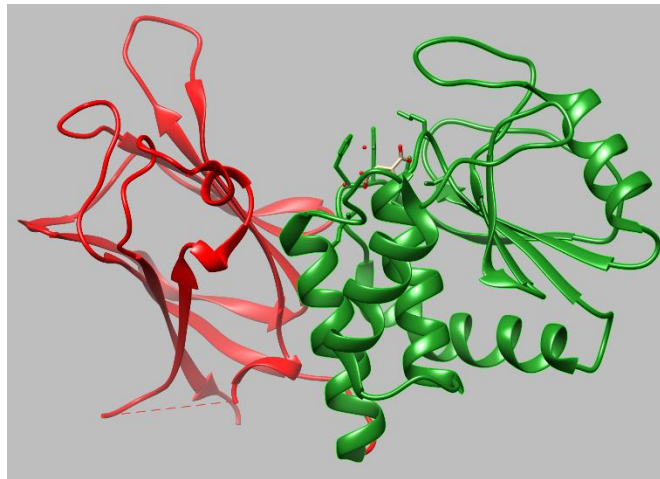


Fig. 5.2: Crystal structure of PTEN protein (PDB -1D5R).

PTEN plays an essential role in the maintenance of chromosomal stability. Overexpression of wild type PTEN results in apoptosis and blocks cell cycle progression, colony formation and cell migration. PTEN protein phosphatase can dephosphorylate protein substrates on serine, threonine

and tyrosine residues [193, 194]. Previously, optimization of PTEN protein fused with glutathione S-transferase tag was studied in order to enhance the solubility. Solubility was checked at different IPTG concentrations, different temperatures and different time intervals. It has been found that temperature, IPTG concentration and induction time affects the expression of protein [191]. Mechanical unfolding of PTEN protein is not known till now. That's why we were interested in measuring the unfolding force for PTEN protein.

5.1.2 T4 Lysozyme

T4 lysozyme is a 164 AA protein and It is used as a model system to understand various factors such as folding, stability and 3D structure of proteins [195]. A mutant has been generated where the two molecules are coming in contact with each other are replaced with the neutral amino acids. T4 lysozyme is mostly α -helix protein (Fig. 5.3). Molecular weight of the protein is 18.5 kDa.

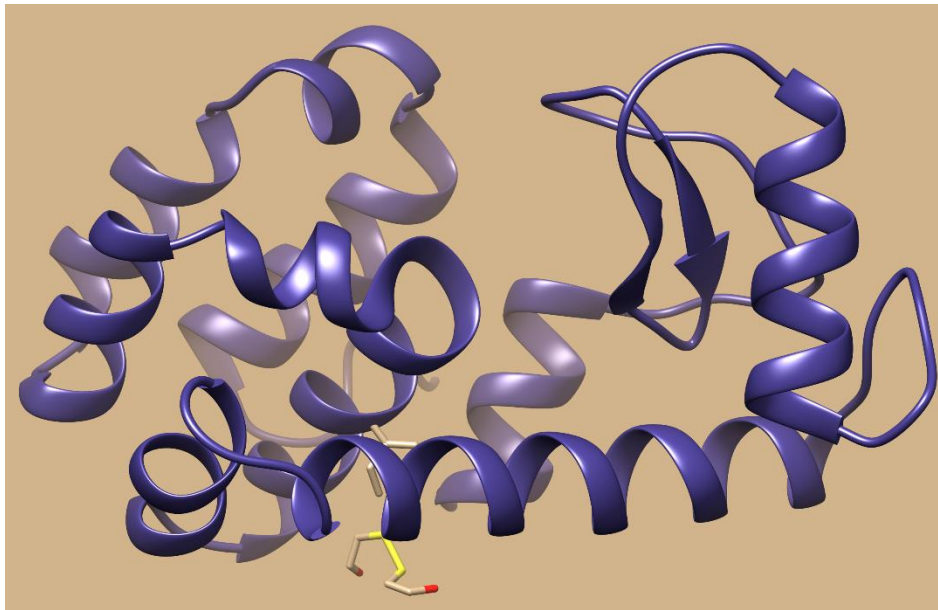


Fig. 5.3: Crystal structure of T4 Lysozyme (PDB -1B6I).

We aimed to study the viscoelasticity of T4 lysozyme using AFM. We tried forming polymers of T4 lysozyme in the solid state. Monomer of T4 lysozyme was purified and oxygen supply was

given in order to form polymers [21]. Previously, the viscoelasticity has been measured for various β -rich proteins [24, 25, 28, 31]. For the measurement of viscoelasticity of α -helix rich protein, we selected T4 lysozyme for our measurement.

In the present chapter, my aim was to measure mechanical unfolding of PTEN protein. In order to do this, we tried optimizing the protein purification at different temperatures and different incubation time durations but the yield was too low to perform the force spectroscopy measurements. For T4 Lysozyme, we were interested in measuring the viscoelasticity. For the purification of monomer, optimization was tried at different parameters but we got very less amount of pure protein. With that, I tried to form polymers. I was able to get the polyprotein but since the amount of protein was very less so we could not proceed further. In future, a more effort can be put to increase the yielding of PTEN and T4 Lysozyme and their mechanical properties can be studied.

5.2 Materials and Methods

5.2.1 Materials

All reagents and media components were purchased from Sigma-Aldrich, Himedia and TCI chemicals unless otherwise stated. Plasmid purification kits were obtained from Agilent.

5.2.2 Optimization for purification of WT-PTEN protein

WT and Mu-PTEN plasmid was transformed into DH5 α cells. To the 5 mL autoclaved LB broth media, 40 μ g/mL kanamycin (Kan) was added and an isolated single colony from the transformed DH5 α cells was inoculated. The culture was kept at 37 °C and 180 revolutions per minute (RPM) for overnight incubation. Plasmid was purified in a similar way as described in the Agilent plasmid purification kit protocol. The purity of the plasmid was checked on the 0.8% agarose gel.

The purified plasmid was transformed in *Escherichia coli* BL21(DE)3 cells. 40 µg/mL of kan was added to the 100 mL LB media. An isolated single colony of the transformed cells was inoculated at 37 °C and 180 RPM for overnight. The cells were grown in LB media at 37 °C until OD600 reached to 0.6. Induction of cells was done at different IPTG concentrations (0, 0.2, 0.4, 0.6, 0.8 and 1.0 mM) at 15 °C for 10, 16 and 18 h. 2 mL of media was taken out from each of the test tube at the above said time intervals. Media was centrifuged at 5000 RPM, 20 min. Pallet was resuspended in 1.5 mL of 1X PBS buffer, sonicated for 1 min and centrifuged at 12500 RPM, 45 min and 4 °C. Supernatant was collected in another 2 mL Eppendorf tube and pallet was resuspended in 1.5 mL of 1X PBS buffer.

The purity and molecular weight of the protein was analyzed using 12% SDS-PAGE gel electrophoresis and it has been found out that protein was going in the pallet. For that reason, different temperatures at different IPTG concentrations were tried and overexpression was checked. Similarly, IPTG optimization at 18 °C with incubation time of 18 h and 30 °C with incubation time of 6 h was checked.

But again we saw that only a little band can be seen in the supernatant (at 18 °C and 18 h incubation time) while a thick band can be seen in the pallet. So, we thought of purifying the protein at 18 °C and 18 h incubation time with a large amount of culture.

5.2.3 Large scale purification of WT - PTEN

WT-PTEN plasmid was transformed in *E. Coli* BL21(DE3) cells. The transformed cells were grown in LB media until OD600 reached 0.6. Cells were induced with 1 mM IPTG at 18 °C for 18 h. Purification was done using Ni-NTA affinity chromatography using Akta pure FPLC system (GE Healthcare). Equilibration buffer was 50 mM Tris-HCl pH 8.0, 300 mM NaCl, 20 mM Imidazole and 0.025% β-Mercaptoethanol. Protein was eluted with 250 mM imidazole buffer (50 mM Tris-HCl pH 8.0, 300 mM NaCl, 250 mM Imidazole, and 0.025% β-Mercaptoethanol).

The purity and molecular weight of the protein was checked using 12% SDS-PAGE gel electrophoresis. The imidazole was removed by dialyzing the protein in 100 mM Tris-HCl pH 8.0, 200 mM NaCl, 0.025% β -Mercaptoethanol. The fractions showing the corresponding molecular weight were pooled together, concentrated and flash frozen in liquid nitrogen with 10% glycerol. Before every measurement, concentration of protein was measured using nanodrop.

5.2.4 Purification of mutant (Mu) - PTEN

Mu-PTEN was purified in a similar way as WT - PTEN was purified at 18 °C and 18 h incubation time.

5.2.5 Optimization for purification of T4 Lysozyme mutant protein

T4 lysozyme mutant plasmid was transformed in DH5 α cells. 100 mg/mL ampicillin was added to the 10 mL of LB media. One isolated colony from the transformed DH5 α cells was inoculated and kept for incubation at 37 °C for overnight. Plasmid was purified using the protocol described in Agilent plasmid prep kit. 0.8% agarose gel was run to see the purity of the desired plasmid.

The purified plasmid was transformed in *E. coli* BL21(DE3) cells. No colony was found in the control plate while only 3 colonies were found in T4 lysozyme labelled plate. However, colonies were less in the lysozyme plate but we thought of checking the overexpression with that only. 100 mg/mL ampicillin was added to the 25 mL of LB media. Single isolated colony from the transformed BL21(DE3) cells was inoculated and kept for incubation at 37 °C and 180 RPM for overnight. Media was slightly turbid after overnight incubation. 50 mL of autoclaved LB media supplemented with 100 mg/mL ampicillin was inoculated with 1% culture. The obtained media was kept for incubation at 37 °C. When OD600 reached 0.8, 1 mM IPTG was induced and kept for incubation at 37 °C, 120 RPM for 3 h. After 3 h, the media was centrifuged at 4500 RPM, 4 °C for 30 min. A Small amount of pallet was dissolved in the lysis buffer (20 mM Tris-HCl pH 8.0, 5 μ L of 1M dithiothreitol (DTT) and 0.5 μ L of 0.1 M PMSF and the obtained cells were sonicated for 15-20 min (60% amplitude, 1s on- 3s off cycle). The sonicated protein sample was centrifuged

at 4 °C, 14500 RPM for 30 min. Supernatant was separated out and the pellet was dissolved in 20 mM Tris-HCl. 18% SDS-PAGE gel electrophoresis was run to check the protein of desired molecular weight.

We did not see any band of the desired molecular weight of the protein (gel image not shown). So, we thought of trying Rosetta cells. The protein purification was tried in a similar way as done with BL21(DE3) cells. A large number of colonies were found with the transformed Rosetta cells but we did not see any band in the 18% SDS-PAGE gel when purification was tried at 30 °C and 37 °C for 3 h and 6 h (gel images not shown). So, we thought of trying protein purification with the pLysS cells.

Till now, we were trying purification from one colony only but we did not see any band of the desired molecular weight. Then, we thought of checking the purification with 4 different colonies. For doing that, plasmid was transformed with pLysS cells. 34 mg/mL chloramphenicol and 100 mg/mL ampicillin was added to the 10 mL of autoclaved LB media. Single isolated colony from 4 different places were inoculated in 4 different falcons and kept for incubation at 37 °C. Protein was purified in a similar way as described above.

The protein of interest was checked on 18% SDS-PAGE gel, a band was seen in the pellet 4. So, we thought of purifying the protein with large culture at 37 °C for 3 h.

5.2.6 Large scale purification of T4 Lysozyme

To the 30 mL of LB solution, 100 mg/mL ampicillin (Amp) and 34 mg/mL of chloramphenicol (CLM) was added. The media was inoculated with the transformed pLysS colony 4 and kept for incubation at 37 °C for overnight. The 8 L of autoclaved LB media was supplemented with 100 mg/mL ampicillin and 34 mg/mL CLM and inoculated with 1% starter culture. The media was incubated at 37 °C until OD₆₀₀ reached 0.6-0.8. 1 mM IPTG was induced and left at 37 °C for 3 h. After 3 h, solutions were centrifuged at 4 °C, 4500 RPM and 15 min. The pellet was dissolved in 8 M urea and 20 mM Tris-HCl pH 8.0 buffer. The cells were sonicated for 45 min and the media was centrifuged at 14500 RPM, 4 °C and 45 min. Supernatant and pellet were separated. Start

buffer (8M urea and 20 mM tris-HCl pH 8.0) and elution buffer (8 M urea, 1 M NaCl and 20 mM tris-HCl pH 8.0) were filtered and kept at 4 °C. Purification was done using Carboxymethyl Sepharose (CM-Sepharose) column (GE Healthcare). 18% SDS-PAGE gel was run to check the purity and molecular weight of the desired protein. Protein was refolded with 20 mM Tris-HCl pH 8.0 and 1 M Dithiothreitol (DTT) buffer. The purity of the refolded protein was checked on 18% SDS-PAGE gel electrophoresis. The concentration of the protein was found out to be 0.337 mg/mL i.e. 18 μ M.

5.2.7 Matrix-assisted laser desorption/ionization (MALDI)

4.5 mg of DAHC (Diammonium hydrogen citrate) and 3.5 mg of DHAP (Dihydroxyacetone phosphate) were weighed separately in microcentrifuge tubes. 200 μ L of milli-Q water and 150 μ L of ethanol were added to each tube, respectively. Both the solutions were sonicated for 1 min and vortexed for another minute. Then 50 μ L of DAHC solution was transferred to DHAP solution and the resulting matrix mixture was vortexed for another minute. In a 500 μ L microcentrifuge tube, 1:1:1 ratio of T4 lysozyme protein solution, 2% trifluoroacetic acid and final matrix mixture were mixed, vortexed for 1 minute.

5.2.8 Formation of polymers from monomer of T4 Lysozyme

Since AFM has been widely applied on polyproteins. Therefore, we tried to make polymers of T4 Lysozyme protein from the monomer itself. Since, the concentration of protein was found to be very less, so we concentrated the protein to 114 μ M (500 μ L only) using amicon tubes. 18% SDS-PAGE gel was run to check the purity. The protein was pure but it was in the monomeric form. After one week, MALDI of the concentrated protein was done and peaks of the desired molecular weights till pentamers were seen with the small intensity but we were not able to see the bands in the SDS-PAGE gel. To enhance the intensity, 500 μ L of the protein sample was taken in a 5 mL eppendorf and atmospheric oxygen was purged through the balloon continuously until the protein

sample got reduced to $\sim 50 \mu\text{L}$. The eppendorf was kept open for 3 days. All the sample got evaporated and it was redissolved in 20 mL of milli-Q. The sample was given for MALDI.

5.3 Results

5.3.1 Agarose gel of PTEN and T4 Lysozyme protein

Fig. 5.4 shows the 0.8% agarose gel of PTEN and T4 Lysozyme plasmid.

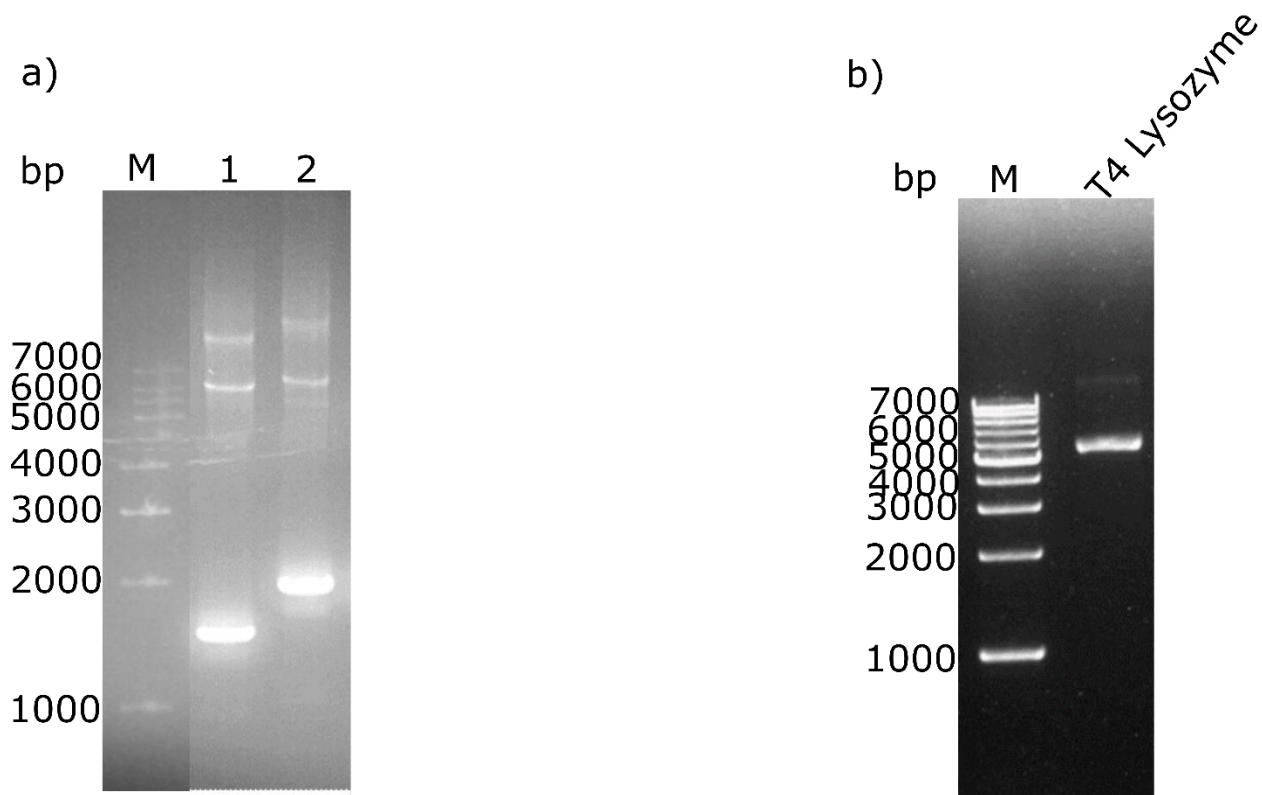


Fig. 5.4: Agarose gel images of a) PTEN and b) T4 lysozyme plasmid, where M stands for marker and bp stands for base pairs.

5.3.2 Optimization of overexpression of PTEN protein

After getting the plasmid of our interest, protein purification was tried under different conditions. Fig. 5.5, 5.6 and 5.7 shows the SDS-PAGE gel images for the IPTG optimization at 15°C for 10 h, 16 h and 18 h respectively.

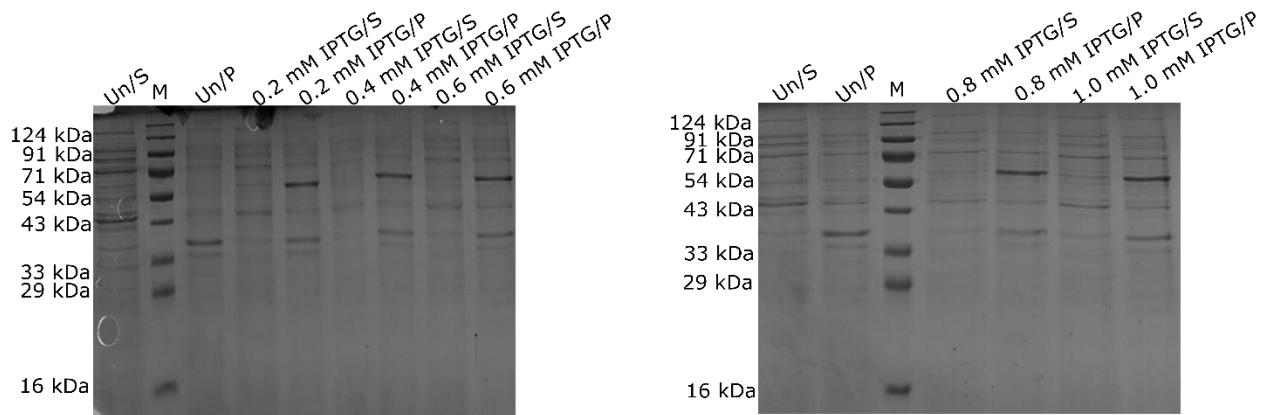


Fig. 5.5: SDS-PAGE gel for IPTG optimization at 15 °C and 10 h incubation time, where M stands for marker, S for supernatant, P for pellet and Un for uninduced.

It can be seen from the below gel images that a little band is there in the pellet between 54-71 kDa which is the molecular weight of protein but no band was seen in supernatant for 10 h incubation time.

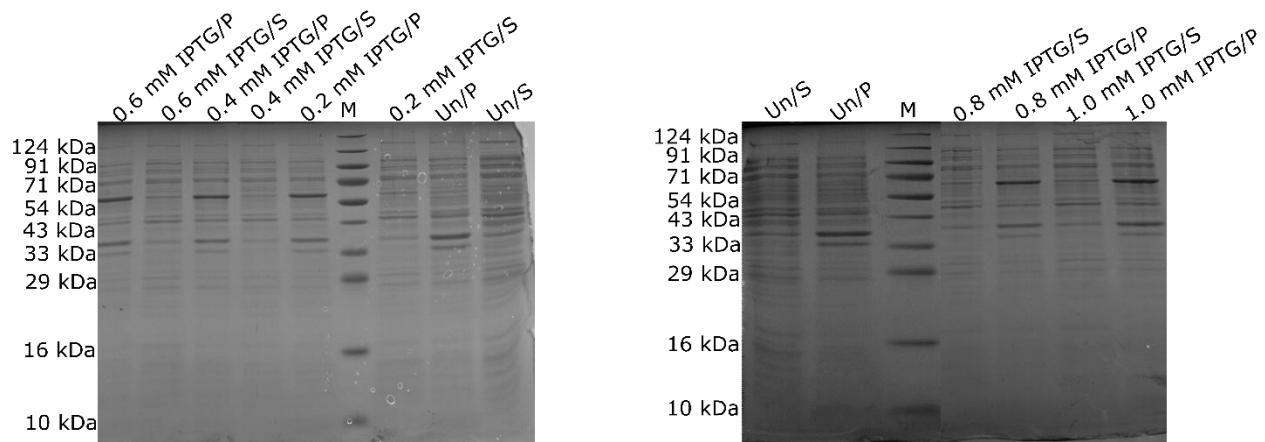


Fig. 5.6: SDS-PAGE gel for IPTG optimization at 15 °C and 16 h incubation time where M stands for marker, S for supernatant, P for pellet and Un for uninduced.

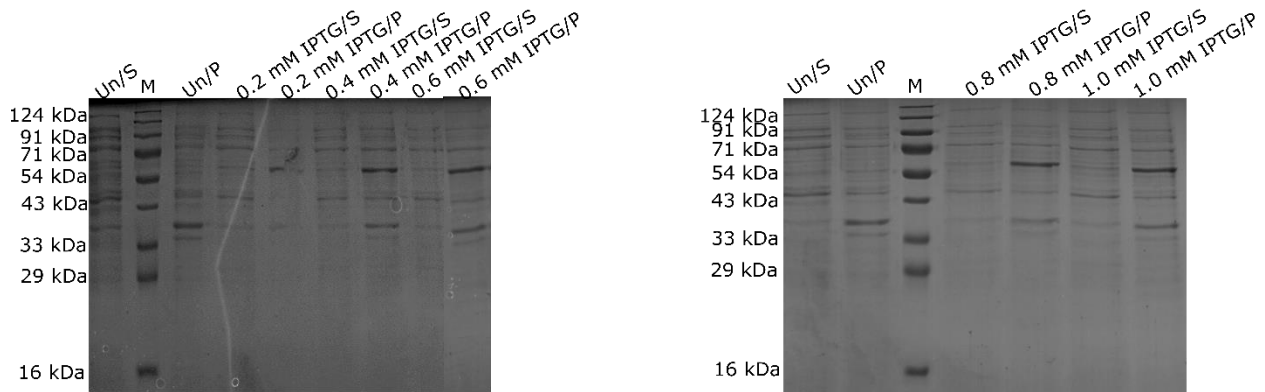


Fig. 5.7: SDS-PAGE gel for IPTG optimization at 15 °C and 18 h incubation time where M stands for marker, S for supernatant, P for pellet and Un for uninduced.

For the 16 h and 18 h incubation time, it can be seen that more of the protein was going in the pellet and a little band can be seen in supernatant. Since more of the protein was going in the pellet so, we thought of trying at 18 °C and 18 h incubation time. Fig. 5.8 shows that a slight thick band at 18 °C and 18 h incubation time was observed in pellet between 54-71 kDa as compared to 15 °C.

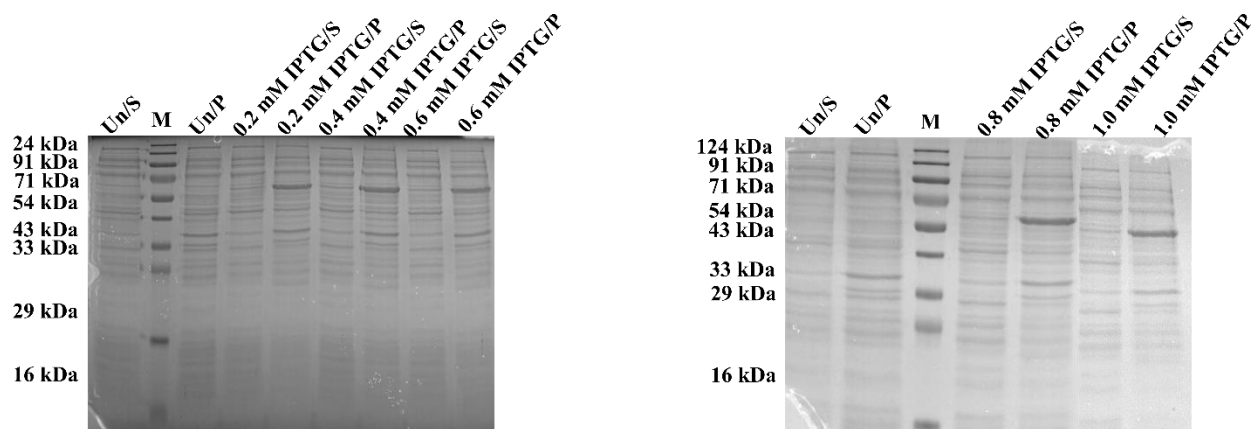


Fig. 5.8: SDS-PAGE gel for IPTG optimization at 18 °C and 18 h incubation time where M stands for marker, S for supernatant, P for pellet and Un for uninduced.

Since at 18 °C and 18 h incubation time, there was some amount of protein in the supernatant so, we thought of proceeding large culture at 18 °C and 18 h incubation time.

5.3.3 Large scale purification of WT- PTEN

Fig. 5.9 shows the SDS-PAGE gel with 2 L of LB media at 18 °C and 18 h incubation time. Below are the gel images for 150 mM elution, 300 mM elution and 500 mM elution. The protein was not so pure. The protein was not expressed that much as we can see from the below gel images.



Fig. 5.9: SDS-PAGE gel for WT-PTEN purification at 18 °C and 18 h incubation time with 2 L culture where M stands for marker.

5.3.4 Purification of Mu-PTEN

Overexpression of Mu-PTEN was checked at 18 °C and 18 h incubation time. Fig. 5.10 shows the SDS-PAGE gel image for that. It can be seen from the below gel images that a small band is there in the supernatant with small culture, however, the protein was going in the pellet also.

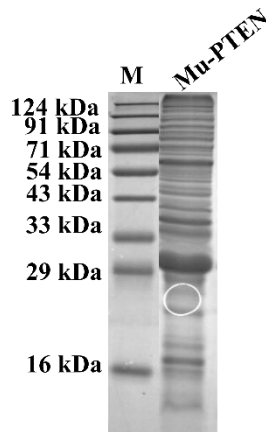


Fig. 5.10: SDS-PAGE gel for Mu-PTEN at 18 °C and 18 h incubation time where M stands for marker.

Since the protein was going in pellet for both the WT as well as for Mu-PTEN, we did not get good amount of protein for our measurement. That's why we could not proceed further.

5.3.5 Optimization of overexpression of T4 Lysozyme

After purification of the plasmid, optimization of T4 lysozyme was carried out under different conditions. Optimization with *E. coli* BL21(DE3) as well as rosetta cells was tried at 37 °C for 3 h but we did not see any band of our interest. Then we tried optimizing with pLysS cells at 37 °C for 3 h with 4 different colonies. Fig. 5.11 shows the SDS-PAGE gel image of 4 different isolated colonies.

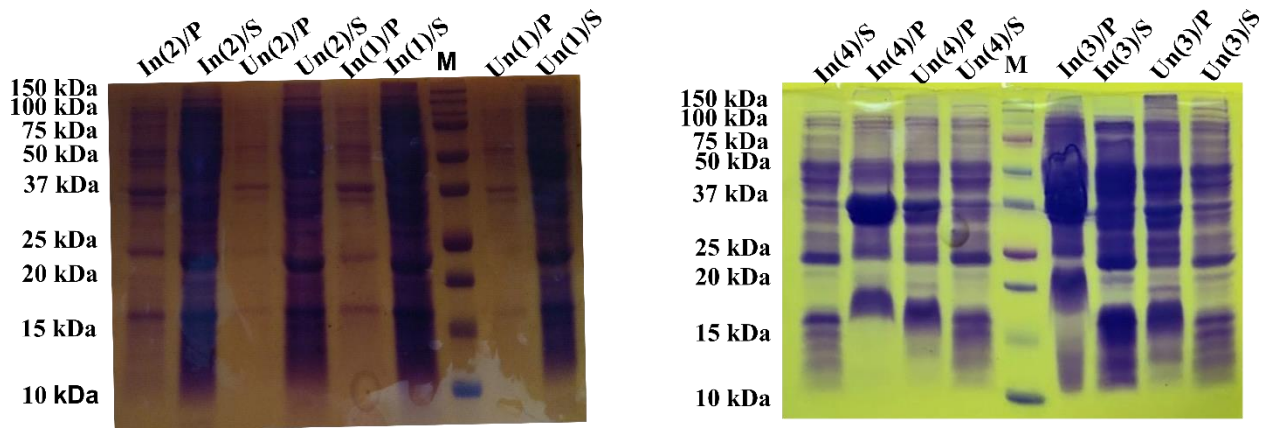


Fig. 5.11: SDS-PAGE gel for T4 Lysozyme mutant at 37 °C and 3 h incubation time (transformation done with pLysS cells), where Un stands for uninduced, In for induced, 1- 4 for single isolated colony respectively, S for supernatant and P for pellet.

It can be seen that colony 4 has a band around 18 kDa but the protein was going in the pellet.

5.3.6 Large scale purification of T4 Lysozyme

Fig. 5.12 a) shows the SDS-PAGE gel image of the protein in 8 M urea buffer. We were able to see a little band but we did not see a thick band around 18 kDa. Therefore, the protein was not getting overexpressed.

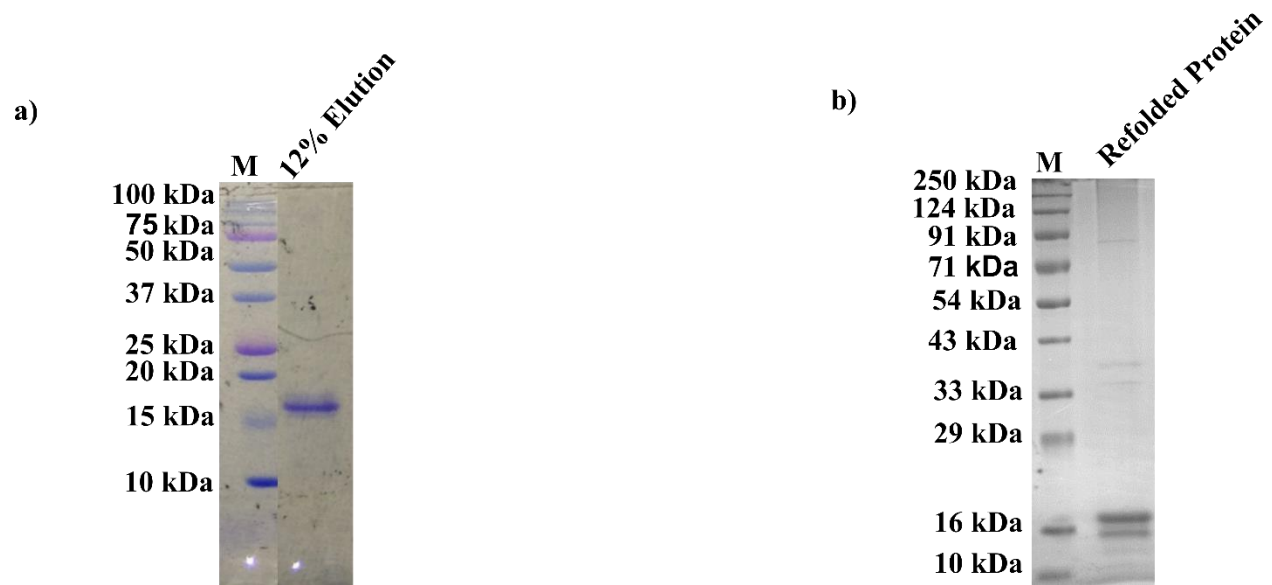


Fig. 5.12: SDS-PAGE gel image of T4 Lysozyme mutant in a) 8 M urea at 37 °C and 5 h incubation time, b) 20 mM Tris-HCl buffer pH 8.0 (transformation done with pLysS cells) where M stands for marker.

With 8 L of culture, concentration of protein was found to be 18 μ M. However, the protein was pure to some extent. Since the protein was in urea buffer so we refolded the protein in 20 mM Tris-HCl buffer pH 8.0. Fig. 5.12 b) shows the SDS-PAGE gel image of the protein refolded in 20 mM Tris-HCl pH 8.0.

5.3.7 MALDI of T4 Lysozyme protein

The protein was concentrated to 114 μ M using amicon tubes. MALDI data after one week shows the peaks till pentamers with small intensity. Fig. 5.13 shows the MALDI of T4 Lysozyme concentrated protein after one week.

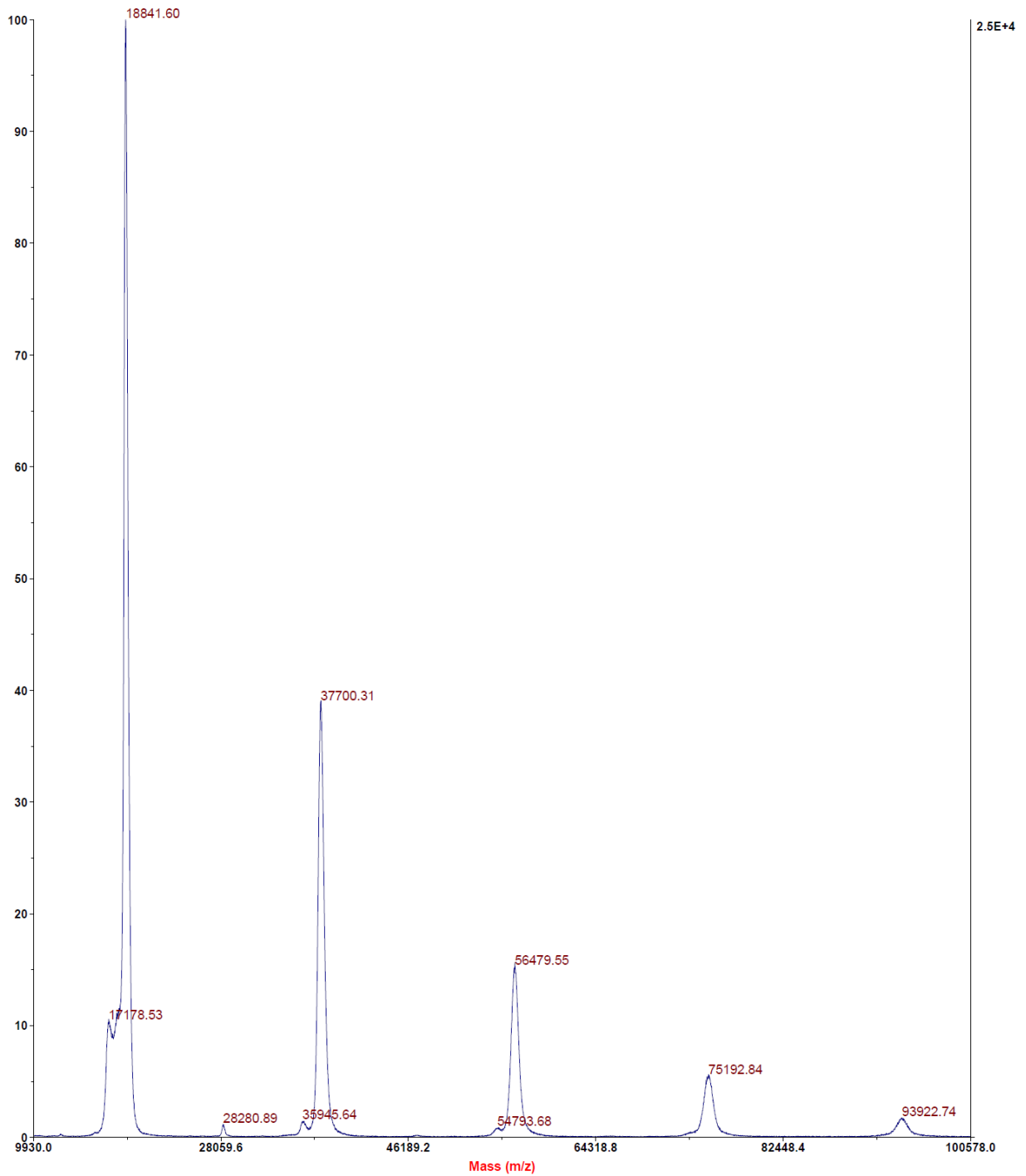


Fig. 5.13: MALDI of T4 Lysozyme mutant in DAHC and DHAP matrix.

However, the peaks were of small intensity, we have purged atmospheric oxygen for 6-7 h at room temperature Fig. 5.14 shows the MALDI of T4 lysozyme protein after supplying atmospheric oxygen. It can be seen that intensity of polymers was increased to some extent.

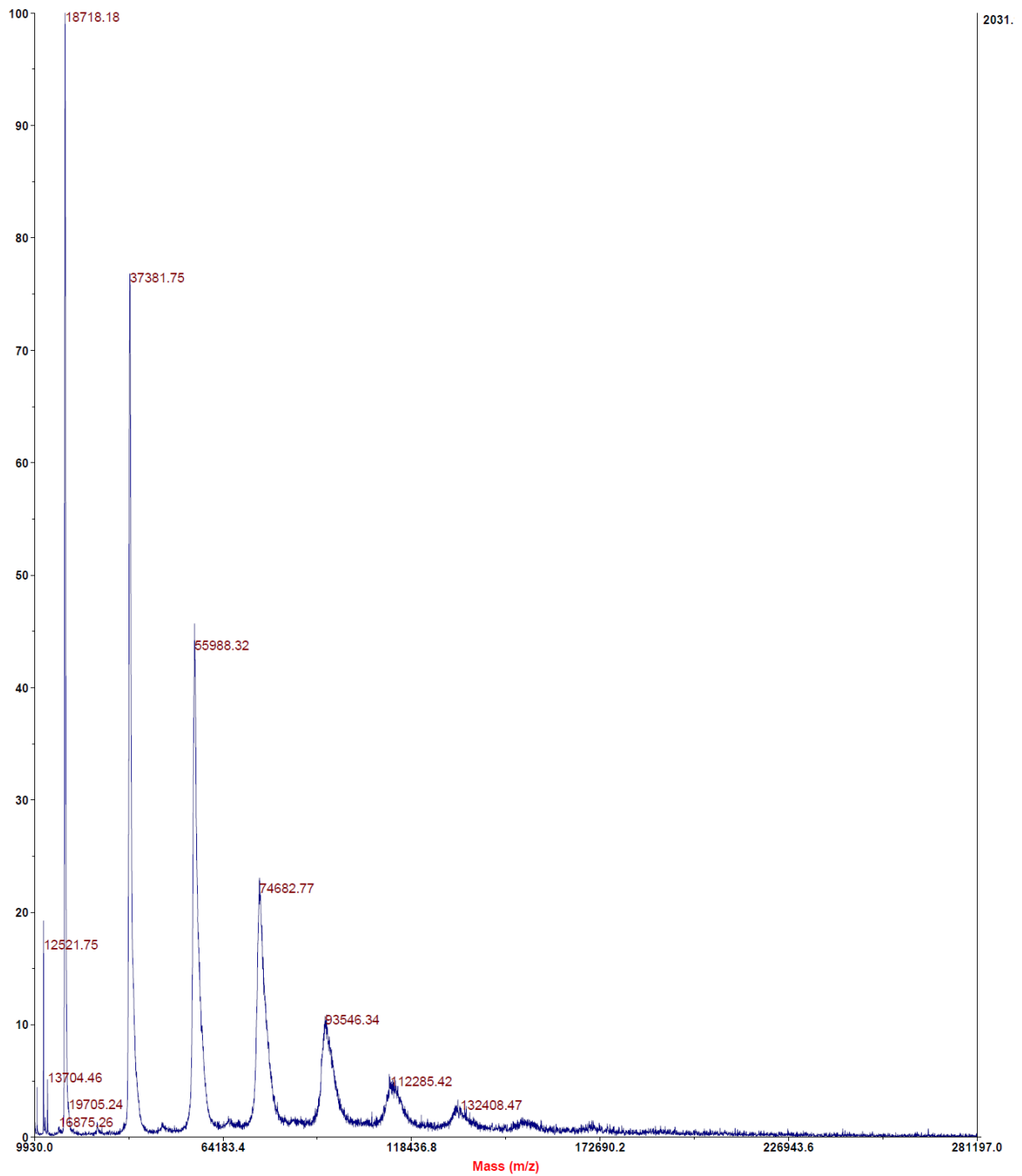


Fig. 5.14: MALDI of T4 Lysozyme mutant in DAHC and DHAP matrix after providing atmospheric oxygen with balloon for 6-7 h at room temperature.

After 5 days, we run the SDS-PAGE gel and we saw many bands in the gel. That means, t4 lysozyme was getting polymerized.

5.3.8 SDS-PAGE of the polymeric T4 Lysozyme protein

Fig. 5.15 shows the SDS-PAGE gel image of the polymeric T4 Lysozyme protein after supplying atmospheric oxygen.

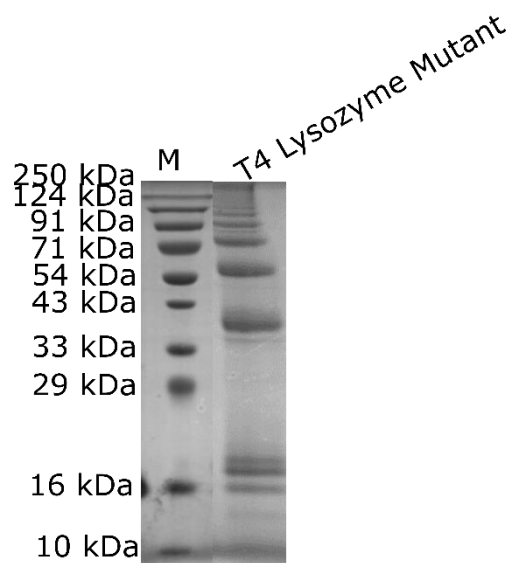


Fig. 5.15: SDS-PAGE gel for T4 Lysozyme mutant after purging atmospheric oxygen for 6-7 h, where M stands for marker.

Later, we tried to get pure protein but we did not get pure protein.

5.4 Conclusion

Purification of PTEN protein was tried at different temperature and different incubation time. It has been found out that the protein was going in the pellet. We got very less amount of protein for our measurement. So we could not proceed further.

Purification of t4 lysozyme was also tried under different conditions. Here too, the protein was going in the pellet. We tried purifying the protein from the pellet, however even with large amount of culture, we got very less amount of pure protein. We were able to form polymers from monomer by purging atmospheric oxygen using a balloon. The formation of polymers is confirmed by MALDI and SDS-PAGE. Since the amount of the protein was very less, we could not proceed for AFM experiments. Later on we tried to get pure protein but we did not get pure protein. So, we could not proceed further.

Chapter 6

Conclusion and future possibilities

6.1 Conclusion

This thesis is mainly focused on studying the mechanical properties of mouse embryonic stem cells (mESCs) and proteins when a drug molecule binds to it. Protein-drug interaction is usually studied by fluorescence, UV-Visible, circular dichroism (CD), calorimetric techniques and atomic force microscope (AFM). Previously, interaction of chloramphenicol (CLM) with human serum albumin (HSA), bovine serum albumin (BSA), lysozyme, hemoglobin and bovine pancreatic system was studied using fluorescence, CD and UV-Visible techniques [76, 78, 79, 81, 83, 181]. There are a few studies where AFM has been used for checking the alteration in mechanical properties of protein when a drug molecule binds to it. Previously, interaction of I27 with calcium was studied using AFM where unfolding force is increased by 40 pN and stiffness is measured as a result of persistence length [8]. Effect of osmolytes on the mechanical properties of fibronectin were also studied in past. The results suggest that there is an enhancement in the mechanical stability of folded domains [140–143].

As we know that mESCs has the ability to differentiate and mechanical properties vary at different stages of differentiation. Therefore, it becomes very important to study the mechanical properties as it plays an important role various functions such as cell differentiation and cell migration. Previously, it has been shown that mESCs show low cellular stiffness in comparison to differentiated cells but mechanical properties on loss of *Cltc* were not known.

In the 1st part of my thesis, interaction of CLM with titin I27 was studied using single molecule measurements (AFM) and bulk measurements (fluorescence spectroscopy) whereas In the 2nd part of my thesis, mechanical properties of mESCs were determined using AFM.

6.1.1 Interaction of Chloramphenicol with titin I27

Following conclusions can be drawn from this work:

1. Formation of protein-drug complex

It has been found that with an increase in concentration of drug, the fluorescence intensity of the protein decreases which shows that the drug is binding to protein. In order to confirm whether quenching is happening because of the drug proximity PatchDock was performed. PatchDock results showed that quenching is happening when drug comes within 5 Å of I27 protein. Mechanism of quenching was also studied using Stern-Volmer plot. The plot shows that binding is happening as a result of formation of protein-drug complex.

2. Mechanical stability of the protein as a result of protein-drug interaction

From the fluorescence data, we came to know that the interaction between the protein and drug is happening as a result of formation of protein-drug complex. To confirm the alteration in the mechanical properties of protein, AFM is used. The experiments were performed at the same concentrations as fluorescence measurements were done. The results showed that at 40 µM drug concentration, the unfolding force increased by 25 pN and decrease in the persistence length was observed in comparison to I27 alone while for other drug concentrations, there was no significant change in the unfolding force. So, the mechanical stability of the protein gets enhanced at 40 µM drug concentration. Further, to confirm the chemical stability, equilibrium denaturation experiments were performed.

3. Equilibrium denaturation experiment

Denaturation experiments were performed for I27-WT, I27 with 30 μM , 40 μM and 50 μM drug concentration. The results showed that the free energy of stabilization was more for I27 with 40 μM drug concentration in comparison to I27-WT only while there were no significant changes in free energy of stabilization for other drug concentrations. Therefore, the chemical stability of the protein is enhanced at 40 μM drug concentration.

6.1.2 Mechanical properties of mouse Embryonic Stem Cells (mESCs)

The conclusions from this work can be summarized as:

1) Clathrin knockdown results in an increased cell stiffness

Young's modulus was measured for live shScrambled, shCltc1, shCltc3 and mESCs cells treated with retinoic acid. We have found out that the Young's modulus was increased by 2.2 fold for shCltc1, 1.7 fold for shCltc3 and 2.8 fold for retinoic acid treated cells.

2) F-actin depolymerizing agents reduces the cellular stiffness of mESCs lacking *Cltc*

Young's modulus was measured for mESCs when treated with actin depolymerizing agents such as LatA and CytoD. The results showed that the young's modulus was found to be in the similar range as the young's modulus was for shScrambled cells.

6.2 Future possibilities

6.2.1 Effect of temperature and chemical denaturants on protein-drug complex

I have studied the interaction of I27 protein with CLM using AFM and fluorescence. It has been found out that the drug is stabilizing the protein chemically and mechanically. We have not

checked the effect of temperature as well as the effect of chemical denaturants on the protein-drug complex. Since, temperature and chemical denaturants such as GdmCl and urea denatures the protein. So, the effect of these on the stability of the protein-drug complex can be studied. We can check the effect on native state as well as intermediate state of protein. The same effect can be checked with other Ig domains of protein also.

6.2.2 Interaction of various antibiotics and muscle relaxants on titin I27 protein

The interaction of antibiotics such as tetracycline, kanamycin, streptomycin, gentamicin and muscle relaxants with titin I27 protein can also be checked. As tetracycline act as calcium chelator, they may result in the relaxation of the contracting muscle. Also, it has been found that matrix metalloproteinase 2(MMP-2) is a protein which is activated in heart at the time of heart attack. Doxycycline, the derivative of tetracycline, has been found to be the only drug which inhibits the MMP-2 protein [196]. Therefore, it becomes very important to study the interaction between I27 and tetracycline. Previously, effect of various antibiotics such as kanamycin, streptomycin on the isometric contraction of rat heart muscle has been studied and the effect was found to be concentration dependent [197] whereas in another study, direct negative inotropic effect on isolated rat heart muscle has been found [198]. Min et al. have compared the effects of certain antibiotics such as kanamycin, streptomycin, gentamycin and neomycin with muscle relaxants such as baclofen, tubocurarine, pancuronium, succinylcholine, and papaverine. A strong effect of these antibiotics on muscles have been found whereas baclofen, tubocurarine, pancuronium, succinylcholine does not show significant effect on the contraction of rat bladder muscle [199]. So, the effect of all these antibiotics and muscle relaxants on the chemical and mechanical stability of titin I27 protein can be studied.

6.2.3 Mechanics of PTEN and T4 Lysozyme

As we have discussed in the chapter 5, we were interested in measuring the mechanical unfolding of PTEN protein and viscoelastic behavior of T4 lysozyme protein.

For the purification of PTEN protein, we can try with the large amount of culture at 18 °C and 18 h incubation time. We can compare the unfolding behavior of WT as well as Mu-PTEN protein. For the T4 Lysozyme protein, we can try to get the pure protein with the terrific broth media with the transformed pLysS cells and then making polymers from monomer by purging atmospheric oxygen at room temperature.

References

1. Williams, P.M., Fowler, S.B., Best, R.B., Luis Toca-Herrera, J., Scott, K.A., Steward, A., Clarke, J.: Hidden complexity in the mechanical properties of titin. *Nature*. 422, 446–449 (2003). <https://doi.org/10.1038/nature01517>
2. Brockwell, D.J., Beddard, G.S., Clarkson, J., Zinober, R.C., Blake, A.W., Trinick, J., Olmsted, P.D., Smith, D.A., Radford, S.E.: The Effect of Core Destabilization on the Mechanical Resistance of I27. *Biophys. J.* 83, 458–472 (2002). [https://doi.org/10.1016/S0006-3495\(02\)75182-5](https://doi.org/10.1016/S0006-3495(02)75182-5)
3. Navizet, I., Cailliez, F., Lavery, R.: Probing protein mechanics: Residue-level properties and their in defining domains. *Biophys. J.* 87, 1426–1435 (2004). <https://doi.org/10.1529/biophysj.104.042085>
4. Gosline, J., Lillie, M., Carrington, E., Guerette, P., Ortlepp, C., Savage, K.: Elastic proteins: Biological roles and mechanical properties. *Philos. Trans. R. Soc. B Biol. Sci.* 357, 121–132 (2002). <https://doi.org/10.1098/rstb.2001.1022>
5. Hao, Y., Cheng, S., Tanaka, Y., Hosokawa, Y., Yalikun, Y., Li, M.: Mechanical properties of single cells: Measurement methods and applications. *Biotechnol. Adv.* 45, 107648 (2020). <https://doi.org/10.1016/j.biotechadv.2020.107648>
6. Granzier, H., Labeit, D., Wu, Y., Labeit, S.: Titin as a modular spring: Emerging mechanisms for elasticity control by titin in cardiac physiology and pathophysiology. *J. Muscle Res. Cell Motil.* 23, 457–471 (2002). <https://doi.org/10.1023/A:1023458406346>
7. Oravcová, J., Lindner, W.: Protein–Drug Interactions. *Encycl. Anal. Chem.* 1–26 (2000). <https://doi.org/10.1002/9780470027318.a1627>
8. DuVall, M.M., Gifford, J.L., Amrein, M., Herzog, W.: Altered mechanical properties of titin immunoglobulin domain 27 in the presence of calcium. *Eur. Biophys. J.* 42, 301–307 (2013)
9. Dong, M., Husale, S., Sahin, O.: Determination of protein structural flexibility by

- microsecond force spectroscopy. *Nat. Nanotechnol.* 4, 514–517 (2009).
<https://doi.org/10.1038/nnano.2009.156>
10. Rico, F., Su, C., Scheuring, S.: Mechanical Mapping of Single Membrane Proteins at Submolecular Resolution. 3983–3986 (2011)
 11. Herruzo, E.T., Dietz, C., Garcia, R.: Noninvasive Protein Structural Flexibility Mapping by Bimodal Dynamic Force Microscopy. 198101, 1–4 (2011).
<https://doi.org/10.1103/PhysRevLett.106.198101>
 12. Cecconi, G., Shank, E.A., Bustamante, C., Marqusee, S.: Biochemistry: Direct observation of the three-state folding of a single protein molecule. *Science* (80-.). 309, 2057–2060 (2005). <https://doi.org/10.1126/science.1116702>
 13. Jollymore, A., Lethias, C., Peng, Q., Cao, Y., Li, H.: Nanomechanical Properties of Tenascin-X Revealed by Single-Molecule Force Spectroscopy. *J. Mol. Biol.* 385, 1277–1286 (2009). <https://doi.org/10.1016/j.jmb.2008.11.038>
 14. Krieg, M., Fläschner, G., Alsteens, D., Gaub, B.M., Roos, W.H., Wuite, G.J.L., Gaub, H.E., Gerber, C., Dufrêne, Y.F., Müller, D.J.: Atomic force microscopy-based mechanobiology. *Nat. Rev. Phys.* 1, 41–57 (2019). <https://doi.org/10.1038/s42254-018-0001-7>
 15. Kellermayer, M.S.Z., Smith, S.B., Granzier, H.L., Bustamante, C.: Folding-unfolding transitions in single titin molecules characterized with laser tweezers. *Science* (80-.). 276, 1112–1116 (1997). <https://doi.org/10.1126/science.276.5315.1112>
 16. Wang, H., Gao, X., Hu, X., Hu, X., Hu, C., Li, H.: Mechanical Unfolding and Folding of a Complex Slipknot Protein Probed by Using Optical Tweezers. *Biochemistry.* 58, 4751–4760 (2019). <https://doi.org/10.1021/acs.biochem.9b00320>
 17. Carrion-Vazquez, M., Oberhauser, A.F., Fowler, S.B., Marszalek, P.E., Broedel, S.E., Clarke, J., Fernandez, J.M.: Mechanical and chemical unfolding of a single protein: A comparison. *Proc. Natl. Acad. Sci. U. S. A.* 96, 3694–3699 (1999).
<https://doi.org/10.1073/pnas.96.7.3694>

18. Rief, M., Gautel, M., Oesterhelt, F., Fernandez, J.M., Gaub, H.E.: Reversible unfolding of individual titin immunoglobulin domains by AFM. *Science* (80-.). 276, 1109–1112 (1997). <https://doi.org/10.1126/science.276.5315.1109>
19. Taniguchi, Y., Brockwell, D.J., Kawakami, M.: The Effect of Temperature on Mechanical Resistance of the Native and Intermediate States of I27. 95, 5296–5305 (2008). <https://doi.org/10.1529/biophysj.108.141275>
20. Peng, Q., Li, H.: Atomic force microscopy reveals parallel mechanical unfolding pathways of T4 lysozyme: Evidence for a kinetic partitioning mechanism. *Proc. Natl. Acad. Sci. U. S. A.* 105, 1885–1890 (2008). <https://doi.org/10.1073/pnas.0706775105>
21. Yang, G., Cecconi, C., Baase, W.A., Vetter, I.R., Breyer, W.A., Haack, J.A., Matthews, B.W., Dahlquist, F.W., Bustamante, C.: Solid-state synthesis and mechanical unfolding of polymers of T4 lysozyme. 97, 139–144 (2000)
22. Amin, S., Rega, C.A., Jankevics, H.: Detection of viscoelasticity in aggregating dilute protein solutions through dynamic light scattering-based optical microrheology. *Rheol. Acta.* 51, 329–342 (2012). <https://doi.org/10.1007/s00397-011-0606-6>
23. Wang, Y., Zocchi, G.: Viscoelastic transition and yield strain of the folded protein. *PLoS One.* 6, (2011). <https://doi.org/10.1371/journal.pone.0028097>
24. Kawakami, M., Byrne, K., Brockwell, D.J., Radford, S.E., Smith, D.A.: Viscoelastic study of the mechanical unfolding of a protein by AFM. *Biophys. J.* 91, L16–L18 (2006). <https://doi.org/10.1529/biophysj.106.085019>
25. Bippes, C.A., Humphris, A.D.L., Stark, M., Müller, D.J., Janovjak, H.: Direct measurement of single-molecule visco-elasticity in atomic force microscope force-extension experiments. *Eur. Biophys. J.* 35, 287–292 (2006). <https://doi.org/10.1007/s00249-005-0023-9>
26. Janovjak, H., Müller, D.J., Humphris, A.D.L.: Molecular force modulation spectroscopy revealing the dynamic response of single bacteriorhodopsins. *Biophys. J.* 88, 1423–1431 (2005). <https://doi.org/10.1529/biophysj.104.052746>

27. Medalsy, I.D., Müller, D.J.: Nanomechanical properties of proteins and membranes depend on loading rate and electrostatic interactions. *ACS Nano*. 7, 2642–2650 (2013). <https://doi.org/10.1021/nn400015z>
28. Benedetti, F., Gazizova, Y., Kulik, A.J., Marszalek, P.E., Klinov, D. V., Dietler, G., Sekatskii, S.K.: Can Dissipative Properties of Single Molecules Be Extracted from a Force Spectroscopy Experiment? *Biophys. J.* 111, 1163–1172 (2016). <https://doi.org/10.1016/j.bpj.2016.08.018>
29. Kawakami, M., Byrne, K., Khatri, B.S., Mcleish, T.C.B., Radford, S.E., Smith, D.A.: Viscoelastic measurements of single molecules on a millisecond time scale by magnetically driven oscillation of an atomic force microscope cantilever. *Langmuir*. 21, 4765–4772 (2005). <https://doi.org/10.1021/la0469699>
30. Khatri, B.S., Byrne, K., Kawakami, M., Brockwell, D.J., Smith, D.A., Radford, S.E., McLeish, T.C.B.: Internal friction of single polypeptide chains at high stretch. *Faraday Discuss.* 139, 35–51 (2008). <https://doi.org/10.1039/b716418c>
31. Rajput, S.S., Deopa, S.P.S., Yadav, J., Ahlawat, V., Talele, S., Patil, S.: The nano-scale viscoelasticity using atomic force microscopy in liquid environment. *Nanotechnology*. 32, (2021). <https://doi.org/10.1088/1361-6528/abc5f3>
32. Yuan, C., Chen, A., Kolb, P., Moy, V.T.: Energy landscape of streptavidin-biotin complexes measured by atomic force microscopy. *Biochemistry*. 39, 10219–10223 (2000). <https://doi.org/10.1021/bi992715o>
33. Fritz, J., Katopodis, A.G., Kolbinger, F., Anselmetti, D.: Force-mediated kinetics of single P-selectin/ligand complexes observed by atomic force microscopy. *Proc. Natl. Acad. Sci. U. S. A.* 95, 12283–12288 (1998). <https://doi.org/10.1073/pnas.95.21.12283>
34. McAllister, C., Karymov, M.A., Kawano, Y., Lushnikov, A.Y., Mikheikin, A., Uversky, V.N., Lyubchenko, Y.L.: Protein interactions and misfolding analyzed by AFM force spectroscopy. *J. Mol. Biol.* 354, 1028–1042 (2005). <https://doi.org/10.1016/j.jmb.2005.10.012>

35. Shimizu, Y., Kihara, T., Haghparast, S.M.A., Yuba, S., Miyake, J.: Simple display system of mechanical properties of cells and their dispersion. *PLoS One*. 7, (2012).
<https://doi.org/10.1371/journal.pone.0034305>
36. Pollard, T.D., Cooper, J.A.: Actin, a central player in cell shape and movement. *Science* (80-.). 326, 1208–1212 (2009). <https://doi.org/10.1126/science.1175862>
37. Oosterwyck, P.H. Van: Cell mechanics and mechanotransduction
38. A-hassan, E., Heinz, W.F., Antonik, M.D., Costa, N.P.D., Nageswaran, S., Schoenenberger, C., Hoh, J.H.: Relative Microelastic Mapping of Living Cells by Atomic Force Microscopy. *Biophys. J.* 74, 1564–1578 (1998). [https://doi.org/10.1016/S0006-3495\(98\)77868-3](https://doi.org/10.1016/S0006-3495(98)77868-3)
39. Bustanji, Y., Arciola, C.R., Conti, M., Mandello, E., Montanaro, L., Samorí, B.: Dynamics of the interaction between a fibronectin molecule and a living bacterium under mechanical force. *Proc. Natl. Acad. Sci. U. S. A.* 100, 13292–13297 (2003).
<https://doi.org/10.1073/pnas.1735343100>
40. Touhami, A., Nysten, B., Dufrêne, Y.F.: Nanoscale mapping of the elasticity of microbial cells by atomic force microscopy. *Langmuir*. 19, 4539–4543 (2003).
<https://doi.org/10.1021/la034136x>
41. Rico, F., Roca-Cusachs, P., Gavara, N., Farré, R., Rotger, M., Navajas, D.: Probing mechanical properties of living cells by atomic force microscopy with blunted pyramidal cantilever tips. *Phys. Rev. E - Stat. Nonlinear, Soft Matter Phys.* 72, 1–10 (2005).
<https://doi.org/10.1103/PhysRevE.72.021914>
42. Rosenbluth, M.J., Lam, W.A., Fletcher, D.A.: Force microscopy of nonadherent cells: A comparison of leukemia cell deformability. *Biophys. J.* 90, 2994–3003 (2006).
<https://doi.org/10.1529/biophysj.105.067496>
43. Faria, E.C., Ma, N., Gazi, E., Gardner, P., Brown, M., Clarke, N.W., Snook, R.D.: Measurement of elastic properties of prostate cancer cells using AFM. *Analyst*. 133, 1498–1500 (2008). <https://doi.org/10.1039/b803355b>

44. Hammerick, K.E., Huang, Z., Sun, N., Lam, M.T., Prinz, F.B., Wu, J.C., Commons, G.W., Longaker, M.T.: Elastic properties of induced pluripotent stem cells. *Tissue Eng. - Part A*. 17, 495–502 (2011). <https://doi.org/10.1089/ten.tea.2010.0211>
45. Pillarisetti, A., Desai, J.P., Ladjal, H., Schiffmacher, A., Ferreira, A., Keefer, C.L.: Mechanical phenotyping of mouse embryonic stem cells: Increase in stiffness with differentiation. *Cell. Reprogram.* 13, 371–380 (2011). <https://doi.org/10.1089/cell.2011.0028>
46. Beaussart, A., El-Kirat-Chatel, S., Herman, P., Alsteens, D., Mahillon, J., Hols, P., Dufrêne, Y.F.: Single-cell force spectroscopy of probiotic bacteria. *Biophys. J.* 104, 1886–1892 (2013). <https://doi.org/10.1016/j.bpj.2013.03.046>
47. Magonov, S.N., Reneker, D.H.: Characterization of polymer surfaces with atomic force microscopy. *Annu. Rev. Mater. Sci.* 27, 175–222 (1997). <https://doi.org/10.1146/annurev.matsci.27.1.175>
48. Radmacher, M.: Measuring the elastic properties of biological samples with the AFM. *IEEE Eng. Med. Biol. Mag.* 16, 47–57 (1997). <https://doi.org/10.1109/51.582176>
49. Frey, M.T., Engler, A., Discher, D.E., Lee, J., Wang, Y.L.: Microscopic Methods for Measuring the Elasticity of Gel Substrates for Cell Culture: Microspheres, Microindenters, and Atomic Force Microscopy. *Methods Cell Biol.* 83, 47–65 (2007). [https://doi.org/10.1016/S0091-679X\(07\)83003-2](https://doi.org/10.1016/S0091-679X(07)83003-2)
50. Engler, A.J., Rehfeldt, F., Sen, S., Discher, D.E.: Microtissue Elasticity: Measurements by Atomic Force Microscopy and Its Influence on Cell Differentiation. *Methods Cell Biol.* 83, 521–545 (2007). [https://doi.org/10.1016/S0091-679X\(07\)83022-6](https://doi.org/10.1016/S0091-679X(07)83022-6)
51. Ludwig, T., Kirmse, R., Poole, K., Schwarz, U.S.: Probing cellular microenvironments and tissue remodeling by atomic force microscopy. *Pflugers Arch. Eur. J. Physiol.* 456, 29–49 (2008). <https://doi.org/10.1007/s00424-007-0398-9>
52. Nautiyal, P., Alam, F., Balani, K., Agarwal, A.: The Role of Nanomechanics in Healthcare. *Adv. Healthc. Mater.* 7, 1–28 (2018).

<https://doi.org/10.1002/adhm.201700793>

53. Rosenhek-Goldian, I., Cohen, S.R.: Nanomechanics of Biomaterials – from Cells to Shells. *Isr. J. Chem.* 1171–1184 (2020). <https://doi.org/10.1002/ijch.202000079>
54. Style, R.W., Boltyanskiy, R., German, G.K., Hyland, C., Macminn, C.W., Mertz, A.F., Wilen, L.A., Xu, Y., Dufresne, E.R.: Traction force microscopy in physics and biology. *Soft Matter*. 10, 4047–4055 (2014). <https://doi.org/10.1039/c4sm00264d>
55. Du Roure, O., Saez, A., Buguin, A., Austin, R.H., Chavrier, P., Siberzan, P., Ladoux, B.: Force mapping in epithelial cell migration. *Proc. Natl. Acad. Sci. U. S. A.* 102, 2390–2395 (2005). <https://doi.org/10.1073/pnas.0408482102>
56. Dembo, M., Wang, Y.L.: Stresses at the cell-to-substrate interface during locomotion of fibroblasts. *Biophys. J.* 76, 2307–2316 (1999). [https://doi.org/10.1016/S0006-3495\(99\)77386-8](https://doi.org/10.1016/S0006-3495(99)77386-8)
57. Trepap, X., Wasserman, M.R., Angelini, T.E., Millet, E., Weitz, D.A., Butler, J.P., Fredberg, J.J.: Physical forces during collective cell migration. *Nat. Phys.* 5, 426–430 (2009). <https://doi.org/10.1038/nphys1269>
58. Evans, E., Ritchie, K., Merkel, R.: Sensitive force technique to probe molecular adhesion and structural linkages at biological interfaces. *Biophys. J.* 68, 2580–2587 (1995). [https://doi.org/10.1016/S0006-3495\(95\)80441-8](https://doi.org/10.1016/S0006-3495(95)80441-8)
59. Gourier, C., Jegou, A., Husson, J., Pincet, F.: A Nanospring Named Erythrocyte. The Biomembrane Force Probe. *Cell. Mol. Bioeng.* 1, 263–275 (2008). <https://doi.org/10.1007/s12195-008-0030-x>
60. Litvinov, R.I., Shuman, H., Bennett, J.S., Weisel, J.W.: Binding strength and activation state of single fibrinogen-integrin pairs on living cells. *Proc. Natl. Acad. Sci. U. S. A.* 99, 7426–7431 (2002). <https://doi.org/10.1073/pnas.112194999>
61. Thalhammer, G., Steiger, R., Bernet, S., Ritsch-Marte, M.: Optical macro-tweezers: Trapping of highly motile micro-organisms. *J. Opt.* 13, (2011).

<https://doi.org/10.1088/2040-8978/13/4/044024>

62. Huber, F., Hegner, M., Gerber, C., Güntherodt, H.J., Lang, H.P.: Label free analysis of transcription factors using microcantilever arrays. *Biosens. Bioelectron.* 21, 1599–1605 (2006). <https://doi.org/10.1016/j.bios.2005.07.018>
63. Wang, X., Hu, X., Kawazoe, N., Yang, Y., Chen, G.: Manipulating Cell Nanomechanics Using Micropatterns. *Adv. Funct. Mater.* 26, 7634–7643 (2016). <https://doi.org/10.1002/adfm.201601585>
64. Manuscript, A.: Ac D Par Te a U G Cl Ía U It Es Ac Ac It Es Ac. *Nat. Methods.* 5, 491–505 (2012). <https://doi.org/10.1038/nmeth.1218>. Single-molecule
65. Plotnikov, S. V., Sabass, B., Schwarz, U.S., Waterman, C.M.: High-Resolution Traction Force Microscopy. Elsevier Inc. (2014)
66. Sobyte, A., Kolding, A., Lund, M.-L.K., Jensen, M.D.: Protein Stability - A study of the stability of Hen Egg-White Lysozyme exposed to chemical and thermal denaturation at pH 4, pH 7, and pH 10. 95 (2015)
67. Chignell, C.F.: Physical Methods for Studying Drug-Protein Binding. *Concepts Biochem. Pharmacol.* 187–212 (1971). https://doi.org/10.1007/978-3-642-65052-9_9
68. Lázaro, E., Lowe, P.J., Briand, X., Faller, B.: New approach to measure protein binding based on a parallel artificial membrane assay and human serum albumin. *J. Med. Chem.* 51, 2009–2017 (2008). <https://doi.org/10.1021/jm7012826>
69. Vuignier, K., Schappler, J., Veuthey, J.L., Carrupt, P.A., Martel, S.: Drug-protein binding: A critical review of analytical tools. *Anal. Bioanal. Chem.* 398, 53–66 (2010). <https://doi.org/10.1007/s00216-010-3737-1>
70. Cao, Y., Balamurali, M.M., Sharma, D., Li, H.: A functional single-molecule binding assay via force spectroscopy. *Proc. Natl. Acad. Sci. U. S. A.* 104, 15677–15681 (2007). <https://doi.org/10.1073/pnas.0705367104>

71. Aggarwal, V., Kulothungan, S.R., Balamurali, M.M., Saranya, S.R., Varadarajan, R., Ainavarapu, S.R.K.: Ligand-modulated parallel mechanical unfolding pathways of maltose-binding proteins. *J. Biol. Chem.* 286, 28056–28065 (2011).
<https://doi.org/10.1074/jbc.M111.249045>
72. Hu, X., Li, H.: Force spectroscopy studies on protein-ligand interactions: A single protein mechanics perspective. *FEBS Lett.* 588, 3613–3620 (2014).
<https://doi.org/10.1016/j.febslet.2014.04.009>
73. Ainavarapu, S.R.K., Li, L., Badilla, C.L., Fernandez, J.M.: Ligand binding modulates the mechanical stability of dihydrofolate reductase. *Biophys. J.* 89, 3337–3344 (2005).
<https://doi.org/10.1529/biophysj.105.062034>
74. Hann, E., Kirkpatrick, N., Kleanthous, C., Smith, D.A., Radford, S.E., Brockwell, D.J.: The effect of protein complexation on the mechanical stability of Im9. *Biophys. J.* 92, L79–L81 (2007). <https://doi.org/10.1529/biophysj.106.102475>
75. Bi, S., Song, D., Tian, Y., Zhou, X., Liu, Z., Zhang, H.: Molecular spectroscopic study on the interaction of tetracyclines with serum albumins. *Spectrochim. Acta - Part A Mol. Biomol. Spectrosc.* 61, 629–636 (2005). <https://doi.org/10.1016/j.saa.2004.05.028>
76. Zhang, J., Chen, L., Zeng, B., Kang, Q., Dai, L.: Study on the binding of chloroamphenicol with bovine serum albumin by fluorescence and UV-vis spectroscopy. *Spectrochim. Acta - Part A Mol. Biomol. Spectrosc.* 105, 74–79 (2013).
<https://doi.org/10.1016/j.saa.2012.11.064>
77. Guo, X.J., Jing, K., Guo, C., Jiang, Y.C., Tong, J., Han, X.W.: The investigation of the interaction between oxybutynin hydrochloride and bovine serum albumin by spectroscopic methods. *J. Lumin.* 130, 2281–2287 (2010).
<https://doi.org/10.1016/j.jlumin.2010.07.005>
78. Panov, V., Shipanova, I., Michtchenko, A., Shabunin, I., Shimanovskii, N., Sibeldina, L., Sergeev, P.: ¹H and ¹³C NMR study of the molecular interaction mechanism between chloramphenicol and human serum albumin. *Biochem. Mol. Biol. Int.* 35, 457–460 (1995)

79. Ding, F., Zhao, G., Chen, S., Liu, F., Sun, Y., Zhang, li: Chloramphenicol binding to human serum albumin: Determination of binding constants and binding sites by steady-state fluorescence. *J. Mol. Struct.* 929, 159-166. (2009).
<https://doi.org/10.1016/j.molstruc.2009.04.018>
80. Yasseen, Z.J., El Ghossain, M.O.: Studies on Binding of Widely used Drugs with Human Serum Albumin at Different Temperatures and PHs. *J. Biomed. Sci.* 5, 1–8 (2016).
<https://doi.org/10.4172/2254-609x.100033>
81. Ding, F., Liu, W., Sun, Y., Sun, Y., Yang, X.L., Zhang, L.: Analysis of conjugation of chloramphenicol and hemoglobin by fluorescence, circular dichroism and molecular modeling. *J. Mol. Struct.* 1007, 81–87 (2012).
<https://doi.org/10.1016/j.molstruc.2011.10.022>
82. Yue, Y., Chen, X., Qin, J., Yao, X.: Spectroscopic investigation on the binding of antineoplastic drug oxaliplatin to human serum albumin and molecular modeling. *Colloids Surfaces B Biointerfaces.* 69, 51–57 (2009).
<https://doi.org/10.1016/j.colsurfb.2008.10.016>
83. Ding, F., Zhao, G., Huang, J., Sun, Y., Zhang, li: Fluorescence spectroscopic investigation of the interaction between chloramphenicol and lysozyme. *Eur. J. Med. Chem.* 44, 4083-4089. (2009). <https://doi.org/10.1016/j.ejmech.2009.04.047>
84. Daneshgar, P., Moosavi-Movahedi, A.A., Norouzi, P., Ganjali, M.R., Madadkar-Sobhani, A., Saboury, A.A.: Molecular interaction of human serum albumin with paracetamol: Spectroscopic and molecular modeling studies. *Int. J. Biol. Macromol.* 45, 129–134 (2009). <https://doi.org/10.1016/j.ijbiomac.2009.04.011>
85. Cao, H., Yi, Y.: Study on the interaction of chromate with bovine serum albumin by spectroscopic method. *BioMetals.* 30, 529–539 (2017). <https://doi.org/10.1007/s10534-017-0022-1>
86. AFM assesment of mechanical properties of stem cells during differentiation.pdf
87. Wang, X., Bleher, R., Brown, M.E., Garcia, J.G.N., Dudek, S.M., Shekhawat, G.S.,

- Dravid, V.P.: Nano-Biomechanical Study of Spatio-Temporal Cytoskeleton Rearrangements that Determine Subcellular Mechanical Properties and Endothelial Permeability. *Sci. Rep.* 5, 1–11 (2015). <https://doi.org/10.1038/srep11097>
88. Li, M., Dang, D., Liu, L., Xi, N., Wang, Y.: Atomic force microscopy in characterizing cell mechanics for biomedical applications: A review. *IEEE Trans. Nanobioscience.* 16, 523–540 (2017). <https://doi.org/10.1109/TNB.2017.2714462>
89. Li, M., Liu, L., Xiao, X., Xi, N., Wang, Y.: Viscoelastic Properties Measurement of Human Lymphocytes by Atomic Force Microscopy Based on Magnetic Beads Cell Isolation. *IEEE Trans. Nanobioscience.* 15, 398–411 (2016). <https://doi.org/10.1109/TNB.2016.2547639>
90. Docheva, D., Padula, D., Popov, C., Mutschler, W., Clausen-Schaumann, H., Schieker, M.: Researching into the cellular shape, volume and elasticity of mesenchymal stem cells, osteoblasts and osteosarcoma cells by atomic force microscopy: *Stem Cells. J. Cell. Mol. Med.* 12, 537–552 (2008). <https://doi.org/10.1111/j.1582-4934.2007.00138.x>
91. Titushkin, I., Cho, M.: Modulation of cellular mechanics during osteogenic differentiation of human mesenchymal stem cells. *Biophys. J.* 93, 3693–3702 (2007). <https://doi.org/10.1529/biophysj.107.107797>
92. Zweier: 基因的改变 NIH Public Access. *Bone.* 23, 1–7 (2014). <https://doi.org/10.1097/MAT.0b013e31802deb2d>. Cytoskeletal
93. Yadav, J., Kumar, Y., Singaraju, G.S., Patil, S.: Interaction of chloramphenicol with titin I27 probed using single-molecule force spectroscopy. 191–204 (2021)
94. Mote, R.D., Yadav, J., Singh, S.B., Tiwari, M., Shinde, L. V., Patil, S., Subramanyam, D.: Pluripotency of embryonic stem cells lacking clathrin-mediated endocytosis cannot be rescued by restoring cellular stiffness. *J. Biol. Chem.* 295, 16888–16896 (2020). <https://doi.org/10.1074/jbc.AC120.014343>
95. Gunning, A.P., Morris, V.J.: Food Hydrocolloids Getting the feel of food structure with

- atomic force microscopy. *Food Hydrocoll.* 78, 62–76 (2018).
<https://doi.org/10.1016/j.foodhyd.2017.05.017>
96. Techniques for characterizing the structure and properties of polymer nanocomposites. 74–88 (2013). <https://doi.org/10.1533/9780857097828.1.74>
97. Farre, M.: *Introduction to the Analysis and Risk of Nanomaterials in Environmental and Food.* (2012)
98. Stylianou, A., Kontomaris, S.V., Grant, C., Alexandratou, E.: Atomic force microscopy on biological materials related to pathological conditions. *Scanning.* 2019, (2019).
<https://doi.org/10.1155/2019/8452851>
99. Scheuring, S., Ringler, P., Borgnia, M., Stahlberg, H., Müller, D.J., Agre, P., Engel, A.: High resolution AFM topographs of the Escherichia coli water channel aquaporin Z. *EMBO J.* 18, 4981–4987 (1999). <https://doi.org/10.1093/emboj/18.18.4981>
100. Walz, T., Tittmann, P., Fuchs, K.H., Müller, D.J., Smith, B.L., Agre, P., Gross, H., Engel, A.: Surface topographies at subnanometer-resolution reveal asymmetry and sidedness of aquaporin-1. *J. Mol. Biol.* 264, 907–918 (1996). <https://doi.org/10.1006/jmbi.1996.0686>
101. Müller, D.J., Schabert, F.A., Büldt, G., Engel, A.: Imaging purple membranes in aqueous solutions at sub-nanometer resolution by atomic force microscopy. *Biophys. J.* 68, 1681–1686 (1995). [https://doi.org/10.1016/S0006-3495\(95\)80345-0](https://doi.org/10.1016/S0006-3495(95)80345-0)
102. Drolle, E., Hane, F., Lee, B., Leonenko, Z.: Atomic force microscopy to study molecular mechanisms of amyloid fibril formation and toxicity in Alzheimer’s disease. *Drug Metab. Rev.* 46, 207–223 (2014). <https://doi.org/10.3109/03602532.2014.882354>
103. Garcia, R.: Nanomechanical mapping of soft materials with the atomic force microscope: Methods, theory and applications. *Chem. Soc. Rev.* 49, 5850–5884 (2020).
<https://doi.org/10.1039/d0cs00318b>
104. Cascione, M., Matteis, V.D.E., Rinaldi, R., Leporatti, S.: Atomic Force Microscopy Combined with Optical Microscopy for Cells Investigation. 00, 1–15 (2016).

<https://doi.org/10.1002/jemt.22696>

105. Staunton, J.R., Doss, B.L., Lindsay, S., Ros, R.: Correlating confocal microscopy and atomic force indentation reveals metastatic cancer cells stiffen during invasion into collagen I matrices. *Nat. Publ. Gr.* 1–15 (2016). <https://doi.org/10.1038/srep19686>
106. Stylianou, A., Politopoulos, K., Kyriazi, M., Yova, D.: Biomedical Signal Processing and Control Combined information from AFM imaging and SHG signal analysis of collagen thin films. *Biomed. Signal Process. Control.* 6, 307–313 (2011).
<https://doi.org/10.1016/j.bspc.2011.02.006>
107. Santos, N.C., Castanho, M.A.R.B.: An overview of the biophysical applications of atomic force microscopy. *Biophys. Chem.* 107, 133–149 (2004).
<https://doi.org/10.1016/j.bpc.2003.09.001>
108. Unfolding, S.P., Rief, M.: Chapter 13. 783, 233–250. <https://doi.org/10.1007/978-1-61779-282-3>
109. Brukman, M.J., Bonnell, D.A.: Probing physical properties at the nanoscale. *Phys. Today.* 61, 36–42 (2008). <https://doi.org/10.1063/1.2947647>
110. Faulk, J.K., Edwards, D.T., Bull, M.S., Perkins, T.T.: Improved Force Spectroscopy Using Focused-Ion-Beam-Modified Cantilevers. Elsevier Inc. (2017)
111. Bull, M.S., Sullan, R.M.A., Li, H., Perkins, T.T.: Improved single molecule force spectroscopy using micromachined cantilevers. *ACS Nano.* 8, 4984–4995 (2014).
<https://doi.org/10.1021/nn5010588>
112. Edwards, D.T., Perkins, T.T.: Optimizing force spectroscopy by modifying commercial cantilevers: Improved stability, precision, and temporal resolution. *J. Struct. Biol.* 197, 13–25 (2017). <https://doi.org/10.1016/j.jsb.2016.01.009>
113. Tortonese, M.: Marco Tortonese. *Eng. Med. Biol.* (1997)
114. Hertz, T.: Determining the elastic modulus of biological samples using atomic force

microscopy. 1–9

115. Duf re, Y.F., Mart nez-Mart n, D., Medalsy, I., Alsteens, D., M ller, D.J.: Multiparametric imaging of biological systems by force-distance curve-based AFM. *Nat. Methods*. 10, 847–854 (2013). <https://doi.org/10.1038/nmeth.2602>
116. Hansma, H.G., Kim, K.J., Laney, D.E., Garcia, R.A., Argaman, M., Allen, M.J., Parsons, S.M.: Properties of biomolecules measured from atomic force microscope images: A review. *J. Struct. Biol.* 119, 99–108 (1997). <https://doi.org/10.1006/jsbi.1997.3855>
117. Hansma, H.G., Sinsheimer, R.L., Li, M., Hansma, P.K.: Atomic force microscopy of single- and double-stranded DNA. 20, 3585–3590 (1992)
118. Bustamante, C., Vesenka, A., Lin, C.T., Rees, W., Guthold, M., Keller, R.: Circular DNA Molecules Imaged in Air by Scanning Force Microscopy. *Biochemistry*. 31, 22–26 (1992). <https://doi.org/10.1021/bi00116a005>
119. Umemura, K., Ishikawa, M., Kuroda, R.: Controlled immobilization of DNA molecules using chemical modification of mica surfaces for atomic force microscopy: Characterization in air. *Anal. Biochem.* 290, 232–237 (2001). <https://doi.org/10.1006/abio.2001.4996>
120. Shlyakhtenko, L.S., Gall, A.A., Weimer, J.J., Hawn, D.D., Lyubchenko, Y.L.: Atomic force microscopy imaging of DNA covalently immobilized on a functionalized mica substrate. *Biophys. J.* 77, 568–576 (1999). [https://doi.org/10.1016/S0006-3495\(99\)76913-4](https://doi.org/10.1016/S0006-3495(99)76913-4)
121. Lyubchenko, Y., Shlyakhtenko, L., Harrington, R., Oden, P., Lindsay, S.: Atomic force microscopy of long DNA: Imaging in air and under water. *Proc. Natl. Acad. Sci. U. S. A.* 90, 2137–2140 (1993). <https://doi.org/10.1073/pnas.90.6.2137>
122. Jensen, T.R., Balashev, K., Bj rnholm, T., Kjaer, K.: Novel methods for studying lipids and lipases and their mutual interaction at interfaces. Part II. Surface sensitive synchrotron X-ray scattering. *Biochimie*. 83, 399–408 (2001). [https://doi.org/10.1016/S0300-9084\(01\)01265-2](https://doi.org/10.1016/S0300-9084(01)01265-2)

123. Hui, S.W., Viswanathan, R., Zasadzinski, J.A., Israelachvili, J.N.: The structure and stability of phospholipid bilayers by atomic force microscopy. *Biophys. J.* 68, 171–178 (1995). [https://doi.org/10.1016/S0006-3495\(95\)80172-4](https://doi.org/10.1016/S0006-3495(95)80172-4)
124. Malkin, A.J., Plomp, M., McPherson, A.: Application of atomic force microscopy to studies of surface processes in virus crystallization and structural biology. *Acta Crystallogr. Sect. D Biol. Crystallogr.* 58, 1617–1621 (2002). <https://doi.org/10.1107/S090744490201274X>
125. Silva, L.P.: Imaging Proteins with Atomic Force Microscopy : An Overview. 387–395 (2005)
126. Zhihua, W.U., Xuehua, Z., Xiaodong, Z., Jieli, S.U.N., Yaming, D., Jun, H.U.: In situ AFM observation of BSA adsorption on HOPG with nanobubble. 52, 1913–1919 (2007). <https://doi.org/10.1007/s11434-007-0288-8>
127. Whited, A.M., Park, P.S.H.: Atomic force microscopy: A multifaceted tool to study membrane proteins and their interactions with ligands. *Biochim. Biophys. Acta - Biomembr.* 1838, 56–68 (2014). <https://doi.org/10.1016/j.bbamem.2013.04.011>
128. Krautbauer, R., Pope, L.H., Schrader, T.E., Allen, S., Gaub, H.E.: Discriminating small molecule DNA binding modes by single molecule force spectroscopy. *FEBS Lett.* 510, 154–158 (2002). [https://doi.org/10.1016/S0014-5793\(01\)03257-4](https://doi.org/10.1016/S0014-5793(01)03257-4)
129. Yokota, H., Nickerson, D.A., Trask, B.J., Van Den Engh, G., Hirst, M., Sadowski, I., Aebbersold, R.: Mapping a protein-binding site on straightened DNA by atomic force microscopy. *Anal. Biochem.* 264, 158–164 (1998). <https://doi.org/10.1006/abio.1998.2851>
130. Xiao, A., Li, H.: Direct monitoring of equilibrium protein folding-unfolding by atomic force microscopy: Pushing the limit. *Chem. Commun.* 55, 12920–12923 (2019). <https://doi.org/10.1039/c9cc06293a>
131. Oesterhelt, F., Oesterhelt, D., Pfeiffer, M., Engel, A., Gaub, H.E., Müller, D.J.: Unfolding pathways of individual bacteriorhodopsins. *Science (80-.)*. 288, 143–146 (2000). <https://doi.org/10.1126/science.288.5463.143>

132. Cao, Y., Yoo, T., Li, H.: Single molecule force spectroscopy reveals engineered metal chelation is a general approach to enhance mechanical stability of proteins. *Proc. Natl. Acad. Sci. U. S. A.* 105, 11152–11157 (2008). <https://doi.org/10.1073/pnas.0803446105>
133. Guo, S., Zhu, X., Jańczewski, D., Lee, S.S.C., He, T., Teo, S.L.M., Vancso, G.J.: Measuring protein isoelectric points by AFM-based force spectroscopy using trace amounts of sample. *Nat. Nanotechnol.* 11, 817–823 (2016). <https://doi.org/10.1038/nnano.2016.118>
134. Evans, E.: Probing the Relation Between Force Lifetime and Chemistry. *Annu. Rev. Biophys. Biomol. Struct.* 30, 105–128 (2001)
135. Oberhauser, A.F., Marszalek, P.E., Erickson, H.P., Fernandez, J.M.: Structural protein tenascin. *Nature.* 393, 181 (1998)
136. Marszalek, P.E., Lu, H., Li, H., Carrion-Vazquez, M., Oberhauser, A.F., Schulten, K., Fernandez, J.M.: Mechanical unfolding intermediates in titin modules. *Nature.* 402, 100–103 (1999). <https://doi.org/10.1038/47083>
137. Wang, C.C., Tsong, T.Y., Hsu, Y.H., Marszalek, P.E.: Inhibitor binding increases the mechanical stability of staphylococcal nuclease. *Biophys. J.* 100, 1094–1099 (2011). <https://doi.org/10.1016/j.bpj.2011.01.011>
138. Li, H., Oberhauser, A.F., Fowler, S.B., Clarke, J., Fernandez, J.M.: Atomic force microscopy reveals the mechanical design of a modular protein. *Proc. Natl. Acad. Sci. U. S. A.* 97, 6527–6531 (2000). <https://doi.org/10.1073/pnas.120048697>
139. Muddassir, M., Manna, B., Singh, P., Singh, S., Kumar, R., Ghosh, A., Sharma, D.: ChemComm surrounding anions and its mechanical stability †. 9635–9638 (2018). <https://doi.org/10.1039/c8cc05557b>
140. Timasheff, N.: Preferential Interactions of Proteins with Solvent Components in Aqueous Amino Acid Solutions †. 224, (1983)
141. Arakawa, T., Timasheff, S.N.: THE STABILIZATION OF PROTEINS BY

- OSMOLYTES. *Biophys. J.* 47, 411–414 (1985). [https://doi.org/10.1016/S0006-3495\(85\)83932-1](https://doi.org/10.1016/S0006-3495(85)83932-1)
142. Roychoudhury, A., Bieker, A., Häussinger, D., Oesterhelt, F.: Membrane protein stability depends on the concentration of compatible solutes - A single molecule force spectroscopic study. *Biol. Chem.* 394, 1465–1474 (2013). <https://doi.org/10.1515/hsz-2013-0173>
143. Schrot, S., Fuchs, H., Galinski, E., Janshoff, A., Oberdo, Y., Friedrich-wilhelms-universita, R.: Impact of compatible solutes on the mechanical properties of fibronectin: a single molecule analysis “. 1876–1881 (2003). <https://doi.org/10.1039/b301022h>
144. Deng, X., Xiong, F., Li, X., Xiang, B., Li, Z., Wu, X., Guo, C., Li, X., Li, Y., Li, G., Xiong, W., Zeng, Z.: Application of atomic force microscopy in cancer research. *J. Nanobiotechnology.* 16, V (2018). <https://doi.org/10.1186/s12951-018-0428-0>
145. Lakowicz, J.R.: General features of protein fluorescence. (2006)
146. Yasseen, Z.J., El Ghossain, M.O.: Studies on Binding of Widely used Drugs with Human Serum Albumin at Different Temperatures and PHs. *J. Biomed. Sci.* 5, 1–8 (2016). <https://doi.org/10.4172/2254-609x.100033>
147. Fraiji, L.K., Hayes, D.M., Werner, T.C.: Static and dynamic fluorescence quenching experiments for the physical chemistry laboratory. *J. Chem. Educ.* 69, 424–428 (1992). <https://doi.org/10.1021/ed069p424>
148. Lehrer, S.S.: Solute Perturbation of Protein Fluorescence. the Quenching of the Tryptophyl Fluorescence of Model Compounds and of Lysozyme by Iodide Ion. *Biochemistry.* 10, 3254–3263 (1971). <https://doi.org/10.1021/bi00793a015>
149. Lakowicz, J.R., Weber, G.: Quenching of Fluorescence by Oxygen. a Probe for Structural Fluctuations in Macromolecules. *Biochemistry.* 12, 4161–4170 (1973). <https://doi.org/10.1021/bi00745a020>
150. Ware, W.R.: Oxygen quenching of fluorescence in solution: An experimental study of the

- diffusion process. *J. Phys. Chem.* 66, 455–458 (1962).
<https://doi.org/10.1021/j100809a020>
151. Han, X. Le, Mei, P., Liu, Y., Xiao, Q., Jiang, F.L., Li, R.: Binding interaction of quincolorac with bovine serum albumin: A biophysical study. *Spectrochim. Acta - Part A Mol. Biomol. Spectrosc.* 74, 781–787 (2009). <https://doi.org/10.1016/j.saa.2009.08.018>
152. Tayyab, S., Siddiqui, M.U., Ahmad, N.: Experimental determination of the free energy of unfolding of proteins. *Biochem. Educ.* 23, 162–164 (1995)
153. Pace, C.N.: Determination and analysis of urea and guanidine hydrochloride denaturation curves *Methods Enzymol.* (1986)
154. Fredrickson, G.H.: The theory of polymer dynamics. *Curr. Opin. Solid State Mater. Sci.* 1, 812–816 (1996). [https://doi.org/10.1016/S1359-0286\(96\)80106-9](https://doi.org/10.1016/S1359-0286(96)80106-9)
155. Saitô, N., Takahashi, K., Yunoki, Y.: *The Statistical Mechanical Theory of Stiff Chains*, (1967)
156. Pillarisetti, A., Desai, J.P., Ladjal, H., Schiffmacher, A., Ferreira, A., Keefer, C.L.: Mechanical phenotyping of mouse embryonic stem cells: Increase in stiffness with differentiation. *Cell. Reprogram.* 13, 371–380 (2011).
<https://doi.org/10.1089/cell.2011.0028>
157. Agarwal, S., Mehrotra, R.: An Overview of Molecular Simulation. *JSM Chem.* 4, 1024 (2016)
158. Morris, G.M., Lim-Wilby, M.: Molecular docking. *Methods Mol. Biol.* 443, 365–382 (2008). https://doi.org/10.1007/978-1-59745-177-2_19
159. Yuriev, E., Ramsland, P.A.: Latest developments in molecular docking: 2010-2011 in review. *J. Mol. Recognit.* 26, 215–239 (2013). <https://doi.org/10.1002/jmr.2266>
160. Tripathi, A., Misra, K.: Molecular Docking: A Structure-Based Drug Designing Approach. *JSM Bioinformatics, Genomics Proteomics.* 5, 1–5 (2017)

161. Bursulaya, B.D., Totrov, M., Abagyan, R., Brooks, C.L.: Comparative study of several algorithms for flexible ligand docking. *J. Comput. Aided. Mol. Des.* 17, 755–763 (2003). <https://doi.org/10.1023/B:JCAM.0000017496.76572.6f>
162. Chen, R., Mintseris, J., Weng, Z.: A Protein – Protein Docking Benchmark. 91, 88–91 (2003)
163. Schneidman-Duhovny, D., Inbar, Y., Nussinov, R., Wolfson, H.J.: PatchDock and SymmDock: Servers for rigid and symmetric docking. *Nucleic Acids Res.* 33, 363–367 (2005). <https://doi.org/10.1093/nar/gki481>
164. Special, W., To, R., Lesions, O.: SIDE-EFFECTS OF CHLORAMPHENICOL AND AUREOMYCIN , WITH SPECIAL REFERENCE TO ORAL LESIONS *. 388–393 (1951)
165. Manten, A.: Side effects of antibiotics. *Tijdschr. Diergeneeskd.* 106, 37–41 (1981). <https://doi.org/10.1080/01652176.1981.9693824>
166. Krasner, J.: Drug-protein interaction. *Pediatr. Clin. North Am.* 19, 51–63 (1972). [https://doi.org/10.1016/S0031-3955\(16\)32666-9](https://doi.org/10.1016/S0031-3955(16)32666-9)
167. Wiest, D.B., Cochran, J.B., Tecklenburg, F.W.: Chloramphenicol toxicity revisited: a 12-year-old patient with a brain abscess. *J. Pediatr. Pharmacol. Ther.* 17, 182–188 (2012)
168. Dajani, A.S., AS, D., RE, K.: The renaissance of chloramphenicol. (1981)
169. Oravcová, J., Böhs, B., Lindner, W.: Drug-protein binding studies new trends in analytical and experimental methodology. *J. Chromatogr. B Biomed. Appl.* 677, 1–28 (1996). [https://doi.org/10.1016/0378-4347\(95\)00425-4](https://doi.org/10.1016/0378-4347(95)00425-4)
170. Abdollahpour, N., Soheili, V., Saberi, M.R., Chamani, J.: Investigation of the Interaction Between Human Serum Albumin and Two Drugs as Binary and Ternary Systems. *Eur. J. Drug Metab. Pharmacokinet.* 41, 705–721 (2016). <https://doi.org/10.1007/s13318-015-0297-y>

171. Maruyama, K.: Connectin/titin, giant elastic protein of muscle. *FASEB J.* 11, 341–345 (1997). <https://doi.org/10.1096/fasebj.11.5.9141500>
172. Kingdom, U.: Mechanical and chemical unfolding of a single protein : 96, 3694–3699 (1999)
173. Banerjee, S., Mitra, C.: Muscle relaxant properties of chloramphenicol. *J. Pharm. Sci.* 65, 704–708 (1976)
174. Sohn, Y.Z., Katz, R.L.: Effects of certain antibiotics on isometric contractions of isolated rat heart muscle. *Can. Anaesth. Soc. J.* 25, 291–296 (1978).
<https://doi.org/10.1007/BF03005651>
175. Sohn, Y.Z., Katz, R.L.: Interaction of halothane and antibiotics on isometric contractions on rat-heart muscle. *Anesth. Analg.* 56, 515—521 (1977).
<https://doi.org/10.1213/00000539-197707000-00011>
176. Glanzer, M.L., Peaslee, M.H.: Inhibition of heart beat development by chloramphenicol in intact and *Cardia bifida* explanted chick embryos. *Experientia.* 26, 370–371 (1970)
177. Pottier, B., Bellon, L.: “Noiseless” thermal noise measurement of atomic force microscopy cantilevers. *Appl. Phys. Lett.* 110, (2017). <https://doi.org/10.1063/1.4977790>
178. Butt, H.J., Jaschke, M.: Calculation of thermal noise in atomic force microscopy. *Nanotechnology.* 6, 1–7 (1995). <https://doi.org/10.1088/0957-4484/6/1/001>
179. Chen, Y., Barkley, M.D.: Toward understanding tryptophan fluorescence in proteins. *Biochemistry.* 37, 9976–9982 (1998). <https://doi.org/10.1021/bi980274n>
180. Sathya, A., Prabhu, T., Ramalingam, S.: Structural, biological and pharmaceutical importance of antibiotic agent chloramphenicol. *Heliyon.* 6, e03433 (2020).
<https://doi.org/10.1016/j.heliyon.2020.e03433>
181. Pramanik, U., Khamari, L., Shekhar, S., Mukherjee, S.: On the role of hydrophobic interactions between chloramphenicol and bovine pancreatic trypsin: The effect of a

- strong electrolyte. *Chem. Phys. Lett.* 742, 137137 (2020).
<https://doi.org/10.1016/j.cplett.2020.137137>
182. Narayana, Y. V., Gadgil, C., Mote, R.D., Rajan, R., Subramanyam, D.: Clathrin-Mediated Endocytosis Regulates a Balance between Opposing Signals to Maintain the Pluripotent State of Embryonic Stem Cells. *Stem Cell Reports.* 12, 152–164 (2019).
<https://doi.org/10.1016/j.stemcr.2018.11.018>
183. Cross, S.E., Jin, Y.S., Rao, J., Gimzewski, J.K.: Nanomechanical analysis of cells from cancer patients. *Nat. Nanotechnol.* 2, 780–783 (2007).
<https://doi.org/10.1038/nnano.2007.388>
184. Duf re, Y.F., Lee, G.U.: Advances in the characterization of supported lipid films with the atomic force microscope. *Biochim. Biophys. Acta - Biomembr.* 1509, 14–41 (2000).
[https://doi.org/10.1016/S0005-2736\(00\)00346-1](https://doi.org/10.1016/S0005-2736(00)00346-1)
185. Fujiwara, I., Zweifel, M.E., Courtemanche, N., Pollard, T.D.: Latrunculin A Accelerates Actin Filament Depolymerization in Addition to Sequestering Actin Monomers. *Curr. Biol.* 28, 3183-3192.e2 (2018). <https://doi.org/10.1016/j.cub.2018.07.082>
186. Shoji, K., Ohashi, K., Sampei, K., Oikawa, M., Mizuno, K.: Cytochalasin D acts as an inhibitor of the actin-cofilin interaction. *Biochem. Biophys. Res. Commun.* 424, 52–57 (2012). <https://doi.org/10.1016/j.bbrc.2012.06.063>
187. Kiss, R., Bock, H., Pells, S., Canetta, E., Adya, A.K., Moore, A.J., De Sousa, P., Willoughby, N.A.: Elasticity of human embryonic stem cells as determined by atomic force microscopy. *J. Biomech. Eng.* 133, 1–10 (2011). <https://doi.org/10.1115/1.4005286>
188. Soofi, S.S., Last, J.A., Liliensiek, S.J., Nealey, P.F., Murphy, C.J.: The elastic modulus of MatrigelTM as determined by atomic force microscopy. *J. Struct. Biol.* 167, 216–219 (2009). <https://doi.org/10.1016/j.jsb.2009.05.005>
189. Xia, S., Lim, Y.B., Zhang, Z., Wang, Y., Zhang, S., Lim, C.T., Yim, E.K.F., Kanchanawong, P.: Nanoscale Architecture of the Cortical Actin Cytoskeleton in Embryonic Stem Cells. *Cell Rep.* 28, 1251-1267.e7 (2019).

- <https://doi.org/10.1016/j.celrep.2019.06.089>
190. Yin, Y., Shen, W.H.: PTEN : a new guardian of the genome. 5443–5453 (2008).
<https://doi.org/10.1038/onc.2008.241>
191. Hu, Y., An, Y., Fang, N., Li, Y., Jin, H., Nazarali, A., Ji, S.: The Optimization of Soluble PTEN Expression in Escherichia coli. 42–48 (2015)
192. Gupta, A.: Controlling PTEN (Phosphatase and Tensin Homolog) Stability A DOMINANT ROLE FOR LYSINE 66 *. 291, 18465–18473 (2016).
<https://doi.org/10.1074/jbc.M116.727750>
193. Song, M.S., Salmena, L., Pandolfi, P.P.: The functions and regulation of the PTEN tumour suppressor. *Nat. Publ. Gr.* 13, 283–296 (2012). <https://doi.org/10.1038/nrm3330>
194. Leslie, N.R., Downes, C.P.: REVIEW ARTICLE PTEN function : how normal cells control it and tumour cells lose it. 11, 1–11 (2004)
195. Alber, T., Matthews, B.W.: Structure and Thermal Stability of Phage T4 Lysozyme. *Methods Enzymol.* 154, 511–533 (1987). [https://doi.org/10.1016/0076-6879\(87\)54093-9](https://doi.org/10.1016/0076-6879(87)54093-9)
196. Bendeck, M.P., Conte, M., Zhang, M., Nili, N., Strauss, B.H., Farwell, S.M.: Doxycycline modulates smooth muscle cell growth, migration, and matrix remodeling after arterial injury. *Am. J. Pathol.* 160, 1089–1095 (2002). [https://doi.org/10.1016/S0002-9440\(10\)64929-2](https://doi.org/10.1016/S0002-9440(10)64929-2)
197. Sohn, Y.-Z., Katz, R.L.: Effects of certain antibiotics on isometric contractions of isolated rat heart muscle. *Can. Anaesth. Soc. J.* 25, 291–296 (1978)
198. Sohn, Y.Z., Katz, R.L.: Interaction of halothane and antibiotics on isometric contractions on rat-heart muscle. *Anesth. Analg.* 56, 515–521 (1977).
<https://doi.org/10.1213/00000539-197707000-00011>
199. Min, C.H., Min, Y.S., Lee, S.J., Sohn, U.D.: The comparative effects of aminoglycoside antibiotics and muscle relaxants on electrical field stimulation response in rat bladder

smooth muscle. *Arch. Pharm. Res.* 39, 863–870 (2016). <https://doi.org/10.1007/s12272-016-0765-1>